



Schweizerische Eidgenossenschaft  
Confédération suisse  
Confederazione Svizzera  
Confederaziun svizra

Eidgenössisches Departement für Umwelt, Verkehr, Energie und Kommunikation UVEK  
Département fédéral de l'environnement, des transports, de l'énergie et de la communication DETEC  
Dipartimento federale dell'ambiente, dei trasporti, dell'energia e delle comunicazioni DATEC

**Bundesamt für Strassen**  
**Office fédéral des routes**  
**Ufficio federale delle Strade**

# Robotic reinforcement of pavements

**Robotergestützte Verstärkung von Belägen**

**Renforcement robotique de chaussées**

**Empa**  
**Martin Arrigada**  
**Saeed Abbasion**  
**Pietro Lura**

**ETH**  
**Petrus Aejmelaesus-Lindstroem**  
**Fabio Gramazio**  
**Matthias Kohler**

**Forschungsprojekt ASTRA 2017/005 auf Antrag des Bundesamt für Strassen (ASTRA)**

**Juli 2023**

**1753**

Der Inhalt dieses Berichtes verpflichtet nur den (die) vom Bundesamt für Strassen unterstützten Autor(en). Dies gilt nicht für das Formular 3 "Projektabschluss", welches die Meinung der Begleitkommission darstellt und deshalb nur diese verpflichtet.

Bezug: Schweizerischer Verband der Strassen- und Verkehrsfachleute (VSS)

Le contenu de ce rapport n'engage que les auteurs ayant obtenu l'appui de l'Office fédéral des routes. Cela ne s'applique pas au formulaire 3 « Clôture du projet », qui représente l'avis de la commission de suivi et qui n'engage que cette dernière.

Diffusion : Association suisse des professionnels de la route et des transports (VSS)

La responsabilità per il contenuto di questo rapporto spetta unicamente agli autori sostenuti dall'Ufficio federale delle strade. Tale indicazione non si applica al modulo 3 "conclusione del progetto", che esprime l'opinione della commissione d'accompagnamento e di cui risponde solo quest'ultima.

Ordinazione: Associazione svizzera dei professionisti della strada e dei trasporti (VSS)

The content of this report engages only the author(s) supported by the Federal Roads Office. This does not apply to Form 3 'Project Conclusion' which presents the view of the monitoring committee.

Distribution: Swiss Association of Road and Transportation Experts (VSS)



Schweizerische Eidgenossenschaft  
Confédération suisse  
Confederazione Svizzera  
Confederaziun svizra

Eidgenössisches Departement für Umwelt, Verkehr, Energie und Kommunikation UVEK  
Département fédéral de l'environnement, des transports, de l'énergie et de la communication DETEC  
Dipartimento federale dell'ambiente, dei trasporti, dell'energia e delle comunicazioni DATEC

**Bundesamt für Strassen**  
**Office fédéral des routes**  
**Ufficio federale delle Strade**

# Robotic reinforcement of pavements

**Robotergestützte Verstärkung von Belägen**

**Renforcement robotique de chaussées**

**Empa**  
**Martin Arrigada**  
**Saeed Abbasion**  
**Pietro Lura**

**ETH**  
**Petrus Aejmelaeus-Lindstroem**  
**Fabio Gramazio**  
**Matthias Kohler**

**Forschungsprojekt ASTRA 2017/005 auf Antrag des Bundesamt für Strassen (ASTRA)**

**Juli 2023**

**1753**

# Impressum

## Forschungsstelle und Projektteam

### Projektleitung

Martin Arraigada, Dr. (Empa)

### Mitglieder

Saeed Abbasion, Dr. (Empa)

Pietro Lura, Prof. Dr. (Empa)

Petrus Aejmelaesus-Lindström, Dr. (ETH)

Fabio Gramazio, Prof. Dr. (ETH)

Matthias Kohler, Prof. Dr. (ETH)

## Begleitkommission

### Präsident

Nicolas Bueche, Prof. Dr. (BFH)

### Mitglieder

Bernhard Hofko, Assoc. Prof. Dipl.-Ing. Dr. techn. (TU Wien)

Gabriele Tebaldi, Prof. Dr. (Uni Parma)

Martin Horat (VSS)

Tobias Bonwetsch, Dr. (ROB Technologies AG)

Gerrit Bartels (ASTRA)

## Antragsteller

Bundesamt für Strassen (ASTRA)

## Bezugsquelle

Das Dokument kann kostenlos von <http://www.mobilityplatform.ch> heruntergeladen werden.

# Inhaltsverzeichnis

<b>Impressum</b> .....	<b>4</b>
<b>Zusammenfassung</b> .....	<b>7</b>
<b>Résumé</b> .....	<b>11</b>
<b>Summary</b> .....	<b>15</b>
<b>1 Introduction</b> .....	<b>19</b>
1.1 State of the art.....	20
<b>2 Objectives of the research</b> .....	<b>25</b>
<b>3 Experimental plan</b> .....	<b>27</b>
3.1 Overview .....	27
3.2 Materials and setup .....	29
3.2.1 Robotic arm .....	29
3.2.2 Aggregates .....	33
3.2.3 String .....	34
3.2.4 Rubber mat.....	35
3.2.5 Setups to apply dynamic mechanical loads .....	37
3.3 Tests description .....	37
3.4 Experimental results.....	41
3.4.1 Experiments on small boxes (50×50×15 cm <sup>3</sup> ) .....	41
3.4.2 Experiments on big boxes (70×70×25 cm <sup>3</sup> ).....	45
3.5 Computer tomography scans .....	50
<b>4 Modelling using the Discrete Element Method</b> .....	<b>53</b>
4.1 Overview .....	53
4.2 Preliminary simulations .....	54
4.3 Simulation of the small box experiment .....	55
4.3.1 Parts .....	56
4.3.2 Particles.....	57
4.3.3 Materials and Interactions .....	66
4.3.4 Particle generation .....	69
4.3.5 Compaction and loading .....	70
4.3.6 Domain .....	70
4.3.7 Implementation through keywords programming with Matlab .....	70
4.4 Results .....	71
<b>5 Conclusions and Outlook</b> .....	<b>75</b>
<b>Glossar</b> .....	<b>79</b>
<b>Literaturverzeichnis</b> .....	<b>81</b>
<b>Projektabschluss</b> .....	<b>83</b>



## Zusammenfassung

Straßenoberbauten sind mehrschichtige Bauwerke, die hauptsächlich aus körnigen Mineralstoffen bestehen, entweder in ungebundener Form oder gebunden mit bituminösen oder hydraulischen Bindemitteln. Körnige Mineralstoffe unterschiedlicher Herkunft, Größe und Form machen das größte Volumen eines Straßenaufbaus aus und tragen entscheidend zu dessen Tragfähigkeit bei. Gesteinskörnungen können sich je nach Einschluss- und Belastungsbedingungen wie ein flüssiges oder festes Material verhalten. Der Übergang vom flüssigen zum festen Zustand eines körnigen Materials wird als Verklemmung (auf English "Jamming") bezeichnet. Im Straßenbau wird dieser Zustand durch Verdichtung erreicht, indem äußere Kräfte und Vibrationen auf das quasi-eingeschlossene Straßenmaterial einwirken. Die Tragfähigkeit ungebundener Schichten hängt sowohl vom Material selbst (Kohäsion und innerer Reibungswinkel) als auch von seinem Spannungszustand ab, der von den aufgebrachtten äußeren Kräften und dem Grad der Einschließung abhängt. Grobkörnige Materialien ohne kohäsive Eigenschaften neigen dazu, durch die Kontaktpunkte des Aggregats entlang der Belastungsrichtung Kraftketten zu bilden. In dieser Situation ist das Material in der Lage, zunehmende Lasten zu tragen und sich wie ein starrer Körper zu verhalten, solange die Kontaktkräfte zwischen den Gesteinskörnern unter ihrer Druckfestigkeit liegen und sich auch die Richtung der einwirkenden Kräfte nicht ändert. Die Einschnürung in Belagskonstruktionen ist sowohl in horizontaler als auch in vertikaler Richtung begrenzt und reicht im Allgemeinen nicht aus, um nach der Verdichtung eine optimale Verdichtung zu erreichen und das Material im Laufe der Zeit zu halten.

Strassenoberbauten können mit handelsüblichen 2D-Gittern, -Gitternetzen oder -Filzen zwischen gebundenen oder ungebundenen Schichten oder Böden im Unterbau verstärkt werden. Diese Verstärkungselemente wirken nur auf Zug, vor allem wenn sich das Bauwerk unter Belastung durch den sogenannten Membraneffekt verformt. Sie verbessern die Tragfähigkeit, indem sie die potenzielle Versagensfläche verändern, sie bieten den Aggregaten durch die Verzahnung mit der Gitteröffnung seitlichen Halt und sie sorgen für Reibungs- und Scherkräfte. Diese 2D-Gitter befinden sich jedoch kaum in der besten vertikalen Position innerhalb einer Schicht, um eine optimale seitliche Begrenzung zu aktivieren, und wenn sie innerhalb der Asphaltsschichten verwendet werden, könnten sie die Grenzflächenhaftung stören. Neuere Forschungen an der ETH Zürich haben gezeigt, dass eine neuartige Konstruktion diese Nachteile durch den Einsatz einer durchgehenden Bewehrung überwinden kann. Schlanke Objekte wie Fäden oder Drähte, die sorgfältig schichtweise und nach bestimmten Mustern zwischen ungebundenen Gesteinskörpern platziert werden, können eine Verklemmung hervorrufen und verbessern, so dass neuartige tragende Strukturen wie Säulen und Wände entstehen. Um diese so genannten "Jammed Architectural Structures (JAS)" zu bauen, muss ein Roboterarm eingesetzt werden, der in der Lage ist, die Schnüre nach einem genauen Muster durch einen digitalen Bauplan zu verlegen. Die Konstruktion kann vollständig automatisiert werden, indem derselbe Roboterarm die Aggregate additiv gießt und verdichtet, was die Technologie zu einer vielversprechenden digitalen Roboterfertigung macht. Nach der Nutzung können die Komponenten dieser Strukturen einfach recycelt werden, indem man die Schnur herauszieht.

Mit dieser Arbeit wollten wir das Konzept der JAS in die Straßenbau Landschaft einführen, insbesondere zur Entwicklung einer einzigartigen Art der Bewehrung für Beläge. Anstelle von vertikalen Strukturen, die hauptsächlich quasistatischen Belastungen standhalten sollen, wurde das Konzept der durchgehenden Strangbewehrung auf die ungebundenen Schichten von Strassenoberbauten ausgedehnt, die in erster Linie die Aufgabe haben, wiederkehrende, vorübergehende vertikale Verkehrslasten von der Oberfläche aufzunehmen und sie auf eine breitere Bodenfläche zu verteilen, ohne sich übermäßig zu verformen. Der Hauptvorteil eines solchen Ansatzes gegenüber herkömmlichen Methoden besteht darin, dass die Schnüre beispielsweise beim Rückbau eines mit dieser Methode gebauten provisorischen Belags leicht aus den Schichten herausgezogen werden können, so dass die verbleibenden ungebundenen Zuschlagstoffe mit minimalem Aufwand

wiederverwendet werden können. Die Bewehrungsfäden können mit Hilfe automatischer Geräte und sogar in 3D-Fadenanordnungen, die den Bewegungen einer Stricknadel ähneln, verlegt werden.

Im ersten und wichtigsten Teil dieses Berichts werden die experimentellen Arbeiten an Gesteinskörnungen mit und ohne Fadenbewehrung beschrieben. Gesteinskörnungen zweier unterschiedlicher Fraktionen, hauptsächlich 16 - 22,4 mm, aber auch 8 - 11,2 mm, wurden in Holzkisten eingebracht. Hauptsächlich wurden gebrochene Gesteinskörnungen verwendet, aber auch gerundete Gesteinskörnungen wurden in ausgewählten Versuchen eingesetzt. Bei der Schnur handelte es sich um einen umweltfreundlichen, preisgünstigen geflochtenen Faden, der aus recycelten synthetischen und natürlichen Resten der Textilindustrie hergestellt wurde. Hauptsächlich wurden Fäden mit einem Durchmesser von 2,5 mm verwendet, in einzelnen Versuchen auch Fäden mit einem Durchmesser von 1,8 mm und 4 mm. Die ersten Versuche wurden mit Kartons von 50 × 50 × 15 cm<sup>3</sup> (kleine Kartons) durchgeführt, während die Hauptversuchsreihe in Kartons von 70 × 70 × 25 cm<sup>3</sup> (große Kartons) mit einer 1,5 cm dicken Gummimatte am Boden durchgeführt wurde. Ein Roboterarm mit 6 Freiheitsgraden wurde zum Ablegen der Schnur verwendet, wobei ein im Laufe des Projekts entwickelter Endeffektor dazu diente, die Schnur nach vordefinierten Mustern in aufeinanderfolgenden Schichten zu ziehen. Bei den Versuchen wurden verschiedene Arten von Fadenmustern verwendet, darunter kreisförmige Muster mit unterschiedlichen Überlappungsgraden und rechteckige Muster mit unterschiedlich großen Maschen. Die Probekörper wurden durch die Zugabe von aufeinanderfolgenden Lagen von Schnüren und Gesteinskörnungen hergestellt, gefolgt von einer manuellen Verdichtung mit einem Erdstamper. Bei den Big-Box-Proben erfolgte die abschließende Verdichtung mit einer sinusförmigen, über die gesamte Fläche der Probe verteilten Last, bis die aufgezeichnete bleibende Verformung ein Plateau erreichte. Anschließend wurden die einachsigen zyklischen Druckversuche mit Belastungen durch eine Belastungsplatte mit unterschiedlichen Belastungsarten, Höchst- und Mindestwerten und Frequenzen durchgeführt. Die Versuche zeigten sehr deutlich, dass die Verstärkung der Aggregatpackung mit Schnüren einen erheblichen und wiederholbaren Einfluss auf die zyklische Tragfähigkeit des Systems hat. Bei den unverstärkten Probekörpern versank die Ladeplatte nach Hunderten bis Tausenden von Zyklen in der Gesteinsschüttung, was zu starkem Abrieb und zur Zerkleinerung der Aggregate führte, während sie bei den verstärkten Probekörpern im Allgemeinen an der Oberfläche der Schüttung blieb. Kleinere Verformungen wurden sowohl bei den bewehrten als auch bei den unbewehrten Probekörpern mit kleineren Gesteinskörnungen beobachtet. Abgerundete Gesteinskörnungen führten sowohl bei den unbewehrten als auch bei den bewehrten Proben zu wesentlich größeren Verformungen als kantige Gesteinskörnungen mit den gleichen Abmessungen. Die Art der zyklischen Belastung hatte einen entscheidenden Einfluss auf das Verhalten der Probekörper: Bei einer hohen Maximallast und einer niedrigen Minimallast dringt die Belastungsplatte leicht in die Aggregatpackung ein, während bei niedrigen oder hohen Minimal- und Maximallasten der Kolben nicht in die Packung eindringt, selbst wenn der Probekörper nicht verstärkt ist. Im Gegensatz dazu hatte die Belastungshäufigkeit einen fast vernachlässigbaren Einfluss, wenn die Anzahl der Zyklen gleich blieb. Bei den in diesem Projekt verwendeten Geometrien und Belastungen schnitten Schnüre mit einer Dicke von 2,5 mm ebenso gut ab wie dickere Schnüre, während dünnere Schnüre rissen und zu größeren Verformungen der Aggregatpackungen führten. Es wurde ein allgemeiner Trend zur Verringerung der Verformung mit zunehmender Länge der in die Packungen eingebetteten Schnüre beobachtet, aber kreisförmige Muster schienen besser zu funktionieren als rechteckige Muster. Die beste Leistung wurde bei kreisförmigen Mustern mit Überlappungen beobachtet, aber die Leistung dieser Muster verbesserte sich nicht, wenn zu viele Überlappungen oder Kreise mit kleinem Durchmesser verwendet wurden. Ein geringerer Abstand zwischen den Bewehrungslagen in vertikaler Richtung oder entsprechend mehr Lagen von Schnüren in den Proben führten zu einer Verringerung der bleibenden Verformung.

Es wurden auch Versuche unternommen, mittels Röntgentomographie ein 3D-Bild der bewehrten Aggregatpackungen zu erhalten, um die Umlagerung der Aggregate und der Strings aufgrund von zyklischen Belastungen, die Zerkleinerung der Aggregate und das Reißen der Strings zu untersuchen. Mit einem speziellen Hochenergiegerät, das an der



Empa zur Verfügung steht, konnte zwar die Aggregatpackung in den kleinen Kästen abgebildet werden und auch die Strings waren sichtbar, eine Segmentierung der Strings mit Standardtechniken war jedoch nicht möglich.

Im zweiten Teil dieses Berichts beschreiben wir die Methodik zur Entwicklung numerischer Modelle zur Simulation von Partikel-String-Systemen unter dynamischer Belastung, um eine genaue Darstellung der im experimentellen Teil durchgeführten Tests zu erreichen. In dieser numerischen Arbeit wurden sowohl die Aggregatpackung als auch die Strangbewehrung mit der Methode der diskreten Elemente (DEM) simuliert. Die Hauptziele dieser Modellierungsarbeit waren: 1) Einblicke in die grundlegenden Mechanismen zu gewinnen, die die Verformung der bewehrten Gesteinsschüttung bestimmen; 2) die Auswirkungen kritischer Parameter (z. B. Materialeigenschaften der Gesteinskörner und der Strings, Belastung, Stringmuster und Randbedingungen) auf systematische und einfache Weise zu erforschen, was in den Experimenten schwierig oder unmöglich sein kann; 3) die Versuchsreihe durch zusätzliche numerische Experimente zu erweitern und zu ergänzen, z. B. mit unterschiedlichen Geometrien und Konfigurationen. Als Werkzeug zur Lösung der numerischen Modelle wurde die DEM-Software ThreeParticle/CAE verwendet. Um die Vorbereitung der verschiedenen Modellkonfigurationen zu automatisieren und zu vereinfachen, entwickelten wir ein Skript in Matlab, das die Vorbereitung und die Prüfung der Proben numerisch wiederholen konnte. Im Rahmen der Vorbereitung der Modelle haben wir eine große Anzahl (100) der in der Versuchsphase verwendeten Aggregate gescannt und digitalisiert. Wir haben auch die mechanischen Eigenschaften der verschiedenen Materialien und Vorrichtungen, die in den Versuchen verwendet wurden (d. h. Aggregate, Schnüre, Gummimatten), ermittelt, um Ausgangswerte für die Materialien und Kontaktmodelle zu erhalten. Die komplexesten Versuchsmodelle waren in der Lage, die für die Herstellung der Probekörper erforderlichen Schritte (Gießen der Zuschlagstoffe, Auslegen der Fäden und Verdichtung) mit einer gewissen Genauigkeit zu reproduzieren. Wir haben verschiedene Darstellungen von Partikelformen für die Aggregate ausprobiert, um herauszufinden, dass die Präzision oft mit dem Rechenaufwand geopfert wird. Folglich stellten wir fest, dass nicht immer die Modelle mit der präzisesten Beschreibung der physikalischen Realität die genauesten und zuverlässigsten Ergebnisse lieferten. Insbesondere haben wir festgestellt, dass die Modellierung der Aggregate mit Multikugeln - obwohl sie weniger genau ist als die Verwendung von Polyedern oder drei Gittern - die besten Ergebnisse bei einem akzeptablen Rechenaufwand liefert. Wir modellierten den Strang, indem wir verschiedene Kapselemente miteinander verbanden. Der Entwurf der Muster wurde ebenfalls automatisiert. Mehrere Simulationsversuche zeigten, dass die Komplexität dieser Modelle einen sehr hohen Rechenaufwand erfordert, mit extrem langen Rechenzeiten (bis zu 4 Wochen) auf der verfügbaren Hardware. Während die im Rahmen dieses Projekts durchgeführten Simulationen wertvolle Einblicke lieferten und die Methoden und Werkzeuge vorbereiteten, wird sich die künftige Arbeit auf die Optimierung der Simulationen der verstärkten Proben konzentrieren, um schnelle Ergebnisse zu erzielen.



## Résumé

Les chaussées sont des structures d'ingénierie multicouches construites principalement à l'aide d'agrégats minéraux granulaires, soit dans une configuration non liée, soit liée à un liant bitumineux ou hydraulique. Les granulats minéraux de différentes sources, tailles et formes constituent le volume le plus important d'une structure routière et contribuent de manière critique à sa capacité de charge. Les granulats peuvent se comporter comme des matériaux fluides ou solides en fonction de leur confinement et des conditions de charge. Le passage de l'état fluide à l'état solide d'un matériau granulaire est appelé bourrage. En ingénierie routière, cet état est atteint par le compactage en appliquant des forces externes et des vibrations au matériau de chaussée quasi confiné. La capacité portante des couches non liées dépend à la fois du matériau lui-même (cohésion et angle de frottement interne) mais aussi de son état de tension, qui dépend des forces externes appliquées et du degré de confinement. Les matériaux granulaires grossiers dépourvus de propriétés cohésives ont tendance à former des chaînes de force à travers les points de contact de l'agrégat le long de la direction de chargement. Dans cette situation, le matériau est capable de supporter des charges croissantes et de se comporter comme un corps rigide, tant que les forces de contact entre les agrégats sont inférieures à leur résistance à l'écrasement et que les contraintes appliquées ne changent pas de direction. Le confinement dans les structures de chaussée est limité à la fois dans la direction horizontale et dans la direction verticale et, en général, il est insuffisant pour atteindre une densification optimale après le compactage et pour maintenir le matériau bloqué dans le temps.

Les chaussées peuvent être renforcées en utilisant des grilles 2D commerciales, des mailles ou des feutres entre les couches liées ou non liées ou les sols de la couche de fondation. Ces éléments de renforcement ne fonctionnent qu'en tension, principalement lorsque la structure se déforme sous l'effet de la charge grâce à ce que l'on appelle l'effet de membrane. Ils améliorent la capacité portante en modifiant la surface de rupture potentielle, ils fournissent une retenue latérale aux agrégats grâce à l'imbrication avec l'ouverture de la grille et ils fournissent des forces de frottement et de cisaillement. Cependant, ces grilles 2D ne se trouvent pas dans la meilleure position verticale au sein d'une couche pour activer un confinement latéral optimal et, si elles sont utilisées dans les couches d'asphalte, elles risquent de perturber l'adhérence de l'interface. Des recherches récentes menées à l'ETH Zurich ont montré qu'un type de construction innovant pourrait permettre de surmonter ces inconvénients grâce à l'utilisation d'un renforcement continu. Des objets minces, tels qu'un fil ou un câble, placés avec soin entre des agrégats non liés, en couches successives et selon certains schémas, peuvent induire et améliorer le blocage pour créer de nouveaux types de structures porteuses, y compris des colonnes et des murs. Pour construire ces "structures architecturales brouillées", il est nécessaire d'utiliser un bras robotisé capable de déployer les cordes en suivant un schéma précis à partir d'un plan numérique. La construction peut être entièrement automatisée en utilisant le même bras robotique pour couler et compacter les agrégats de manière additive, ce qui en fait une technologie prometteuse de fabrication robotique numérique. Après utilisation, les composants de ces structures peuvent être facilement recyclés, simplement en retirant la ficelle.

Avec ce travail, nous avons l'intention d'introduire le concept de JAS dans le paysage de l'ingénierie routière, en particulier pour développer un type unique de renforcement pour les chaussées. Au lieu de structures verticales préparées pour supporter principalement des charges quasi statiques, le concept de renforcement continu des cordes a été étendu aux couches non liées des chaussées, dont la fonction principale est de reprendre les charges de trafic verticales transitoires répétitives de la surface et de les distribuer sur une zone inférieure plus large sans se déformer de manière excessive. Le principal avantage de cette approche par rapport aux méthodes traditionnelles est qu'en cas, par exemple, de démantèlement d'une chaussée temporaire construite selon cette méthode, les cordes peuvent être facilement extraites des couches, ce qui permet de réutiliser les agrégats non liés restants avec un minimum d'effort. Les cordes de renforcement peuvent être placées

à l'aide de dispositifs automatiques et même dans des arrangements de cordes en 3D, ressemblant aux mouvements d'une aiguille à tricoter.

Dans la première et principale partie de ce rapport, le travail expérimental sur les paquets de granulats avec et sans renfort de cordes est décrit. Des agrégats de deux fractions différentes, principalement de 16 à 22,4 mm mais aussi de 8 à 11,2 mm, ont été placés dans des boîtes en bois. La plupart du temps, des agrégats concassés ont été utilisés, mais des agrégats arrondis ont également été utilisés dans certaines expériences. La ficelle était un fil tressé écologique et bon marché, fabriqué à partir de déchets synthétiques et naturels recyclés provenant de l'industrie textile. Des cordes d'un diamètre de 2,5 mm ont été principalement utilisées, mais certains essais ont été réalisés avec des cordes d'un diamètre de 1,8 mm et de 4 mm. Les premiers essais ont été réalisés avec des boîtes de 50 × 50 × 15 cm<sup>3</sup> (petites boîtes), tandis que la série expérimentale principale a été réalisée avec des boîtes de 70 × 70 × 25 cm<sup>3</sup> (grandes boîtes) dont le fond était recouvert d'un tapis en caoutchouc de 1,5 cm d'épaisseur. Un bras robotisé à 6 degrés de liberté a été utilisé pour déposer la ficelle, avec un effecteur développé au cours du projet qui a été utilisé pour tirer la ficelle en suivant des motifs prédéfinis dans des couches successives. Différents types de motifs de cordes ont été utilisés dans les expériences, y compris des motifs circulaires avec différents degrés de chevauchement et des motifs rectangulaires avec des mailles de différentes tailles. Les échantillons ont été préparés en ajoutant des couches consécutives de cordes et d'agrégats, suivies d'une densification manuelle à l'aide d'un pilon à terre. Pour les échantillons Big Box, le compactage final a été effectué avec une charge sinusoïdale distribuée sur toute la surface de l'échantillon, jusqu'à ce que la déformation permanente enregistrée atteigne un plateau. Les essais de compression cyclique uniaxiale, avec des charges imposées par une plaque de chargement, ont ensuite été effectués avec différents types de charge, valeurs maximales et minimales et fréquences. Les expériences ont montré très clairement que le renforcement des agrégats par des cordes a un effet considérable et reproductible sur la capacité de charge cyclique du système. Dans les spécimens non renforcés, la plaque de chargement a fini par être enfouie dans les granulats après des centaines ou des milliers de cycles, alors que dans les spécimens renforcés, elle est généralement restée à la surface des granulats. Des déformations plus faibles, tant pour les échantillons renforcés que pour les échantillons non renforcés, ont été observées avec des agrégats plus petits. Les agrégats arrondis ont entraîné des déformations beaucoup plus importantes que les agrégats angulaires de même taille, tant pour les échantillons non renforcés que pour les échantillons renforcés. Le type de charge cyclique a montré une influence primordiale sur la performance des échantillons : avec une charge maximale élevée et une charge minimale faible, la plaque de chargement pénètre facilement dans le paquet de granulats, tandis que lorsque les charges minimale et maximale étaient toutes deux faibles ou élevées, le piston ne pénétrait pas dans le paquet, même si l'échantillon n'était pas armé. En revanche, la fréquence de chargement a eu une influence presque négligeable lorsque le nombre de cycles est resté le même. Avec les géométries et les charges employées dans ce projet, les cordes d'une épaisseur de 2,5 mm se sont comportées aussi bien que les cordes plus épaisses, tandis que les cordes plus fines se sont rompues et ont entraîné des déformations plus importantes des paquets d'agrégats. Une tendance générale à la réduction de la déformation avec l'augmentation de la longueur de la corde incorporée dans les paquets a été observée, mais les motifs circulaires ont semblé mieux fonctionner que les motifs rectangulaires. La meilleure performance a été observée dans les motifs circulaires avec chevauchements, mais la performance de ces motifs ne s'est pas améliorée lorsqu'un chevauchement trop important ou des cercles de petit diamètre ont été utilisés. Une plus petite distance entre les couches de renforcement dans la direction verticale, ou, de manière équivalente, un plus grand nombre de couches de cordes dans les spécimens, a entraîné une réduction de la déformation permanente.

Des premières tentatives ont également été faites pour obtenir une image en 3D des granulats renforcés au moyen de la tomographie à rayons X, afin d'étudier le réarrangement des granulats et des cordes sous l'effet des charges cycliques, l'écrasement des granulats et la rupture des cordes. Une installation spéciale à haute énergie disponible à l'Empa a certes permis de visualiser les agrégats dans les petites boîtes et même les cordes, mais il n'a pas été possible de segmenter les cordes avec les techniques habituelles.

Dans la deuxième partie de ce rapport, nous décrivons la méthodologie utilisée pour développer des modèles numériques permettant de simuler des systèmes de particules et de cordes soumis à des charges dynamiques et d'obtenir une représentation exacte des essais réalisés dans la section expérimentale. Dans ce travail numérique, l'emballage des agrégats et le renforcement de la corde ont été simulés à l'aide de la méthode des éléments discrets (DEM). Les principaux objectifs de cet effort de modélisation étaient les suivants 1) d'obtenir un aperçu des mécanismes fondamentaux qui régissent la déformation du paquet de granulats renforcé ; 2) d'explorer l'effet des paramètres critiques (par exemple, les propriétés des matériaux des granulats et des cordes, la charge, les modèles de cordes et les conditions aux limites) d'une manière systématique et simple, ce qui peut être difficile ou impossible dans les expériences ; 3) d'étendre et de compléter la série expérimentale avec des expériences numériques supplémentaires, par exemple avec des géométries et des configurations différentes. Nous avons utilisé le logiciel DEM ThreeParticle/CAE pour résoudre les modèles numériques. Afin d'automatiser et de simplifier la préparation des différentes configurations des modèles, nous avons développé un script dans Matlab capable de reproduire numériquement la préparation et le test des spécimens. Dans le cadre de la préparation des modèles, nous avons scanné et numérisé un nombre important (100) des agrégats utilisés dans la phase expérimentale. Nous avons également obtenu les propriétés mécaniques des différents matériaux et dispositifs utilisés dans les expériences (agrégats, cordes, tapis en caoutchouc), afin d'obtenir les valeurs initiales des matériaux et des modèles de contact. En conséquence, les modèles d'essai les plus complexes obtenus ont pu reproduire avec un certain degré de précision les étapes nécessaires à la préparation des spécimens (coulage des agrégats, déploiement des cordes et compactage). Nous avons essayé différentes représentations de la forme des particules pour les agrégats et nous avons constaté que la précision est souvent compromise par l'effort de calcul. Par conséquent, nous avons établi que les modèles décrivant le plus précisément la réalité physique ne fournissaient pas toujours les résultats les plus précis et les plus fiables. Plus précisément, nous avons observé que la modélisation des agrégats à l'aide de multi-sphères - bien que moins précise que l'utilisation de polyèdres ou de trois mailles - fournit les meilleurs résultats avec un effort de calcul acceptable. Nous avons modélisé la corde en collant ensemble différents éléments de la capsule. La conception des motifs a également été automatisée. Plusieurs essais de simulation ont montré que la complexité de ces modèles exige un effort de calcul très important, avec des temps de calcul extrêmement longs (jusqu'à 4 semaines) sur le matériel disponible. Bien que les simulations effectuées dans le cadre de ce projet aient fourni des informations précieuses et préparé les méthodes et les outils, les travaux futurs se concentreront sur l'optimisation des simulations des spécimens renforcés afin d'obtenir des résultats rapides.



## Summary

Pavements are multilayered engineering structures constructed mainly using granular mineral aggregates, either in unbound configuration or bound with bituminous or hydraulic binder. Granular mineral aggregates from different sources, sizes and shapes make up the largest volume of a road structure and contribute critically to its bearing capacity. Aggregates can behave as a fluid- or solid-like material depending on their confinement and loading conditions. The transition from fluid- to solid-like state of a granular material is called jamming. In road engineering, this state is reached through compaction by applying external forces and vibration to the quasi-confined pavement material. The bearing capacity of unbound layers depends both on the material itself (cohesion and internal friction angle) but also on its tensional state, which depends on the applied external forces and the degree of confinement. Coarse granular materials with no cohesive properties tend to form force chains through the aggregate's contact points along the loading direction. In this situation, the material is able to support increasing loads and behave as a rigid body, as long as the contact forces among aggregates are below their crushing strength and also if the applied stress does not change in direction. Confinement in pavement structures is limited in both in the horizontal and in the vertical direction and in general it is insufficient to reach an optimum densification after compaction and to maintain the material jammed over time.

Pavements can be reinforced by using commercial 2D grids, meshes or felts between either bound or unbound layers or soils in the subgrade. These reinforcing elements work only on tension, mainly when the structure deforms under load thanks to the so-called membrane effect. They improve the bearing capacity by changing the potential failure surface, they provide lateral restraint to the aggregates thanks to interlocking with the grid aperture and they induce frictional and shear forces. However, these 2D grids are hardly in the best vertical position within a layer for activating optimal lateral confinement and if used between the asphalt layers, they might disturb the interface adhesion. Recent research performed at ETH Zurich has shown that an innovative type of construction might be able to overcome these drawbacks through the use of a continuous reinforcement. Slender objects like a thread or a wire, carefully placed between unbound aggregates in a layer-wise manner and following certain patterns can induce and improve jamming to create new types of loadbearing structures, including columns and walls. In order to build these so-called "Jammed Architectural Structures (JAS)", it is necessary to use a robotic arm capable to deploy the strings following a precise pattern through a digital blueprint. The construction can be fully automatized using the same robotic arm to pour and compact the aggregates additively, making it a promising digital robotic fabrication technology. After use, the components of these structures can be easily recycled, just by pulling out the string.

With this work we intended to introduce the concept of JAS to the road engineering landscape, specifically for developing a unique type of reinforcement for pavements. Instead of vertical structures prepared to withstand mainly quasi static loads, the concept of continuous string reinforcement was extended to the unbound layers of pavements, which have primarily the function of taking repetitive transient vertical traffic loads from the surface and distribute them onto a broader bottom area without deforming excessively. The main advantage of such an approach over traditional methods is that in case of, for example, dismantling a temporary pavement built with this method, the strings can be easily extracted from the layers, allowing to reuse the remaining unbound aggregates with minimal effort. Reinforcement strings can be placed through automatic devices and even in 3D string arrangements, resembling the movements of a knitting needle.

In the first and main part of this report, the experimental work on aggregate packings with and without string reinforcement is described. Aggregates of two different fractions, mainly 16 - 22.4 mm but also 8 - 11.2 mm, were placed into wooden boxes. Mostly, crushed aggregates were used, but also rounded aggregates were used in selected experiments. The string was an eco-friendly, low-priced braided thread made of recycled synthetic and

natural leftovers from the textile industry. Strings with 2.5 mm diameters were mostly used, with selected tests with strings of 1.8 mm and 4 mm diameter. The initial tests were performed with  $50 \times 50 \times 15 \text{ cm}^3$  boxes (small boxes), while the main experimental series was performed using  $70 \times 70 \times 25 \text{ cm}^3$  boxes (big boxes) with a 1.5 cm-thick rubber mat at the bottom. A robotic arm with 6 degrees of freedom was used to deposit the string, with an end effector developed in the course of the project that was used to pull the string following predefined patterns in successive layers. Different types of string patterns were employed in the experiments, including circular patterns with different degrees of overlap and rectangular patterns with meshes of different sizes. The specimens were prepared adding consecutive layers of strings and aggregates followed by a manual densification using an earth rammer. For the big box samples, the final compaction was carried out with a sinusoidal load distributed over the entire area of the specimen, until the recorded permanent deformation reached a plateau. The uniaxial cyclic compression tests, with loads imposed by a loading plate, were then carried out with different load types, maximum and minimum values and frequencies. The experiments showed very clearly that the reinforcement of the aggregate packing with strings has a considerable and repeatable effect on the cyclic load carrying capacity of the system. In unreinforced specimens, the loading plate ended up buried into the aggregate packing after hundreds to thousands of cycles producing high abrasion and crushing of the aggregates, while in reinforced specimens it generally remained at the surface of the packing. Smaller deformations, both for the reinforced and the unreinforced specimens, were observed with smaller aggregates. Rounded aggregates resulted in much larger deformations than angular aggregates with the same sizes, both when unreinforced and when reinforced. The type of cyclic load showed a paramount influence in the performance of the specimens: with a high maximum load and a low minimum load, the loading plate penetrates easily into the aggregate packing, while when both the minimum and the maximum loads were either both low or both high, the piston did not penetrate into the packing, even if the specimen was unreinforced. On the contrary the loading frequency had almost negligible influence when the number of cycles was kept the same. Under the geometries and loads employed in this project, strings with 2.5 mm thickness performed as well as thicker strings, while thinner strings ruptured and resulted in larger deformations of the aggregate packings. A general trend of reduced deformation with increased length of string embedded in the packings was observed, but circular patterns appeared to work better than rectangular patterns. The best performance was observed in circular patterns with overlaps, but the performance of these patterns did not improve when too much overlapping or circles of small diameter were employed. A smaller distance between the reinforcement layers in the vertical direction, or equivalently, more layers of string in the specimens, resulted in a reduction of the permanent deformation.

Initial attempts were also made to obtain a 3D image of the reinforced aggregate packings by means of X-ray tomography, to study the rearrangement of the aggregates and of the strings due to cyclic loads, the crushing of the aggregates and the rupture of the strings. While a special, high-energy setup available at Empa was able to image the aggregate packing in the small boxes and even the strings were visible, segmentation of the strings with standard techniques was not possible.

In the second part of this report, we describe the methodology to develop numerical models to simulate particle-string systems under dynamic loading achieving an accurate representation of the actual tests performed in the experimental section. In this numerical work, both the aggregate packing and the string reinforcement were simulated with the Discrete Element Method (DEM). The main aims of this modelling effort were: 1) to obtain insight about the fundamental mechanisms that govern the deformation of the reinforced aggregate packing; 2) to explore the effect of critical parameters (e.g. material properties of aggregates and strings, load, string patterns and boundary conditions) in a systematic and simple manner, which may be difficult or impossible in the experiments; 3) to extend and complement the experimental series with additional numerical experiments, e.g. with different geometries and configurations. We used the DEM software ThreeParticle/CAE as a tool for solving the numerical models. In order to automatize and simplify the preparation of different model configurations, we developed a script in Matlab that was able to numerically replicate the preparation and the testing of the specimens. As part of the preparation of the models, we scanned and digitalized a significant number (100) of the



aggregates used in the experimental phase. We also obtained the mechanical properties of the different materials and devices used in the experiments (i.e., aggregates, strings, rubber mat), in order to obtain initial values of the materials and contact models. As a result, the most complex trial models obtained were able to replicate with a certain degree of precision the steps required to prepare the specimens (pouring of aggregates, deploying of strings and compaction). We tried different particle shape representations for the aggregates to find out that precision often trades off with computational effort. Consequently, we established that not always the models with the most precise description of the physical reality provided the most accurate and reliable results. Specifically, we observed that modelling of the aggregates with multi-spheres – despite being less accurate than using polyhedrons or three meshes - provides the best results with an acceptable computational effort. We modelled the string by bonding different capsule elements together. The design of the patterns was also automatized. Several simulation trials showed that the complexity of these models is requiring a very important computational effort, with extremely long computation times (up to 4 weeks) on the available hardware. While the simulations performed in the frame of this project provided valuable insight and prepared the methods and the tools, future work will focus on optimizing the simulations of the reinforced specimens to obtain rapid results.



# 1 Introduction

Pavements are multilayered engineering structures constructed mainly using granular mineral aggregates either in unbound configuration or bound with bituminous or hydraulic binders [1]. Crushed or uncrushed granular mineral aggregates from different sources, sizes and shapes take up by far the highest volume of a road structure and contribute most to its bearing capacity. Like any granular matter, aggregates can behave either as a fluid or as a solid, depending on their confinement and loading conditions [2]. The transition from fluid- to solid-like state of a granular material is called jamming. In road engineering, this state is reached through compaction by applying external forces and vibration to the quasi-confined pavement material, until a target bulk density is reached. In this situation, interlocking between the aggregates is usually optimum, thus increasing the yield stress of the in-service jammed material [3]. This optimum mainly depends on the applied compaction regime and energy, layer thickness, the type and granulometry of the aggregates. In addition, also the amount and viscosity of a possible “lubricant” (such as water or bituminous binder) influences the compaction process. In particular, the lubricant reduces the energy consumption for jamming [4]. In the case of hot mix asphalt, the same hot binder that serves as lubricant during the jamming process holds the aggregates together once the temperature drops and in-service loads coming from the traffic (resulting in a complex combination of tension and shear loads) attempt to pull them apart.

Instead, the bearing capacity of unbound layers relies not only on the intrinsic material properties like cohesion and internal friction angle but also on its stress state, which depends on the external forces applied and on its degree of confinement. Particularly, coarse granular materials with no cohesive properties tend to form force chains through the aggregate's contact points along the loading direction. In this situation, the material is able to support increasing loads and behave as a rigid body, as long as the contact forces among the aggregates are below their mechanical threshold (aggregates grinding) and also if the applied stress does not change in direction [5] [6]. Due to this behavior, this type of granular systems is often referred as fragile matter. Confinement in pavement structures might be insufficient to reach an optimum densification after compaction and to maintain the material jammed over time. This is because roads do not have longitudinal boundaries and the lateral boundaries (if any) are relatively far from each other, considering the aggregates' size and the magnitude of the loads. In numerical simulations, the lack of confinement in the horizontal plane may be simulated by applying periodic boundary conditions in both horizontal directions. Further, the confinement in the vertical direction is also limited. In fact, the bottom layers in a road usually have low bearing capacity and relatively high deformability. On the other hand, the surface, if not covered with a bounded layer, is totally unconfined and susceptible to loads that can unjam the material.

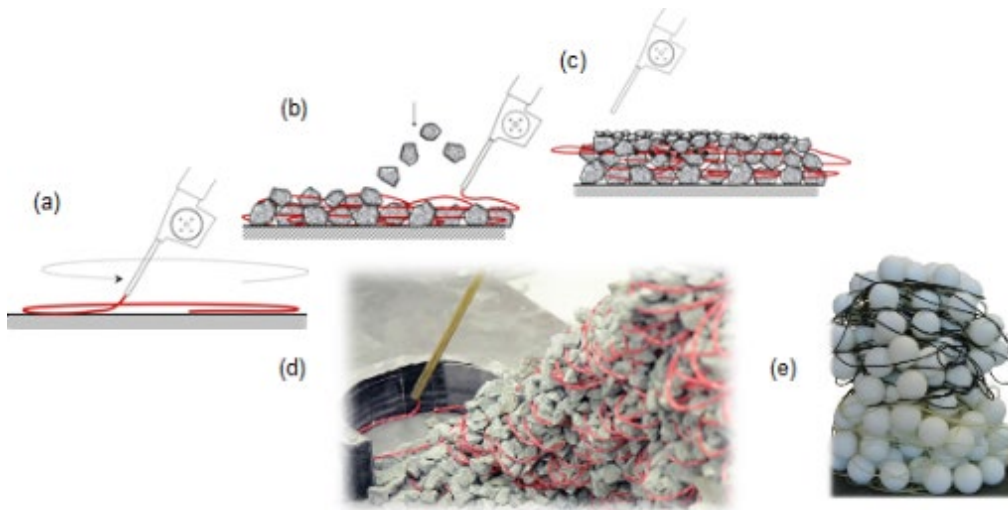
In building construction, reinforced cement concrete structures are designed using a concrete mixture (made of aggregates, cement, water and additives) and steel reinforcement bars. During the construction of a structure, fluid concrete is poured into molds in which the rebars for reinforcement are previously positioned. The main function of the steel reinforcement is to take in-service internal tensile and shear stresses. In contrast, in pavement engineering, the concept of reinforcement is usually related to the use of commercial 2D grids, meshes or felts between either bound or unbound layers or soils in the subgrade (commonly referred as geogrids, reinforcement grids or geomembranes). Their primary use is to enhance the structural performance of roads. From the mechanical point of view, these elements work only in tension, mainly when the structure deforms under load thanks to the so-called membrane effect [7] [8]. Further, they improve the bearing capacity by changing the potential failure surface and they provide lateral restraint to the aggregates thanks to interlocking with the grid aperture and frictional/shear forces [9]. Hence, these 2D reinforcements are mainly designed for broadening the vertical load distribution angle and refine the crack distribution/bridging in the pavement structure [10]. On the other hand, their main disadvantages is that they can be placed only between the pavement's layers and may therefore disturb the interface adhesion. Another disadvantage is that they are hardly in the best vertical position within a layer for activating optimal lateral confinement. Finally, 2D reinforcement grids are also

difficult to remove and to recycle when the pavement needs to be renovated. Because of these disadvantages, traditional construction processes do not include reinforcement meshes during the construction of the pavement, mainly for economic and interlayer bonding reasons. This raises the following questions: what would happen if pavements could hold 3D reinforcements to take complex and changing tensile stresses induced by traffic or due to thermal fluctuations? Could such an approach lead to thinner and therefore more economical and sustainable pavement structures?

## 1.1 State of the art

The past decade has seen a shift from traditional manual construction towards flexible robotic fabrication, 3D printing, and the exploration of novel additive manufacturing processes [11]. This has led to the development of highly versatile and customizable construction systems and the realization of architectural case studies and prototypical structures [12]. Through the seamless integration of design and fabrication, digital fabrication offers the efficient use of production resources, material-specific concepts and durability. This new approach was also promoted with a SNF National Centre of Competence in Research (NCCR) "Digital Fabrication – Innovative Building Processes in Architecture" that was initiated by Gramazio Kohler Research in 2014 (<http://www.snf.ch/en/researchinFocus/nccr/digital-fabrication/Pages/default.aspx9>).

Especially notable is in this context the project "Design and Robotic Fabrication of Jammed Architectural Structures" (2015-2019), funded by an ETH research grant. Partners were Gramazio Kohler Research (ETH) and the Institute for Building Materials (ETH) with the support of the Self-Assembly Lab of the Massachusetts Institute of Technology (MIT). In this and other connected projects, the potential of an innovative type of construction that combines loose aggregates with continuous reinforcement have been explored. Different publications [13] [14], [15] [16], showed that slender objects like a thread or a wire, carefully placed within the aggregates' packing in a layer-wise manner and following certain patterns can induce and improve jamming to create new types of loadbearing structures. In [13], a robot manipulates the dry granular bulk material, while another one positions elements able to take up tensile stresses such that forces are integrally transferred into the depth of the structure in 3D. As a result, it is possible to create structures with different types of granular aggregates (see Abb. 1 ) that are able to carry loads. Most importantly, these structures are fully reversible and recyclable, i.e. the component materials can be fully recovered without chemical or energy-intensive processes, which is in line with sustainability expectations.



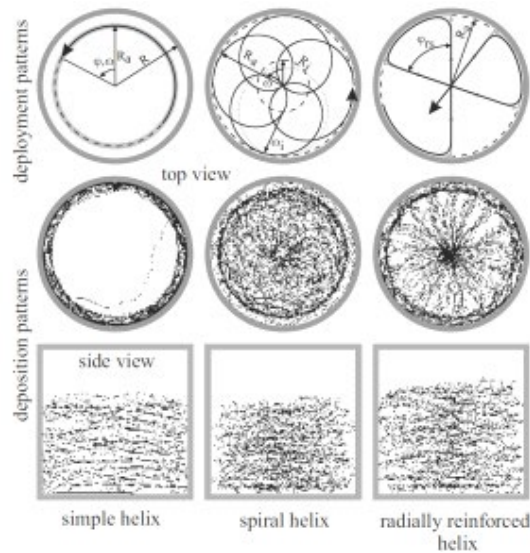
**Abb. 1** construction of a structure made of aggregates and a string reinforcement, no binder: (a) String-extruding robot places a reinforcement filament according to a digital blueprint (b) crushed aggregates are placed on top and (c) repetition of steps (a) and (b). (d) Example of a stone wall (from [13]) and (e) a tennis ball column (from [17]) built with this method.

One exciting aspect of this research has been the introduction of robotic methods for the construction with granular materials. The powerful possibilities emerging from the use of industrial robotic manipulators are at the core of this work, as well in the deployment of the different materials and reinforcements used, as shown in Abb. 2.

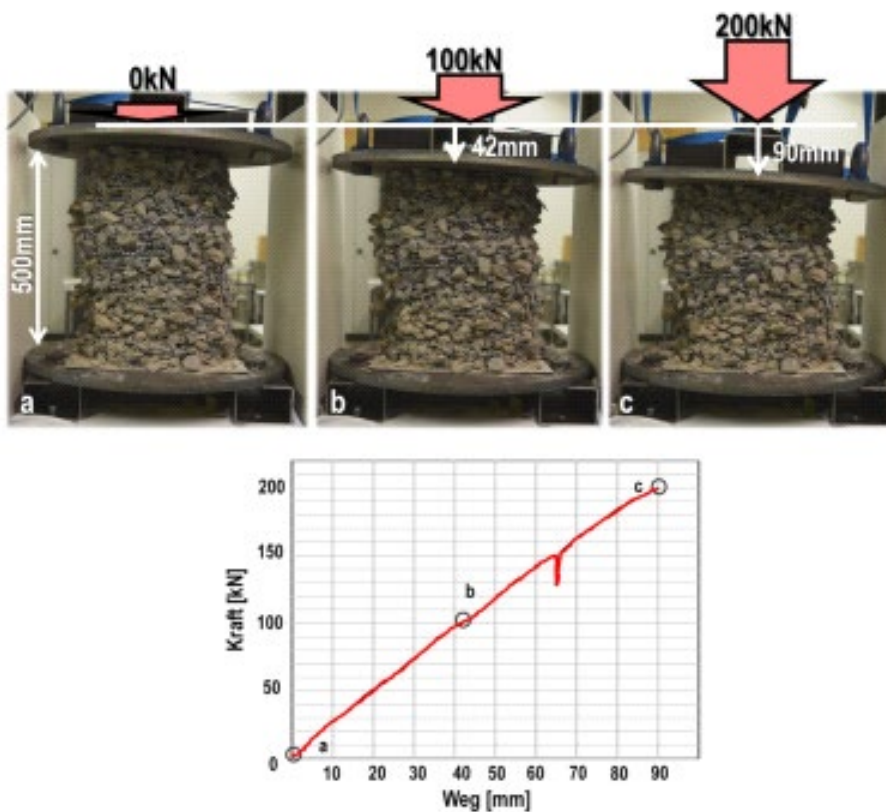


**Abb. 2** compression tests of a wide range of jammed material systems and reinforcements (from [13]).

The ETH research project focused on using irregularly shaped rocks or gravel to build columns or walls, i.e. on readily available types of granular matter for building structural parts. However, instead of employing external confinement to hold aggregates together (like pre-fabricated gabions), confinement is achieved by adding in situ different internal reinforcements following pre-defined patterns (Abb. 3). Thin, flexible strings deployed while building up the aggregates proved to be the strongest combination under compression tests, as shown Abb. 4. For example, a striking result was that a freestanding vertical column of stones reinforced with cotton strings was able to withstand an axial load of up to 200kN.



**Abb. 3** the first row shows schematics of different deployment patterns for a cylindrical specimen: simple helix, spiral helix and radially reinforced helix (from [2]). Below, the top and side views of the final deposition patterns.



**Abb. 4** compression test on 500mm aggregate column (no binder) reinforced with strings. According to the load-displacement diagram, the structure is able to carry 200kN; the displacement at this load level reaches 90mm (Image credit: Gramazio Kohler Research, ETH Zurich, 2017).

In order to build these so-called "Jammed Architectural Structures (JAS)", it is necessary to use a robotic arm capable to deploy the strings following a precise pattern though a digital blueprint. The construction can be fully automatized using the same robotic arm to pour and compact the aggregates additively, making it a promising digital robotic fabrication technology. Several vertical structural elements were built in the laboratory with this

technique, including columns and walls, all of them without the need of a formwork. Based on this concept, an architectural installation was built for the inaugural Chicago Architecture Biennial 2015, called Rock Print [14] (<https://vimeo.com/141097712>). An actual building in the Swiss city of Winterthur was also built with this method, an outdoor pavilion composed by 11 pillars supporting an 8.7 t steel roof. This temporary structure was built in real-world construction conditions and exposed to weathering for 6 weeks until it was dismantled (<https://ethz.ch/de/news-und-veranstaltungen/eth-news/news/2018/09/rock-print-pavilion.html>). Afterwards, the components of the pavilion were easily recycled, just by pulling the string out. By doing this, the aggregates unjammed and separated without the use of labour- or energy-intensive recycling methods [15].

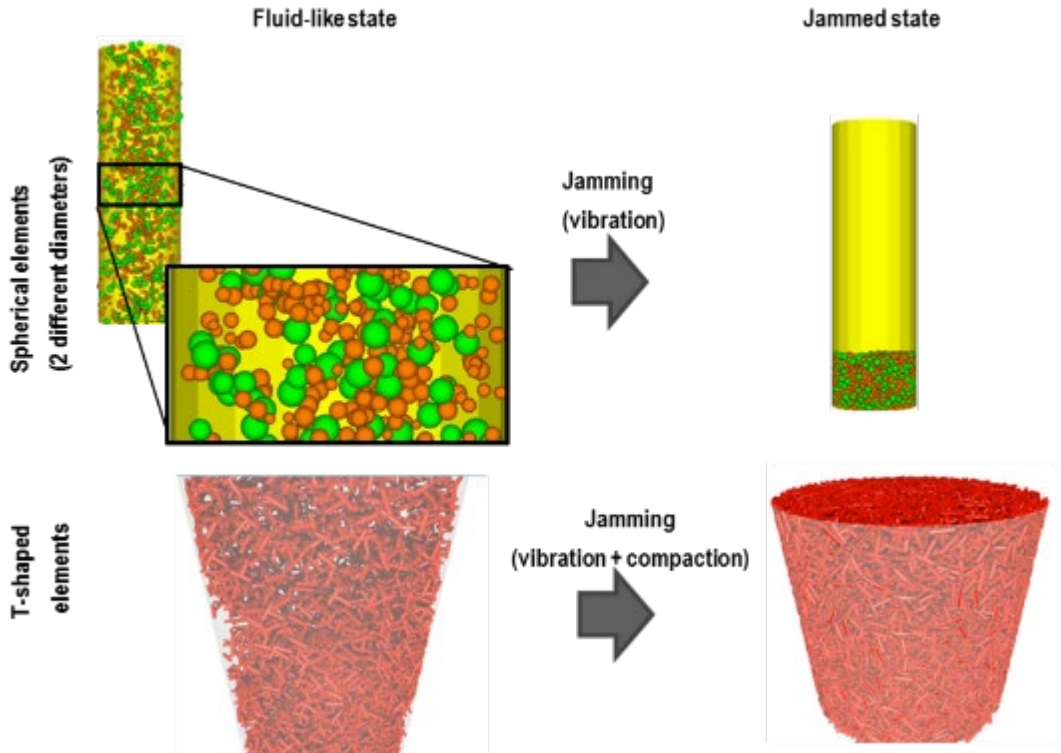
Fundamental understanding of the underlying mechanisms of load resistance of these structures was also obtained through numerical models [18] [19] [2]. In a PhD thesis completely dedicated to modeling [2], a grain-scale numerical model incorporating rigid irregular polyhedral particles and an elastic soft wire was developed to simulate wire-reinforced granular materials. Different analyses have shown the importance of the string's pattern and stiffness, the particles size distribution and friction coefficients and the system size among others, on the stability of reinforced granular columns. The results showed a narrow distribution for the elongation of the wire, and a localization of force chains towards the center of the columns at high loads, shedding light on the confining and load redistribution mechanisms of the reinforcement. The numerical model developed in [2] also incorporated particle breaking, to take into account the observed fracturing of individual grains. This allowed to simulate both the crushing of a single particle between two plates and the crushing of a confined packing at large displacements, taking into account also the shape of the particles.

The SNF-funded PhD project “High Performance Aggregates for Sustainable Road Pavements” 2015-2022 [<http://p3.snf.ch/project-15712215>] focused on the use of artificial engineered aggregates (Abb. 5) to improve asphalt concrete performance [20]. Instead of enhancing the characteristics of the binder, this work concentrated on improving the aggregates, which account for ca. 95% by mass of the asphalt concrete mixture. In particular, it addressed the question whether artificial aggregates could be designed with specific shapes to improve the properties of pavements. This investigation considered unbound materials only, whereas a subsequent future project may evaluate the effect of binder addition. The Discrete Element Method (DEM) was used to simulate the jamming/compaction process of various aggregate's shapes and materials (Abb. 6). The numerical investigation revealed that the stress distribution within the aggregates' packing became more heterogeneous as the aggregate sphericity decreased, with some aggregates being subjected to eight times the average stress. Consequently, the material for the manufacturing of such non-convex artificial aggregates needs to be chosen such that the aggregates can withstand such high stresses. 3D printing was then used for rapid prototyping of different aggregates designs (made of a ceramic material, alumina) that proved to provide the best interlocking in the DEM simulations. Packings of these 3D printed aggregates were also studied in depth concerning their porosity, tortuosity and permeability [21]. In addition, specimens prepared with these aggregates were tested in the laboratory to evaluate their mechanical performance and their permeability. The consortium of laboratories participating in this project involved the Laboratory of Road Engineering/Sealing Components (from 2020, Concrete and Asphalt Laboratory) and the Laboratory for High Performance Ceramics from the Empa side, and the Laboratory of Energy Science and Engineering (Institute of Energy Technology) from the ETH side.



Tetrapods	Dolosse	Tetrahedra
$\psi = 0.87$ $\Omega = 0.86$	$\psi = 0.85$ $\Omega = 0.86$	$\psi = 0.97$ $\Omega = 1$
$\psi = 0.67$ $\Omega = 0.47$	$\psi = 0.73$ $\Omega = 0.65$	$\psi = 0.74$ $\Omega = 0.93$
$\psi = 0.53$ $\Omega = 0.19$	$\psi = 0.55$ $\Omega = 0.28$	$\psi = 0.43$ $\Omega = 0.40$

**Abb. 5** different artificial aggregate types and aggregate sphericities investigated numerically in [21]. The tetrapods (in particular those shown left and below in the figure) were also investigated experimentally, with packing and permeability experiments being performed. The tetrahedra shown below to the right were manufactured with 3D printing out of alumina.



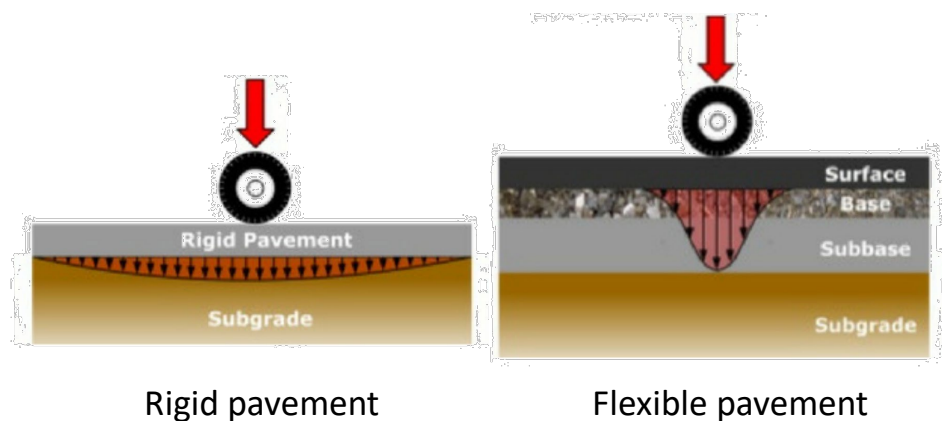
**Abb. 6** simulation of jamming processes for two types of ideal aggregates, using DEM (Image credit: Nicholas Conzelmann, PhD Student, Empa/ETH).



## 2 Objectives of the research

With this work, we intend to introduce the concept of JAS to the road engineering landscape, specifically for developing a unique type of reinforcement for pavements. Instead of vertical structures prepared to withstand mainly quasi-static loads, we intend to use the concept of continuous string reinforcement in the unbound layers of pavements, which have primarily the function of taking repetitive transient vertical traffic loads from the surface and distribute them to a broader underlying area without deforming excessively.

Abb. 7, left, shows a rigid pavement, which redistributes the traffic load to the subgrade without the need of intermediate layers. This is how e.g. a concrete pavement would work. On the contrary, in a flexible pavement (Abb. 7, right), the surface layer (typically made of asphalt) deforms more locally and more substantially under the tire. With flexible pavements, base and subbase layers contribute to the distribution of the traffic loads to the subgrade. Introducing string reinforcement according to the JAS concept into the unbound subbase layer would enhance its load carrying capacity and the capacity of redistributing the loads. As a consequence, the whole thickness of the pavement, and in particular the thickness of the surface layer, could be reduced and thereby material could be spared.



**Abb. 7** schematic representation of rigid pavement (left) and of flexible pavement (right) including their different layers and how loads from tires are redistributed from the surface to the lower layers and to the subgrade (Image credit: <https://pavementinteractive.org/>).

A number of other advantages that could be obtained by employing string reinforcement in the unbound layers are:

- Reinforcement of the unbound layer would allow to extend the service life of the asphalt concrete (the surface layer) under fatigue. This is achieved mainly by limiting the deformations of the surface layer exposed to cyclic loads from the traffic;
- Another main advantage of such an approach over traditional methods (e.g. over reinforcement grids and over using a binder also in the subbase) would be that in case of removing a temporary road/street/parking lot, the strings could be easily extracted from the no longer used pavement. This would allow easy and precise recycling. In fact, the remaining unbound aggregates could be recovered and reused with a minimum of effort, thus fulfilling sustainability requirements in an almost perfect way;
- Pavements constructed with this novel approach would also need less compaction energy. By depositing aggregates and reinforcement stepwise, there will be full aggregate-aggregate contact and no need for skeleton rearrangement. Segregation and damage of the aggregates would decrease and producing savings in compaction energy;
- Further, with this concept, a layer with the same mechanical performance but with increased porosity and less clogging could be achieved, which could be an advantage

- e.g. for water storage in permeable pavements for mild/ hot climates where no freezing is expected;
- Similarly and although it falls outside the scope of this research, the proof of concept presented here could be also used for railway ballast reinforcement.

Placing reinforcement strings can be performed through automatic devices and even in 3D string arrangements. The movement of the robot performing this task resembles the movements of a knitting needle. Reinforcement strings can be placed over the whole pavement width or just locally, e.g. to confine the weaker border zones or embankments or the zones directly underneath the wheelpath, where stresses are highest. Using a robot to place the strings is more precise than in case of manual placement and spares a large amount of labor. Changes in the patterns of the strings can be easily implemented by adapting the software that controls the robot, without any need of training of the workers. Potentially, a large part of pavement construction could be fully automatized, with lower costs and increased quality.

Following the motivation described above, this report summarizes the efforts to use and adapt the existing knowledge about JAS into horizontal structures, with the objective to investigate their behavior under cyclic dynamic repetitive loads considering multiple variables. To that end, box-specimens were prepared with the help of a robotic arm using different types of aggregates, strings and patterns. The specimens were tested in a cyclic compression setup to evaluate their deformation and performance with the accumulation of loading cycles. In the case of unbound layers, the deformation response is usually characterized by a recoverable (resilient) and a residual (permanent) deformation. This plastic deformation accumulates with loading and is typically high during the initial cycles, tending to decrease with the densification and jamming of the material. This behavior, and in particular the advantages of string reinforcement in limiting the deformation, was confirmed by numerical modelling with the discrete element method.

The hypothesis that motivated this work is that string reinforcement deployed through a robotic arm can improve the jamming of the aggregates and can help taking dynamic vertical repetitive loading, increasing the area onto which the stress is distributed and reducing the permanent deformation (rutting). This working hypothesis was confirmed by both the experimental and numerical results obtained in this project. At the same time, the practical implementation of this novel reinforcement concept meets a number of difficulties, some of which became evident during this project. In order to differentiate them from the JAS, these structures will be denoted in this report as continuous string reinforced pavement layers.

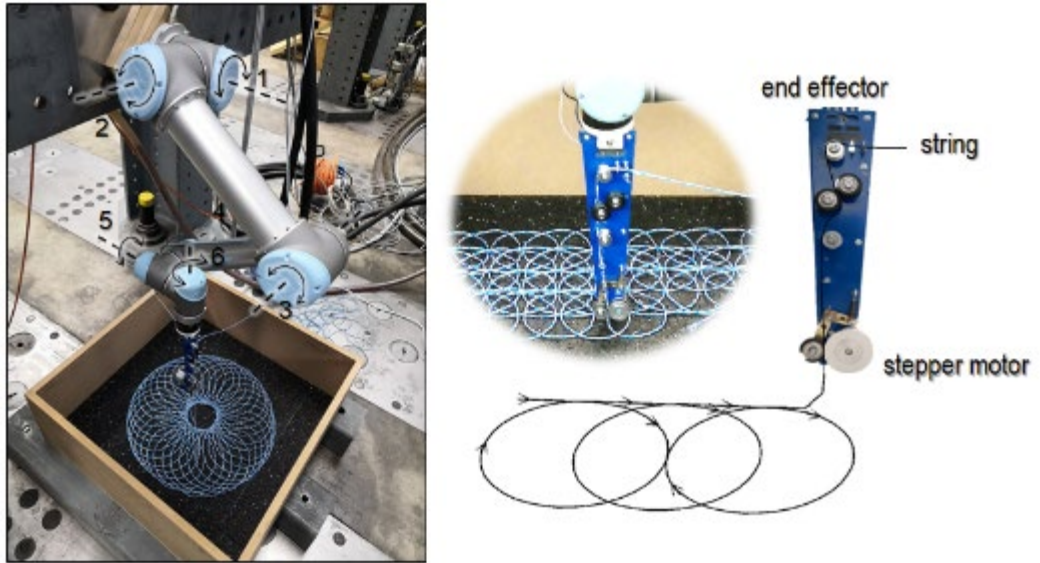
## 3 Experimental plan

### 3.1 Overview

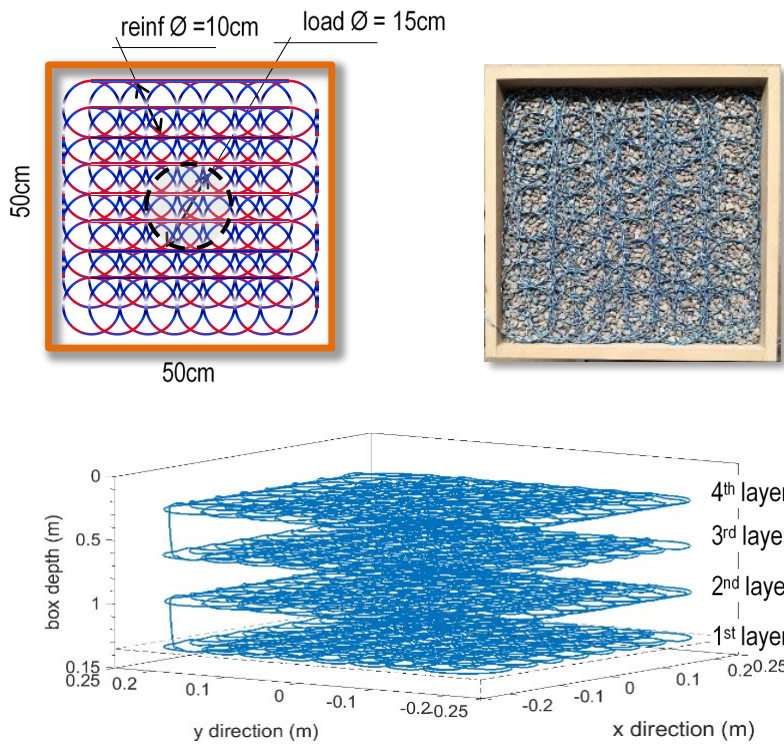
As mentioned in the previous section, continued string reinforced specimens were prepared within wood boxes with a soft, 1.5 cm-thick recycling rubber mat at the bottom, to allow limited elastic deformation under load. This configuration simulates a weak subgrade. The size of the boxes was selected to be as large as possible to minimize the confining effect of the rigid lateral walls, while at the same time being small enough to fit in the testing setups. Therefore, two sizes of boxes were used:  $50 \times 50 \times 15 \text{ cm}^3$  (small boxes) and  $70 \times 70 \times 25 \text{ cm}^3$  (big boxes). The small boxes were designed to fit inside a temperature chamber, whereas the big ones were tested in an open setup without any temperature regulation. The placement of the specimens in a temperature chamber was initially thought to be important for the initial targets of this project, since it would allow to impose also temperature cycles in addition to load cycles to the aggregate packing. However, in the course of the project, this idea was abandoned as the effect of temperature cycles on the deformation was found to be of secondary importance compared to different types of loads and reinforcement patterns. Consequently, most of the experiments explained in the following were performed on the larger specimens, without any temperature regulation. The larger specimens are closer to the field conditions in pavements and allow more freedom in the placement of the string pattern.

The specimens were made mainly using washed aggregates of narrow size distribution typically used for road or concrete construction. The selection of the aggregates was based on the fact that clean, coarse aggregates with a narrow size distribution would provide the maximum porosity with minimum contact points between the aggregates. Further, no cohesion or lubricating effect of fines would influence the jamming, providing result where jamming is mainly depending on the aggregate interlocking, the compaction grade and the type of reinforcement. By choosing narrow aggregate's size distributions by the selection of aggregates between two consecutive sieves, we also wanted to reduce the amount of variables to consider in the data analysis. For similar reasons, the specimens were prepared without surcharge, i.e. without a weight on the surface simulating an upper bound layer. As shown in a previous work on geosynthetics [7], surcharge provides confinement to the aggregates, affecting the reinforcement effect under study.

A robotic arm with 6 degrees of freedom was used to deposit the string (see Abb. 8). An end effector with a stepper motor was responsible to pull the string following predefined patterns in successive layers, as shown in Abb. 9. The specimens were prepared adding consecutive layers of strings and aggregates followed by a manual densification using an earth rammer. To achieve consistently homogeneous samples, equal amounts of aggregates were used in each of the layers, i.e. the mass of the aggregates was previously defined and the amount in each layer was calculated by dividing the total mass by the number of layers in each specimen. For the big box samples, the final compaction was carried out with a sinusoidal load of 3 kN distributed over the entire area of the specimen using a hydraulic actuator at 20 Hz, until the recorded permanent deformation reached a plateau. The uniaxial cyclic compression tests were then carried out with different load types, maximum and minimum values and frequencies using the same setup, as described in section 3.3. The entire preparation and testing procedure is shown in Abb. 10.



**Abb. 8** left: view of the robotic arm (with its 6 degrees of freedom indicated by numbers 1 to 6). Right: view of the end effector for string deployment.



**Abb. 9** example of a 2D reinforcement: schema seen from the top (left), top view of the actual sample (center) and 3D representation of the string deposition (right) of a small box specimen, reinforced using a 10 cm circular pattern and half diameter overlap in 4 layers.





**Abb. 10** specimen preparation: a) deployment of the first string reinforcement layer with a robotic arm, b) addition of first aggregate layer, c) densification of individual layers, d) deployment of consecutive reinforcement and aggregate layers e) final compaction and d) cycling loading setup.

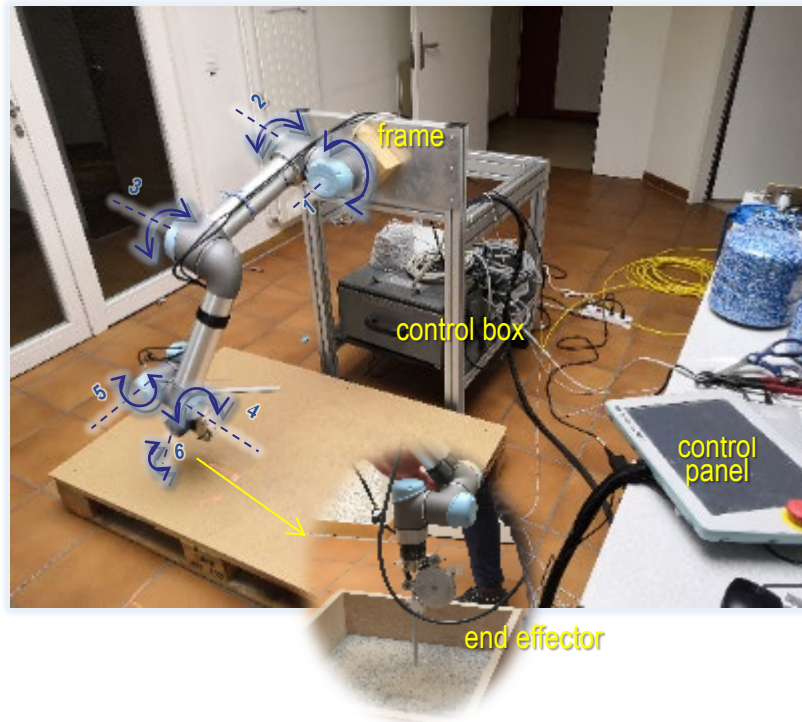
Part of the original testing plan was to evaluate the specimens' performance under repetitive traffic loading in the laboratory using rolling tires. Due to the enormous effort required to perform the cyclic compression tests described below, this was not achieved within this project and left for future follow-up projects. Similarly, interesting factors the influence of water, the effect of a different aggregates distributions or how a surface surcharge affects the performance of the specimens were also not included in this work.

## 3.2 Materials and setup

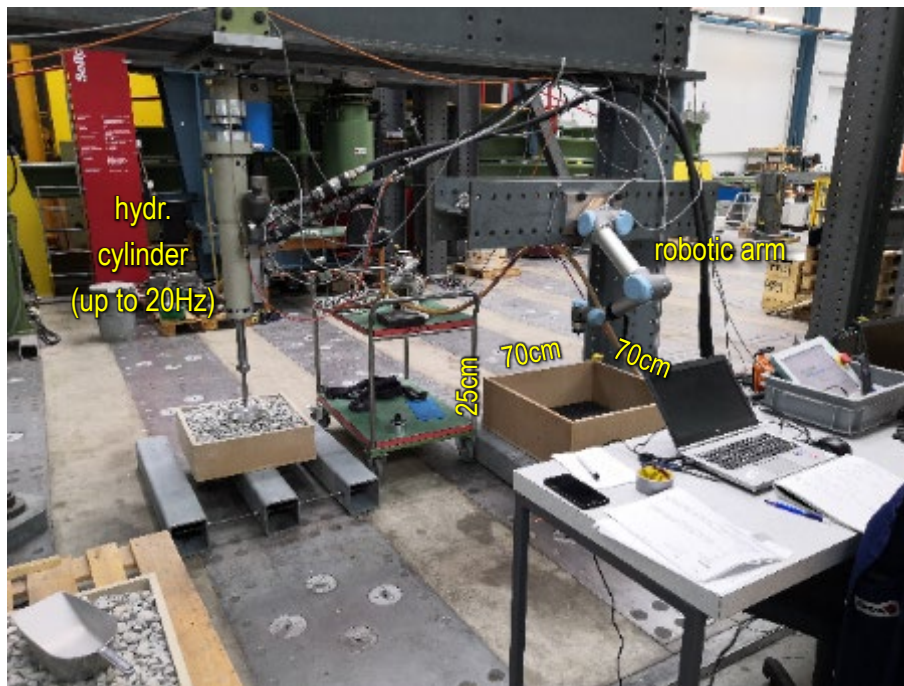
### 3.2.1 Robotic arm

To deploy the strings inside the box specimens we used two collaborative robot arms from Universal Robots, so the procedure could be carried out precisely and automatized. For the small boxes, we used the robotic arm model UR5 and for the big boxes, the UR10 lent from ETH Zurich. The arms of the two robots have a maximum payload of 5 kg and 12.5 kg and a maximum reach of 0.85 m and 1.3 m, respectively. Both robotic arms have 6 degrees of freedom, i.e. the different members of the arm can rotate around 6 axes. For this application, the payload limit did not represent a challenge, because the strings are relatively lightweight, even when an entire string roll is mounted at the end of the arm. Instead, the area that the arm can reach was an important feature to consider as, for example, building the big box specimens with the UR5 was at the limit of its capabilities – thus the UR10 was employed instead.

We mounted the robotic arms on stable rigid frames, so the movements of the arm were fixed relatively to the base. The frame for the UR5 is shown in Abb. 11 and the frame for UR10 is shown in Abb. 12. In this way, the spatial location of the end effector, which is the tool that pulls and deposit the string, can precisely follow the predetermined reinforcement pattern according to a digital blueprint. We designed the blueprints of the string patterns with the software Rihnos and a Grasshoppers/Python plugin.



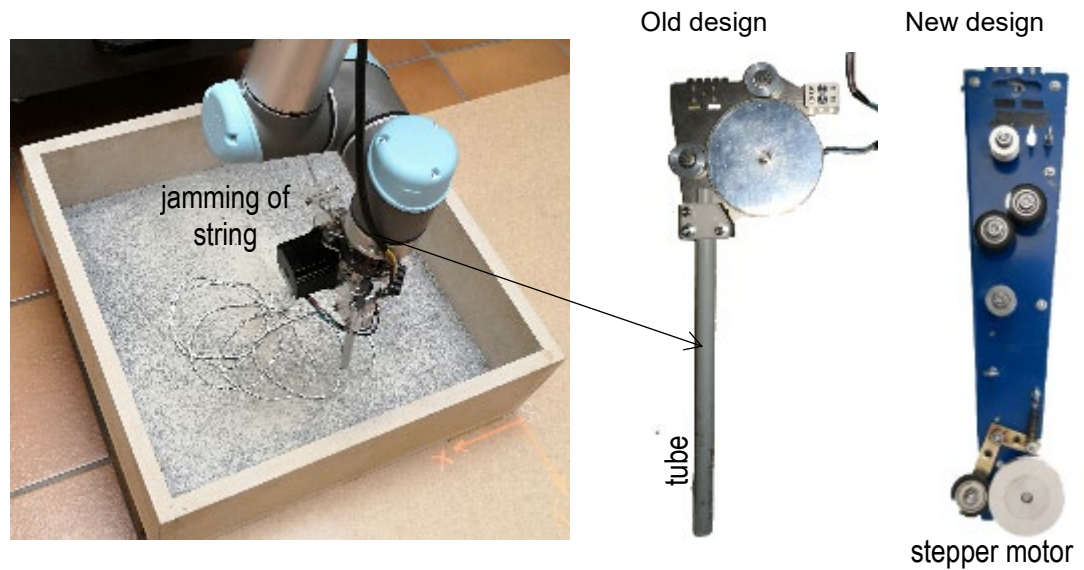
**Abb. 11** view of the robotic arm model UR5, mounted on an aluminum frame. Note the position of the 6 degrees of freedom and the location of the end effector.



**Abb. 12** view of the robotic arm UR10 mounted on the testing setup for big boxes.

It must be pointed out that the original/old design of the end-effector by our ETH collaborator proved to have problems while deploying the string. Initial trials showed the string was jamming at the inlet of the positioning tube. Despite using many different approaches, including changing the tube's inlet size and shape as well as blowing compressed air through the tube to push the string, the problem could not be solved. Therefore, the only remaining option for us was to completely redesign the end-effector and remove the tube entirely. After designing different prototypes, the final setup, shown in the Abb. 13, used a small stepper motor to pull a string through a system of pulleys and springs to a location as close as possible to the final deposition. The string was controlled using Arduino, so it is turning on and off and the speed of the motor matched perfectly with the speed of the moving arm. This is an important aspect when precise patterns need to be realized. Videos showing the performance of the new end-effector is available for downloading in File 1 of the repository available at <https://doi.org/10.5281/zenodo.7786624>.





**Abb. 13** example of the string jamming problem with the old design and view of the new design.

Another attempt to improve the string deployment was to replace the robotic arms though a self-made XYZ rail setup, similar to Cartesian 3D printers. The proposed system consisted of 3 beams with stepper motors and threaded rods to control the position of the end effector. (Abb. 14). We used Arduino and self-made electronics to control the setup. By simplifying the movements of the arm from 6 degrees of freedom to only 3, we expected to have a more efficient and cheap device for our purposes. Although the system proved to work, the incorrect selection of the pieces (due to budget constrains) resulted in an apparatus that was noisy and slower than expected, so the use of the setup was discarded (for a video of the device working, the reader can download File 2 of the repository at <https://doi.org/10.5281/zenodo.7786624>). Nevertheless, this information was included into this report because we believe that a design based on this concept might be useful in future applications.





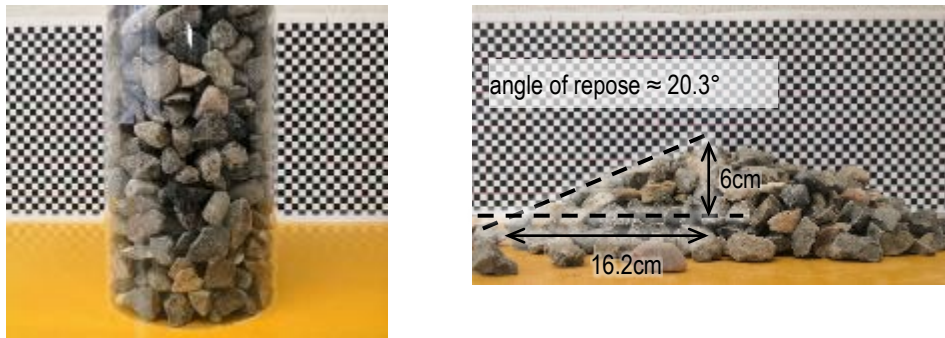
**Abb. 14** view of the beams used to build a self-made Cartesian 3D printer, including the electronics and final setup.

### 3.2.2 Aggregates

The aggregates used to prepare the specimens were selected among typical aggregates that are usually employed in asphalt or concrete mixtures. On one hand, hard rubble with angular shape and good interlocking, typically used in road construction, was the first natural choice. Giving the box sizes and the thickness of the specimens, two fractions corresponding to standardized sieves were selected: 8 mm - 11.2 mm and 16 mm - 22.4 mm. For the sake of simplicity, they are referred in this report as 8-11 and 16-22 *angular* aggregates. On the other hand, rounded aggregates (alluvial gravel, of the type employed in concrete mixtures) with the same sizes were also used and in this report they are denoted as 8-11 and 16-22 *round*. As mentioned in previous sections, the aggregates were washed and dried in the oven to eliminate dust that could affect the internal friction of the jammed aggregates.

In order to obtain a seed value for the DEM simulations (see § 4.3.2), we characterized the interaction between aggregates using the angle of repose, which is a quick way to establish the flowability and interlocking of granular materials. To that end, we filled a plexiglas cylinder with 16-22 angular aggregates (see Abb. 15 left). Then, we removed the cylinder containing the aggregates, and let them flow freely. As all granular media, the aggregates flow to form a heap. We calculated the angle of repose using the height and the radius of

the heap. For the angular aggregates 16-22 an angle of repose of  $20.3^\circ$  was obtained with this method.

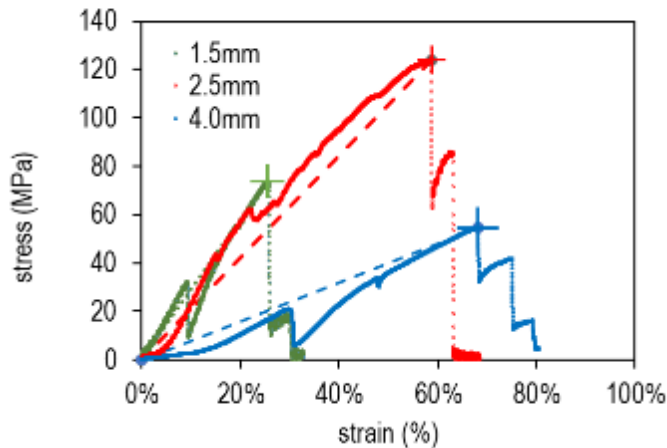


**Abb. 15** calculation of the angle of repose of the 16-22 aggregates

### 3.2.3 String

The selection of the reinforcement string was made based on previous work on JAS [16]. We fabricated all specimens using an eco-friendly, low-priced braided thread made of recycled synthetic and natural leftovers from the textile industry, mostly used for packing purposes. The diameters used in this study were mainly 2.5 mm, but selected specimens were also prepared with strings of thicknesses of 1.8 mm and 4 mm. These strings had the capability to form precise loops with diameters over 6 cm. Other attempts to use strings of jute, cotton or hemp failed. These natural fibers were found to be not suitable, because they were too stiff in bending compared with the synthetic fibers. Once the strings made of natural fibers were placed onto the aggregate packing, they moved and re-arranged due to their stiffness and internal tensions, which disrupted the reinforcement patterns.

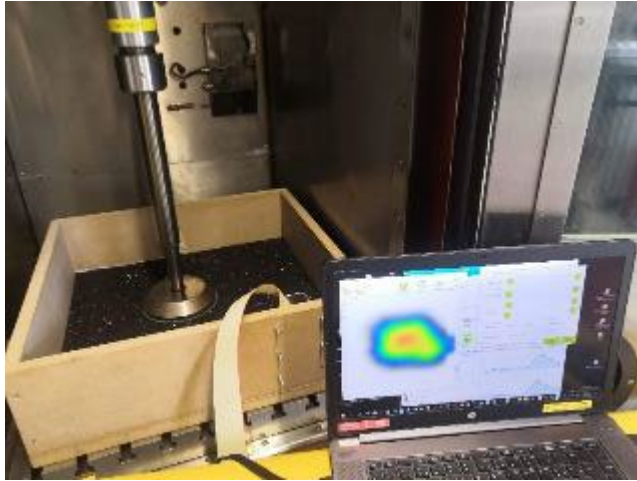
In order to characterize the mechanical performance of the string used in this research and used later as a seed value for the DEM simulations (see § 4.3.2), we obtained the stiffness modulus of the strings through displacement controlled tensile tests with a speed of 5mm/s. As shown Abb. 16, the modulus, calculated based on the inclination of the secant of the stress-strain curve at the initial and breaking points, are 290 MPa, 211 MPa and 80 MPa for the 1.5 mm, 2.5mm and 4.0 mm strings respectively. The stepped shape of the curves are a sign of rupture of individual fibers. In these types of strings, multiple single fibers twisted together into a braid, the distribution of loads is not even and individual fibers might take more load than others. Once one of these fibers breaks, there an internal rearrangement of the tensile forces occurs. Although all strings are supposedly made from the same material, thinner strings tend to take higher stresses and are less ductile than thicker strings. One hypothesis is that this might be a consequence of the so-called size effect, in which larger specimens tend to have lower strength because the probability of having (large) defects increases with the size of the specimen. Another possibility is that, since these strings are made from recycled fibers, the quality of the product is more prone to depend on the raw materials variability.



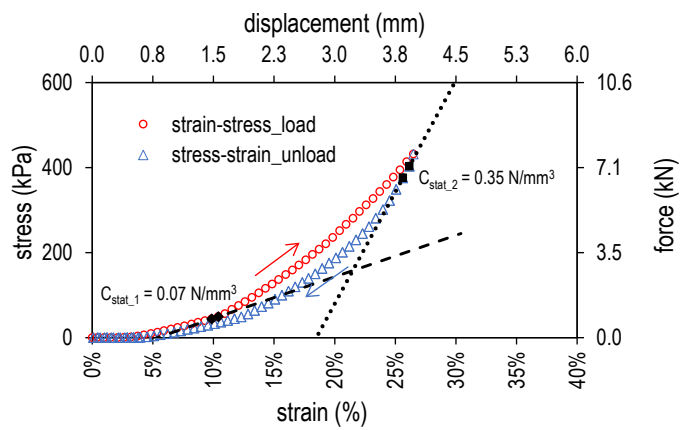
**Abb. 16** stress-strain curves for the 1.8mm, 2.5 mm and 4.0 mm diameter strings. The figure also shows the secant of the stress stress-strain curve at the tension of rupture, whose inclination is the stiffness modulus.

### 3.2.4 Rubber mat

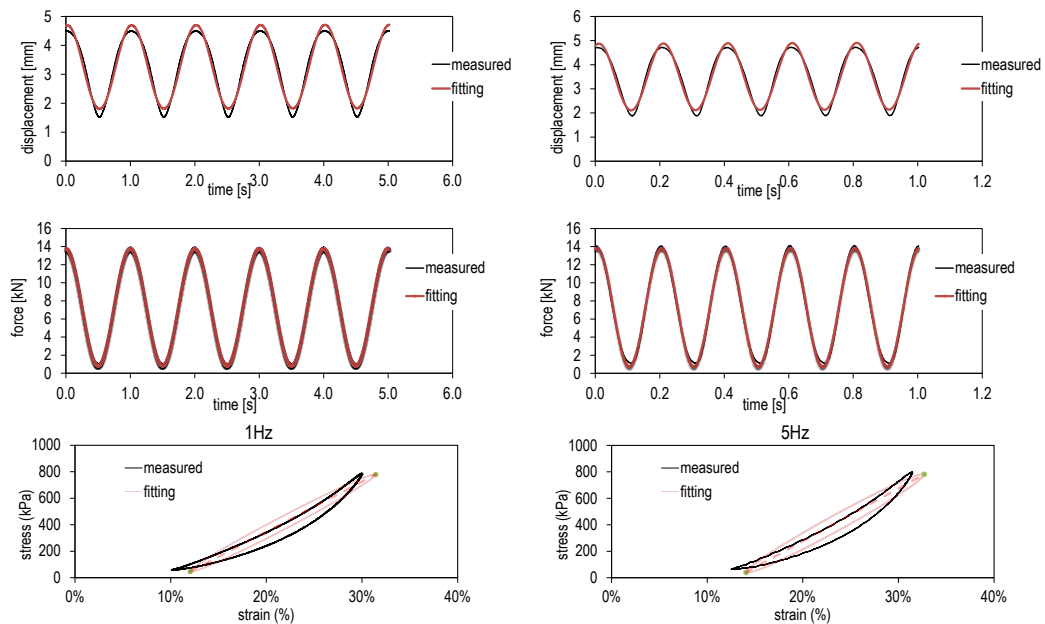
In order to allow some degree of vertical displacement under load, we used a rubber mat with a medium to soft stiffness at the bottom of the boxes, below the aggregates and string system. In order to quantify the mechanical parameters and use them later for the DEM modelling (see § 4.3.2), we measured the stiffness of the mat under static and dynamic loading. As shown in Abb. 17, the mat was placed inside the box and in the center, the loading plate with a diameter of 15 cm applied quasi-static as well as dynamic sinusoidal loads. In Abb. 18, the stress-strain curve resulting from the quasi-static loading shows a physical hardening of the system and a hysteresis loop, i.e. the loading and unloading curves do not match. Then, the value static stiffness  $C_{stat}$ , depends on the loading situation. For example, at one hand, at ca. 10% strain and in the loading segment of the stress-strain curve, the  $C_{stat}$  yields a value of  $0.07 \text{ N/mm}^3$ . On the other hand, at ca. 26% of deformation and in the unloading fragment of the stress-strain curve, the  $C_{stat}$  yields a value of  $0.35 \text{ N/mm}^3$  (see Abb. 18). The observed hardening likely comes from the increasing restraint in the plane perpendicular to the loading direction as the rubber mat is more and more compressed. Despite this observation and for simplicity, in the simulations the rubber mat was modelled with linear behavior. Nevertheless, we did use these experimental strain-stress curves as a calibration tool by comparing them with the simulated strain-stress curves, as shown later in § 4.3.2. Similarly, the dynamic modulus of the rubber mat at 1 Hz and 5 Hz is displayed in Abb. 19. A zero phase angle between load and displacement and the area of the hysteresis loop demonstrate the pure elastic nature and the damping capacity of the rubber mat used in the experimental setup. For the dynamic tests, the stiffness is usually obtained by fitting the last cycles of the measured data (in this case the last 5 loading cycles) with a sinusoidal function. Then, by means of this function is possible to calculate the dynamic modulus as the slope of the hysteresis curves. For our tests it corresponds to values of  $C_{dyn1(1Hz)} = 0.25 \text{ N/mm}^3$  and  $C_{dyn1(5Hz)} = 0.27 \text{ N/mm}^3$  at 1 Hz and 5 Hz respectively. As in the static tests, these values are different as what we could have obtained from the unfitted data. Therefore, we did again use the dynamic stress-strain curves to calibrate the simulation results (see § 4.3.2).



**Abb. 17** view of the rubber mat bedding stiffness measurements.



**Abb. 18** measurements of the static stiffness  $C_{stat}$ . Notice the hardening behavior and the hysteresis loop of the rubber mat. The static stiffness is calculated based on the tangent of the pressure-strain curve.



**Abb. 19** dynamic bedding modulus measurement at 1 Hz (left) and 5 Hz (right).

### 3.2.5 Setups to apply dynamic mechanical loads

Two setups were used to apply dynamic loads to the reinforced and unreinforced specimens. A hydraulic actuator with a maximum force rating of 100 kN, a piston stroke length of 40 cm and a loading frequency limited to approximately 2 Hz was used to test the small box specimens. Because of the limited space in this setup, a wider frame with more room for the manipulation of larger and heavier samples was constructed to test big box specimens. In this case, a 40 kN servo-hydraulic actuator with a piston stroke of 40 cm was used. In addition to these features, the maximum loading frequency of the actuator reached 50 Hz. With both setups, force-controlled loads were applied varying the type (sinusoidal or half-cycle sine), the frequency (between 1 Hz and 20 Hz) and the minimum and maximum values, as detailed in the next section. The load was applied through a plate with a diameter of 15 cm, representing an area of 176.7 cm<sup>2</sup>. The displacement and force of the hydraulic actuators were recorded with the built-in LVDTs and the force sensors of the devices.

## 3.3 Tests description

The approach used to systematically study the influence of different variables in the specimens reinforced by strings was to change variables one by one (both the configuration of the specimen itself and the type of load) and compare the permanent deformation among them and to a specimen without any reinforcement.

A large number of different configurations was realized and tested. Tab. 1 below shows all the different parameters that were varied in the experiments. In the table, the specimen ID is reported, for example SRC108. The first position in the ID indicates the size of the specimen: S for small (50×50×15 cm<sup>3</sup>) and B for big (70×70×25 cm<sup>3</sup>). The second position in the ID indicates the presence of the reinforcement: C for unreinforced and R for reinforced. The third position in the ID indicates the shape of the reinforcement: C for circular, R for rectangular and S for square. The numbers that follow these letters specify the geometry of the reinforcement and can be understood by reading the single entries in Tab. 1. More details about the different patterns used for the reinforcement are illustrated in Abb. 20 until Abb. 22, which show different types of circular and rectangular patterns (see detailed description below). For example, for circular patterns of string deployment,

the radius of the pattern is given in Tab. 1 together with the overlap between the circles (a positive value in the table) or the separation between them (a negative value in the table). For square patterns, the size of the square cell in the pattern is given. Tab. 1 also reports the number of reinforcement layers that were placed one above the other within the thickness of the specimen (4 for small specimens, 5 for big ones) as well as the thickness and the total length of the string in the specimen. Another column reports the size fraction of the aggregates and whether angular or rounded aggregates were used: angular aggregates in the size fraction 16-22 were used in most tests, smaller aggregates occasionally. In a few cases, rounded aggregates were employed only for comparison, considering that angular aggregates are dominant in road construction. The final column in Tab. 1 specifies the load cycles that were imposed onto the specimens: either sinusoidal or half-cycle sine loads, with frequency and maximum/minimum loads also specified.




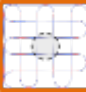
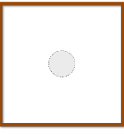

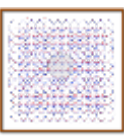
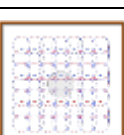
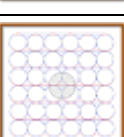
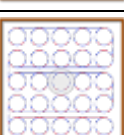

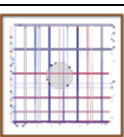
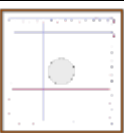

The different configurations of the string reinforcement in 2D are explained in detail in Abb. 20, Abb. 21 and Abb. 22. Abb. 20 shows the string patterns used in the smaller boxes (50×50 cm<sup>2</sup>), both circular and square patterns. Only a limited number of patterns were used in the small boxes. Abb. 21 and Abb. 22 show instead the patterns used for the big boxes (70×70 cm<sup>2</sup>). For the circular patterns shown in Abb. 21,  $D$  is the diameter of the circles, either 15, 10, 8 or 6 cm.  $OL$  is the overlap between the circles in the pattern, which is zero when the circles just touch each other, positive when there is an overlap between the circles, while  $OL$  becomes negative when the circles are detached (as in the pattern in the row above, in the middle). Abb. 22 shows instead the square patterns, in which  $GO$  is the size of the unit in the square patterns.  $GO$  4 cm and 2 cm are shown in the figure, which are the approximate (rounded to cm) sizes of the squares.

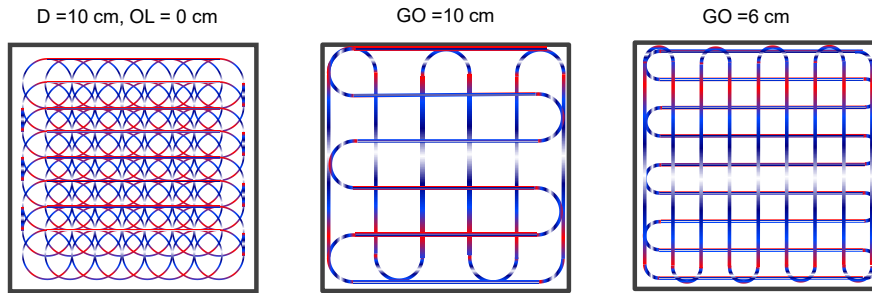
Due to the intensive labor required to prepare and test each sample, the repeatability of the test results was initially verified by running 3 repetitions on both reinforced and unreinforced samples in one single reinforcement configuration, but testing both aggregate sizes 8-11 and 16-22. In the main sequence of tests, experiments with a given configuration or type of load were repeated occasionally. While not all tests could be repeated, the large number of configurations tested (see Tab. 1) and the knowledge of the repeatability in some given configurations allows to reach solid conclusions.

From the large amounts of configurations tested, comparisons were made between specimens among which single parameters were varied. Selected comparisons are plotted in Abb. 23 to Abb. 33 and explained in detail in the following paragraphs.

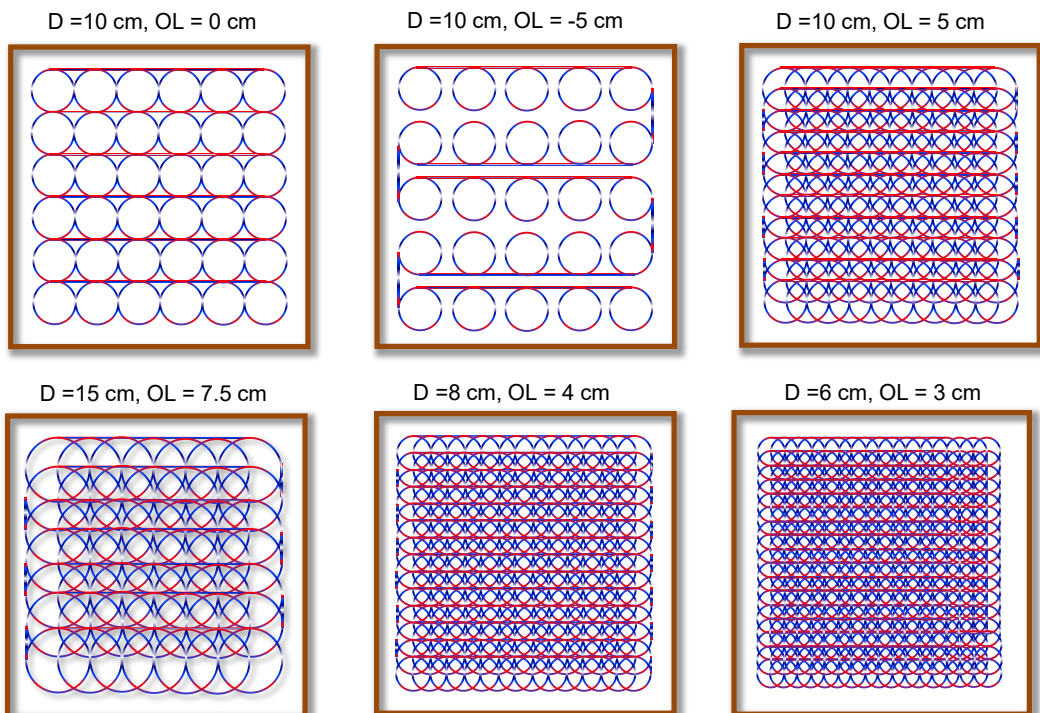


**Tab. 1** summary of the uniaxial cyclic loading tests

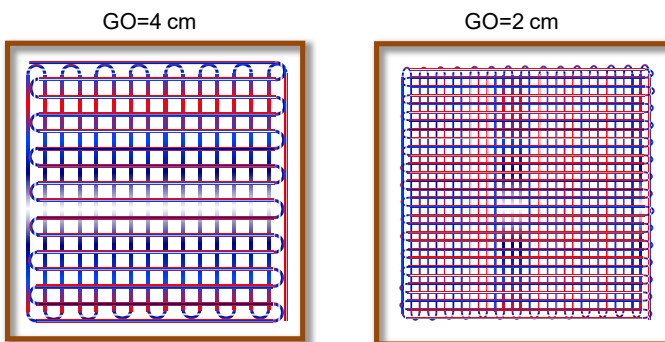
boxsize (cm)	ID	specimen	pattern type	no. layer	string length / thickness	aggregates	load
50 x 50x 15	SC		-(control)	-	-	8-11 & 16-22 round	sinusoidal 1 Hz, 2-8 kN
	SRC108		circular, Ø: 10 cm overlap 5 cm reinf/side 8	4	80 m / 2.4 mm	8-11 & 16-22 round	sinusoidal 1 Hz, 2-8 kN
	SRS69		square, opening: 6 cm reinf/side 9	4	40 m / 2.4 mm	16-22 angular	sinusoidal 1 Hz, 2-8 kN
	SRS106		square, opening 10 cm reinf/side: 6	4	26 m / 2.4 mm	16-22 angular	sinusoidal 1 Hz, 2-8 kN
70 x 70 x 25	BC		-(control)	-	-	8-11 & 16-22 angular	half-cycle sine 1, 5, 10, 20 Hz 0.5-3.5/6.5/9.5 kN 3.5/5.0-9.5 kN
	BRC8_14		circular, Ø: 8 cm overlap: 4 cm circl/side: 14	5	246 m / 2.4 mm	16-22 angular	half-cycle sine 20 Hz
	BRC10_11_5		circular, Ø: 10 cm overlap: 5 cm circles/side 11	5	190 m / 1.8, 2.4, 4.0 mm	16-22 angular	half-cycle sine 1, 5, 10, 20 Hz 0.5-3.5/6.5/9.5 kN 3.5/5.0-9.5 kN
	BRC10_11_6			6	228 m / 2.4 mm	16-22 angular	
	BRC10_7		circular, Ø: 10cm overlap: 2.5 cm circles/side: 7	5		16-22 angular	half-cycle sine 20 Hz 3.5-9.5 kN
	BRC10_6		circular, Ø: 10 cm overlap: 0 cm circles/side: 6	5	113 m / 2.4 mm	16-22 angular	half-cycle sine 20 Hz 3.5-9.5 kN
	BRC10_5		circular, Ø: 10 cm separation: 5 cm circl/side: 5	5	43 m / 2.4 mm	16-22 angular	half-cycle sine 20 Hz 3.5-9.5 kN
	BRC15_7		circular, Ø: 15 cm overlap: 7.5 cm circles/side: 7	5	115 m / 2.4 mm	16-22 angular	half-cycle sine 20 Hz 3.5-9.5 kN
	BRS4_32		square, opening 2 cm reinf/side 32	5	186 m / 2.4 mm	16-22 angular	half-cycle sine 20 Hz 3.5-9.5 kN
	BRS4_16		square, opening 4cm reinf/side 16	5	96 m / 2.4 mm	16-22 angular	half-cycle sine 20 Hz 3.5-9.5 kN



**Abb. 20** different 2D string patterns employed for the reinforcement of aggregate packings in the small boxes. The size of the boxes drawn in the figure is  $50 \times 50 \text{ cm}^2$ . The characteristics of the patterns are explained in the text of the reports and in the legends of Abb. 21 and Abb. 22.



**Abb. 21** different circular 2D string patterns employed for the reinforcement of aggregate packings in the big boxes. The size of the boxes drawn in the figure is  $70 \times 70 \text{ cm}^2$ .  $D$  is the diameter of the circular patterns, while  $OL$  is the overlap between the circles in the pattern, which is zero when the circles just touch each other and becomes negative when the circles are detached.



**Abb. 22** different square 2D string patterns employed for the reinforcement of aggregate packings in the big boxes. The size of the boxes drawn in the figure is  $70 \times 70 \text{ cm}^2$ .  $GO$  is the (approximate) size of the unit in the square patterns.

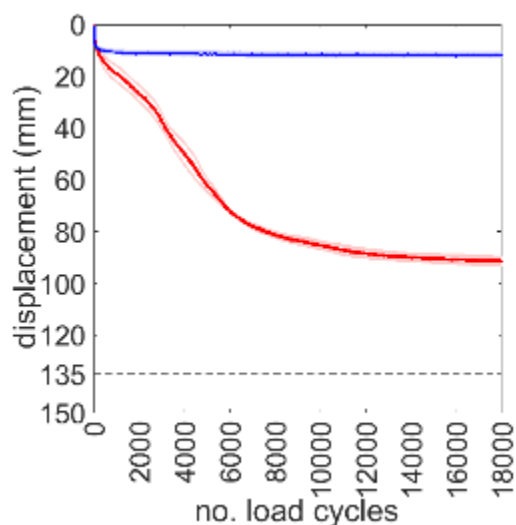


## 3.4 Experimental results

### 3.4.1 Experiments on small boxes (50×50×15 cm<sup>3</sup>)

Abb. 23 shows a comparison of reinforced and unreinforced specimens for aggregate sizes 8-11 (angular aggregates). The displacement of the unreinforced specimens under cyclic loading is shown with the red lines, while the displacement of the reinforced specimens is shown with the blue lines (this convention is repeated in all the results shown in this section). The specimens belonged to the series with smaller size boxes (S, see Tab. 1) and they were reinforced according to the scheme RC108 (see Tab. 1, strings placed in a circular pattern with diameter 10 cm, overlap 5 cm). As Abb. 23 clearly demonstrates, the reinforcement of the aggregate packing with strings has a considerable and repeatable effect on the cyclic load carrying capacity/life of the system. The displacement of the piston that loaded the aggregate packing increased constantly in the unreinforced specimens. The loading plate ended up deeply buried into the aggregate packing after about 5000 cycles (see Abb. 24). A time-lapse video showing this behavior is available to the reader in File 3 of the repository <https://doi.org/10.5281/zenodo.7786624>. The lines in Abb. 25 shows the permanent deformation of the specimens accumulated after each load of the cyclic loading program, through the proxy of the maximum displacement of the piston. This can be better understood by Abb. 25, which shows a snapshot of the whole experiments (only 20 load cycles) in which all the displacements of the piston are seen instead. In Abb. 25 it is evident that the permanent deformation is much higher for the unreinforced specimen (red curve).

In Abb. 23, while some scatter was observed between the maximum displacement-versus-load cycles curve of individual specimens in unreinforced conditions, the behavior of all specimens was equivalent. In the case of the reinforced specimens, after an initial compaction (increasing displacement of the piston) taking place in the first hundreds of cycles, almost no further deformation was observed for the subsequent several thousands of cycles. The scatter between the reinforced specimens was also substantially smaller than for the unreinforced specimens. The initial compaction of the aggregate packing apparently is necessary for the strings to be tensioned and start restraining the aggregates. After this point, the packing is in the jammed state and resists further compaction with limited deformation.

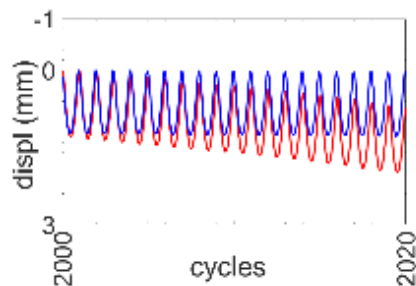


**Abb. 23** cyclic loading tests repeatability for aggregate sizes 8-11, in unreinforced (red lines) and reinforced (blue lines) according to a circular pattern SRC108. Measurements performed in the small boxes (50×50×15 cm<sup>3</sup>). Notice that the dashed line close to the bottom (here at 135 mm) indicates the position of the rubber mat that was placed on the bottom of the box. Each light-colored line in the figure shows a single experiment (3

repetitions for each configuration), while the dark-colored lines are the average of the repetitions.

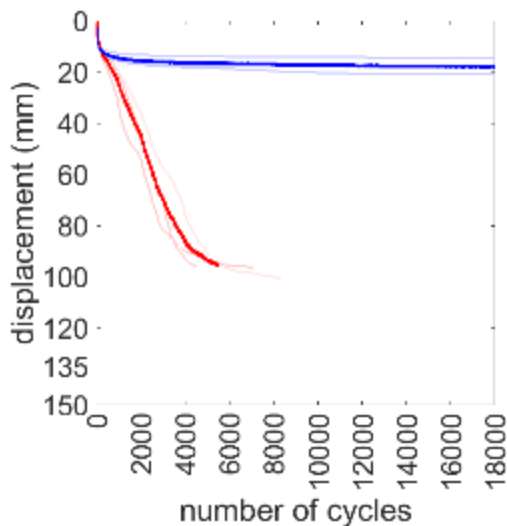


**Abb. 24** photographs of the test specimens described in Abb. 23 at the end of the testing process (after several thousand of loading cycles). In the unreinforced specimens (left), the piston ended up deeply buried into the aggregate packing, while in the reinforced specimens (right), the piston with the loading plate is still visible at the surface of the aggregate packing.



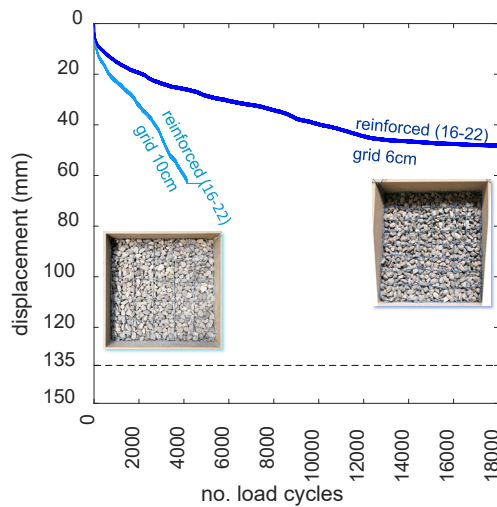
**Abb. 25** snapshot (only 20 load cycles) of a cycling loading experiment (same as in Abb. 23) in which all the displacements of the piston are seen. The curves shown in Abb. 23 are instead only describing the evolution of the permanent deformation of the specimens, which can be traced by connecting the lowermost points in each curve in Abb. 23.

Abb. 26 shows a comparison of reinforced and unreinforced specimens for larger aggregate sizes, 16-22. Also in this case, as in Abb. 23, the experiments were performed with angular aggregates. The differences between the two aggregate sizes (compare Abb. 23 and Abb. 26) are minor, with somewhat smaller deformations and less scatter observed in the tests with the smaller aggregates (8-11). Since these differences are observed both in the unreinforced and in the reinforced specimens, the origin of this behavior has to be found in the characteristics of the aggregate packing. A possible explanation of the different behavior observed with different aggregate sizes is that the initial compaction of the 8-11 aggregates, before the test was started, was more efficient (with a smaller amount of voids in the packing) than for the 16-22 aggregates. Another possibility is that smaller aggregates have more contact points among them and the packing in general is more homogeneous. Possibly, these effects are more visible with the small boxes than they might be with the larger boxes.



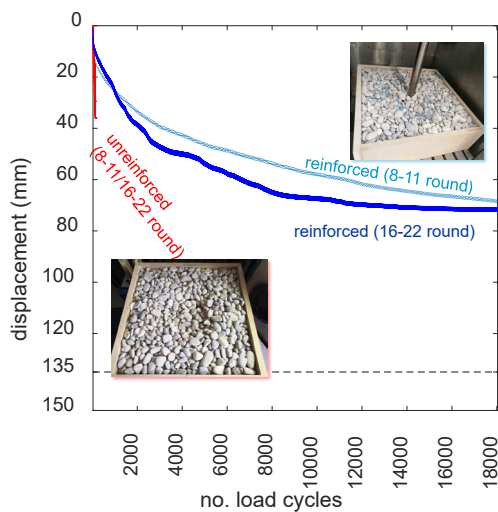
**Abb. 26** cyclic loading tests repeatability for aggregate sizes 16-22, in unreinforced (red lines) and reinforced (blue lines) according to the circular pattern SRC108. Measurements performed in the small boxes ( $50 \times 50 \times 15 \text{ cm}^3$ ). Notice that the dashed line close to the bottom (here at 135 mm) indicates the position of the rubber mat that was placed on the bottom of the box. Each light-colored line in the figure shows a single experiment (3 repetitions for each configuration), while the dark-colored lines are the average of the repetitions.

From first principles, it can be expected that multiple aspects of the geometry of the string and of the reinforcement pattern will have an effect on the deformation response of the packing. A first candidate is the pattern shape and in particular the size of the gaps between the strings in the pattern. In particular, the relative dimensions of the gaps in the pattern and the aggregates should be of importance. A too dense reinforcing pattern might be difficult to place and may even disrupt the packing of the aggregates. On the other hand, too little string in the aggregate packing or too large gaps in the pattern might allow aggregates to slip through. In addition, also the shape of the pattern (see Abb. 20, Abb. 21 and Abb. 22) may be important. In the results presented in Abb. 26 (with angular aggregates 16-22), a circular pattern with overlap was used, corresponding to the leftmost pattern in Abb. 20. In order to consider the effect of pattern shape, a square mesh shape was also considered and the results are shown in Abb. 27. Whereas also the square patterns were able to reinforce the aggregate packing and reduce the displacement of the piston, there is a clear difference between the two shapes. The circular pattern (Abb. 26) results in much less deformation than both square patterns, even for the denser square pattern (6 cm square, see Tab. 1 and Abb. 20). The large square pattern of 10 cm edge had a very limited effect on the deformations. These first results showed clearly that the shape of the pattern has a major influence on the performance of the reinforcement. However, if one compares in Tab. 1 specimens with ID SRC108 (circular pattern with half diameter overlap, results in Abb. 26), SRS69 and SRS106 (results in Abb. 27), it is clear that the length of the reinforcement string in the circular pattern is double that of the specimen with square pattern 6 cm and over 3 times that of the specimen with square pattern 10 cm (80 m vs. 40 m and 26 m, respectively). This is also clearly visible in Abb. 20, where these patterns are shown in detail for the whole box. For that reason, it is more immediate to attribute the differences in deformation behavior seen between the circular pattern and the square patterns to the different length of the reinforcement string in the specimens (however, see also the later section about the large boxes in which the effect of string length and type of pattern is dealt with in further detail). When working with the small  $50 \times 50 \text{ cm}^2$  boxes, the possible geometries of the pattern were limited by space constraints and only a few different patterns could be realized and investigated. In the later experimental campaign performed in the big boxes, it was possible to realize a larger number of patterns (see Abb. 21 and Abb. 22), which allowed to understand much better the influence of the pattern shape and of the total length of string embedded in the aggregate packings.



**Abb. 27** permanent deformation of square reinforcement pattern with 6 cm and 10 cm grid opening (ID SRS69 and SRS106 in Tab. 1).

Finally, as the last case of the first series of specimens in the small boxes, the influence of the aggregates' shape on the deformations is studied, in particular the difference between angular and rounded aggregates. Although rounded aggregates are forbidden for road applications, because the positive effect of interlocking of angular aggregates is known in the field, rounded aggregates of different size fractions were nevertheless examined, both to cover an extreme case of aggregates shape (in fact, aggregates of different angularity might be used in pavements) and more important to gain fundamental understanding on the mechanical behavior of the packing, both with and without reinforcement. From a fundamental understanding point of view, two different aspects of the aggregates' shape and surface characteristics may be of importance for the deformation response of the packing: the interlocking between the aggregates and the interaction of the aggregate shape with the string. The first aspect is obvious: round aggregates have smaller contact areas between each other and a packing with round aggregates is expected to be less stable and have larger deformations. The second aspect regards the fact that the aggregates' shape plays a role in the force transfer between aggregates and string. The string might be activated in tension both due to the friction at the aggregates' surface and due to blocking between adjacent aggregates. In both cases, round aggregates are expected to be less efficient than round ones. Abb. 28 shows the results with rounded aggregates and should be compared to Abb. 23 for the 8-11 size and with Abb. 26 for the 16-22 size. The shape of the aggregates is confirmed to have a very significant effect on the deformation behavior of the packing. Unreinforced specimens with rounded aggregates showed much less resistance to deformation than unreinforced specimens with angular aggregates (compare the red curves in Abb. 28 with those in Abb. 23 and Abb. 26). With rounded aggregates, the piston became buried within the packing after only hundreds of cycles, compared to a couple of thousands for the angular aggregates. In the case of the reinforced specimens (compare the red curves in Abb. 23 and Abb. 26, in both cases the specimen ID is SRC108, corresponding to circular pattern with half-diameter overlap) the loading plates penetrated after some thousands of cycles deeper inside the specimens compared to the angular aggregates. Nevertheless, the deployment of string reinforcement was able to increase the service life of the sample under cyclic compressive loads in comparison of the unreinforced one. Since the unreinforced specimens with rounded aggregates had very poor performance, it is clear that the aggregate to aggregate jamming is much worse in these systems. A clear conclusion about the efficiency of the force transfer between aggregates and strings in dependence of the aggregates' surface cannot however be drawn at this point. Further experiments and numerical analyses are needed to shed light on this fundamental aspect.



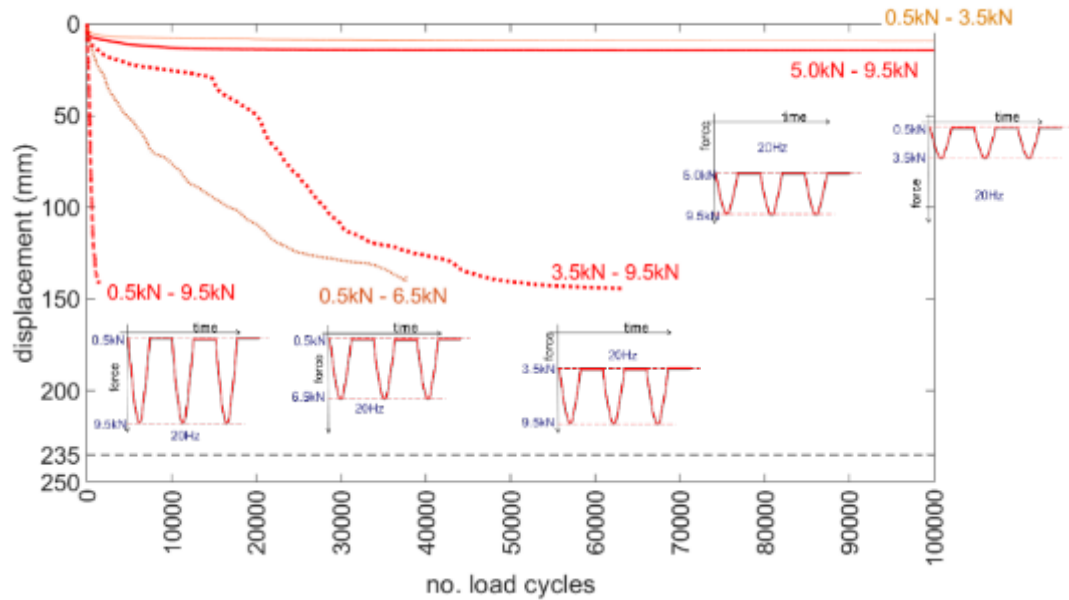
**Abb. 28** comparison of unreinforced and reinforced conditions using round aggregates of different sizes (both 8-11 and 16-22). These results should be compared with both Abb. 23 and Abb. 26, which show the results with angular aggregates.

### 3.4.2 Experiments on big boxes (70×70×25 cm<sup>3</sup>)

All the experimental results presented in the following section (starting from Abb. 29) were obtained with the larger boxes ("big boxes") with dimensions (70×70×25 cm<sup>3</sup>). The substantial larger dimensions (more than 3 times in volume, which directly translates into the weight of the filled boxes) result in more issues with handling and testing of the specimens. This also means that the larger samples took more time to build and test than the smaller ones. On the other hand, the larger samples are arguably more representative of the envisaged application of string reinforcement in roads, where the lateral boundaries are not expected to restrain the deformation of the aggregate packing. In addition, larger specimens allow to test more string patterns and more complex ones (see Abb. 21 and Abb. 22), because there is a lower limit to the local radius of the pattern and the small boxes thus limit the possible pattern geometries. Notice that the dashed line close to the bottom, at 235 mm in Figures 20-24, indicates the position of the rubber mat (with thickness 15 mm) that was placed on the bottom of the box.

Abb. 29 shows all results on unreinforced specimens. Each line represent a test where the first number is the minimum load and the second is the peak load. The frequency of the loading cycles was 20Hz for all test and the shape of the loading curve was a half-sine, with 40Hz pulse load and 40Hz resting period. This is different from the shape of the loading curve for the small boxes samples, which was sinusoidal (see Abb. 25 for example); in the following experiments on the big boxes, the shape of the loading cycles was always half-sine. This specific type of cyclic loading was chosen for the main experimental series on the big boxes because it resembles a traffic pulse in a pavement more closely than a sinusoidal curve. In Abb. 29, the general shape of the loading curve was kept always constant but different combinations of the minimum load (either 0.5, 3.5 or 5kN) and of the peak load (either 3.5, 6.5 or 9.5kN) were imposed onto the specimens. The results show clearly that the load level has a paramount influence in the performance of the specimens, even in the aggregate packings with no reinforcement. If the maximum load is high and the minimum load is low (0.5kN-9.5kN), the loading plate penetrates easily into the aggregate packing, because the maximum force tends to break the aggregates particles and then the low minimum load allows the rearrangement of the aggregate packing. On the contrary, when both the minimum and the maximum loads are low (0.5kN-3.5kN), the piston does not penetrate into the packing, even if the specimen is unreinforced. The same is true when both the minimum and the maximum loads are high (5.0kN-9.5kN). For these reasons, for the comparison of unreinforced and reinforced specimens, only specific combinations of

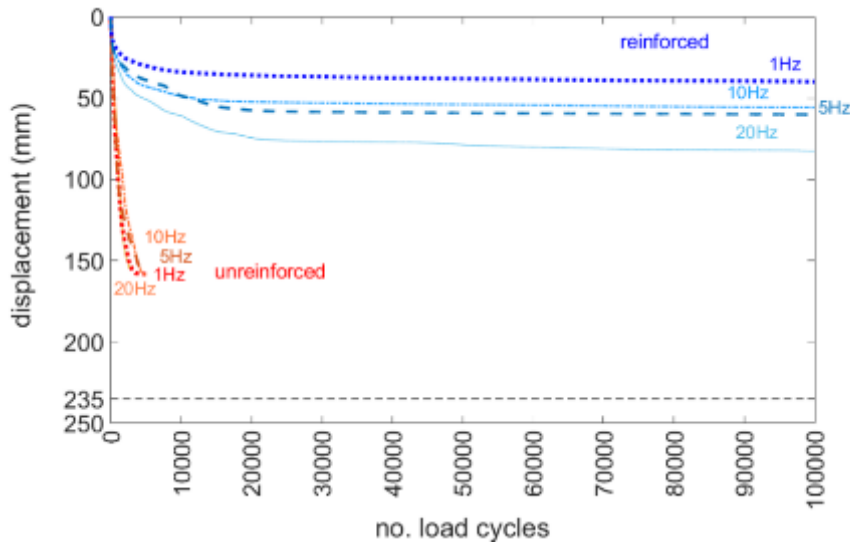
the maximum and minimum loads in the half-cycle sine pulse loading were selected (either 0.5kN-9.5kN or 3.5kN-9.5kN), for which the advantage given by the string reinforcement is evident (see Abb. 30).



**Abb. 29** effect of different half-cycle sine pulse load amplitudes on the deformation of unbound specimens; the frequency used in all cases was 20Hz. Notice that the dashed line close to the bottom (here at 235 mm, because the big boxes were 250 mm deep) indicates the position of the rubber mat that was placed on the bottom of the box.

Abb. 30 shows the influence of the loading frequency on the deformation of the specimens under cyclic compression tests. All tests were performed with half-cycle sine pulse loading with minimum load 0.5kN and maximum load 9.5kN (see comment to Abb. 29 about this choice). Both unreinforced and reinforced (all with circular pattern with  $D=10\text{cm}$  and overlap 5 cm) specimens were tested. This figure shows that the loading frequency has no substantial influence on the results, in particular on the permanent deformation and on the deformation rate. The permanent deformation of the aggregate packing, both unreinforced and reinforced, mainly depends on the number of loading cycles (when the maximum and minimum load are kept constant). One can postulate that the deformation of the packing depends on the energy that is transferred into the system, which induces local crushing of the aggregates at the contact points [2] and rearrangements of the aggregate packing. It is remarked here that the behavior of an asphalt pavement under the same type of cyclic loads would on the contrary be critically dependent on the load frequency, because the bituminous binder shows viscoelastic behavior and would manifest more permanent deformation under lower frequency loads than under higher frequency loads. Since the load frequency had only a minor influence on the deformation behavior, all following tests were performed at 20Hz, because they are much faster to complete and allow more specimens to be tested in the allocated time.

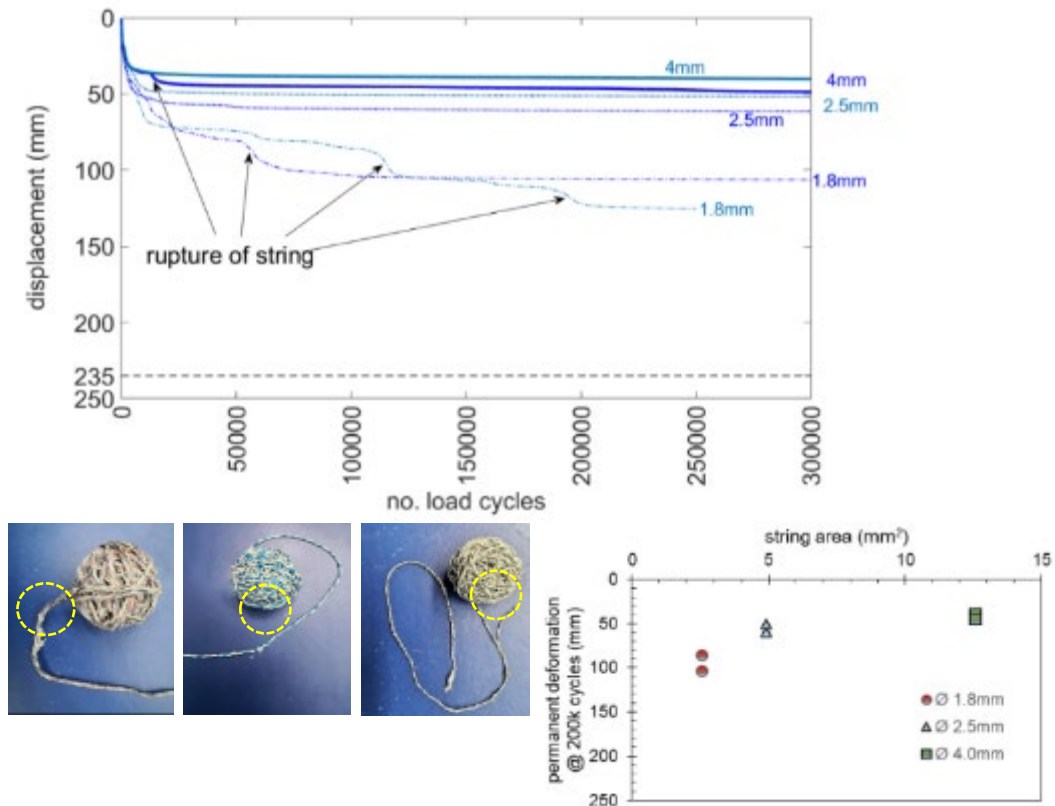




**Abb. 30** influence of loading frequency on the deformation of the specimens under cyclic compression tests. Half-cycle sine pulse loading with minimum load 0.5kN and maximum load 9.5kN. The reinforced specimens were with circular pattern ( $D=10\text{cm}$ ) with half diameter overlap.

Abb. 31 shows the influence of the diameter of the string reinforcement on the permanent deformation of reinforced specimens in cyclic tests. The loading was half-cycle sine pulse with minimum load 0.5kN and maximum load 9.5kN. The specimens were reinforced with a circular string pattern ( $D=10\text{cm}$ ) with half diameter overlap. String diameters of 1.8, 2.5 and 4.0 mm were employed and each string diameter was tested twice. The main graph in Abb. 31 (above to the left) shows the deformation of the packing (i.e., the displacement of the loading piston) as a function of the load cycles. In the graph, distinct breaks/steps with sudden increase of the displacement are visible in the displacement curve, which correspond to the rupture of the string. Multiple ruptures are evident with the smaller strings, which then induce a rearrangement of the aggregates' packing (and a displacement of the loading piston) until the aggregates reach a new stable position. This indicates that the string is loaded to high tensile stresses and in particular, the thinner strings are loaded to failure due to the fatigue tensile loading and ultimately break. However, when the string breaks locally, after rearrangement of the packing it may be still able to carry tensile stresses, possibly because it is jammed in between the aggregates at other locations. The ductile behavior of the strings, even after snapping, may be due to load redistribution within the fibers of the braid when some of the fibers snap (see Abb. 31). Even after the string snaps, and even after multiple ruptures, the displacement of the aggregate packing is still limited by the string. The very fact that multiple ruptures of the string are observed in the same packing with increased number of loads shows that a ductile branch likely follows the rupture, even in the case of the thinner strings that are more brittle (Abb. 31). Possibly, the string actually may not have necessarily to be continuous through the packing to be active (though this is practical when placing the string). In summary, the response of the reinforced aggregate packing is overall ductile also after the string breaks. For this particular load, a string diameter of 2.5mm provides good results, with displacement comparable to the 4mm diameter. This is clear in the smaller graph to the right in Abb. 31, which shows the permanent deformation after 200k cycles versus the area of the string. In fact, in Abb. 31 it is shown that the 2.5mm strings carry higher stress and are almost as ductile as the larger 4mm strings. The last subfigure of Abb. 31 (below) shows some examples of retrieved string after the experiments, in which ruptures are evident also in the thicker strings. Besides considerations about the capacity to carry the tensile forces in the packing, it should be pointed out that, the thicker the string, the more rigid it is, which also means that it might be more difficult to deploy. On the other hand, thicker strings are heavier

per unit of length, so once put in place, they tend to lay flat and do not move much during the preparation of the specimen.

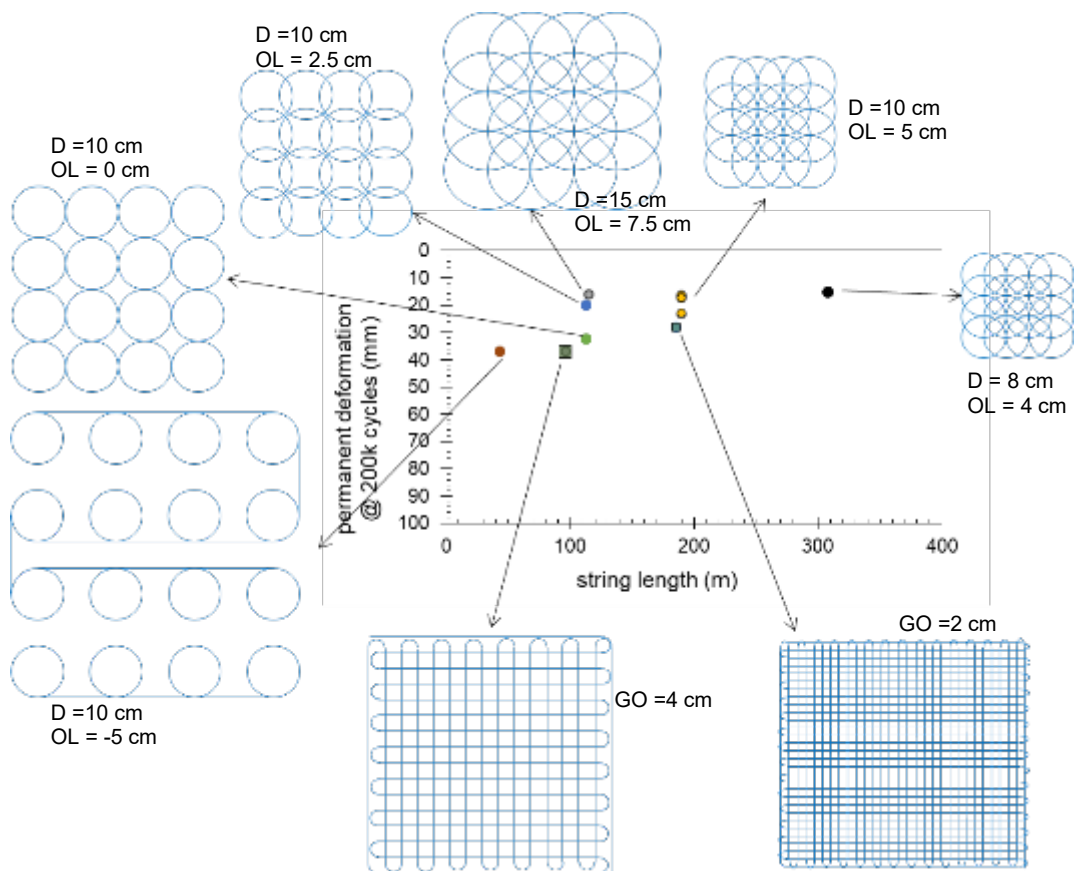


**Abb. 31** influence of string thickness (diameters 1.8, 2.5 and 4.0 mm) on the permanent deformation of the cyclic tests. Half-cycle sine pulse loading with minimum load 0.5kN and maximum load 9.5kN. The reinforced specimens were with circular pattern ( $D=10\text{cm}$ ) with half diameter overlap. Top left: displacement vs number of cycles. Top right: permanent deformation after 200k cycles versus the area of string. Bottom: retrieved strings after the experiments showing ruptures (4mm string to the left, 2.5mm string in the middle and 1.8mm string to the right).

Abb. 32 shows the deformation measured after 200'000 load cycles with different reinforcement patterns versus the total length of string; this particular number of loading cycles was selected because it was reached in all experiments. The loading was half-cycle sine pulse with minimum load 3.5kN and maximum load 9.5kN. The diameter of the string was always 2.5mm in these tests. In the figure, the different patterns to which the points in the permanent deformation vs string length graph refer are also schematically shown (a general view and more details about the patterns can be found in Abb. 21 and Abb. 22). As expected, a rough trend of reduced deformation with increased length of string can be identified in Abb. 32. However, it appears that the specific pattern of the string reinforcement is even more significant than the amount of reinforcing materials used. In general, circular patterns appear to work better than rectangular patterns. However, circular patterns with no overlaps ( $D=10\text{cm}$ ,  $OL=0\text{cm}$  or  $OL=-5\text{cm}$ ) are less efficient than those with overlaps. It appears that the circles in the pattern should embrace as many aggregates as possible. On the other hand, too much overlapping or circles with small diameters (see  $D=8\text{cm}$ ,  $OL=4$ ) do not result in further improvements, although the total amount of strings was 308m (about 50% more than in  $D=10\text{cm}$ ,  $OL=0\text{cm}$ ). In terms of efficiency of string

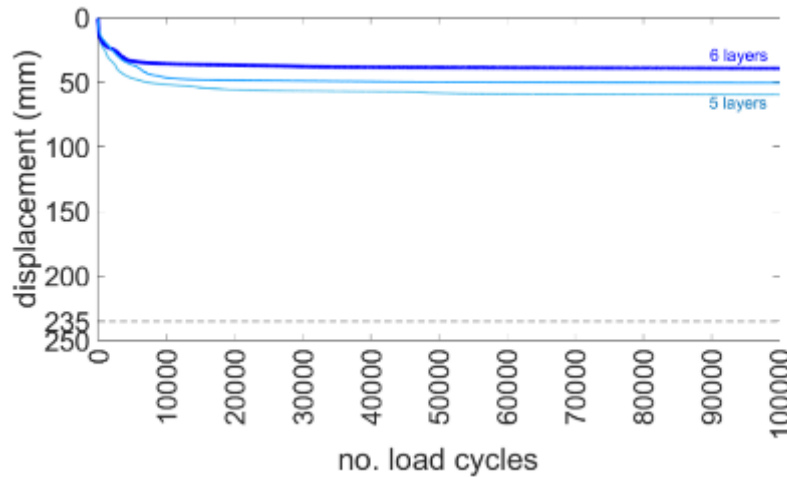


used, the pattern with  $D=15$ ,  $OL=7.5$ cm provides the best results (less rutting, i.e. less permanent deformation) with limited length of string of 115m.



**Abb. 32** deformation measured after 200'000 load cycles with different reinforcement patterns vs total length of string. Half-cycle sine pulse loading with minimum load 3.5kN and maximum load 9.5kN.

Abb. 33 shows effect of the number of layers in the permanent deformation under cyclic loading. In the big boxes specimens described in this section, the reinforcement was generally laid out in 5 layers in the vertical direction and different patterns were tried in each layer (see Abb. 32). In this figure, the reinforcement was always with a circular string pattern ( $D=10$ cm) with half diameter overlap and the difference between 5 and 6 layers is shown. For 5 layers of reinforcement, the distance between the layers was about 4.7cm and the total amount of string in the specimen was 190m. For 6 layers of reinforcement, the distance between the layers was about 3.9cm and the total amount of string in the specimen was 228m. The loading was half-cycle sine pulse with minimum load 0.5kN and maximum load 9.5kN. This figure demonstrates that also a smaller distance between the reinforcement layers in the vertical direction, or equivalently, more layers of string in the specimens, results in a reduction of the permanent deformation. A possible explanation, in line with what was found also for the patterns in the reinforcement plane (see Abb. 32) is that it is beneficial when the confining effect of the string is better distributed also throughout the thickness of the boxes. In fact, the distance of the reinforcing layers in the vertical direction (4.7 cm for 5 layers and 3.9 cm for 6 layers) is comparable with the aggregates' size (1.6-2.2 cm). This geometry is expected to result in efficient confinement.



**Abb. 33** effect of the number of layers in the permanent deformation under cyclic loading. Half-cycle sine pulse loading with minimum load 0.5kN and maximum load 9.5kN. Reinforcement with circular pattern ( $D=10\text{cm}$ ) with half diameter overlap.

### 3.5 Computer tomography scans

While the experimental setup described above allowed to capture the general behavior of the specimens subjected to cyclic loads through the displacement of the piston, the rearrangement of the aggregates and any displacement and rearrangement of the string reinforcement remained unknown. To solve this problem, a possible solution was performing 3D imaging of the aggregate packing with X-rays, ideally observing the same specimen before and after cyclic loading. However, even the small specimens, with side 50 cm, would be extremely large for most X-ray tomography setups available at research institutions. In case a setup able to handle samples of this large size would be available, its resolution might be too low to detect small displacements of the aggregates, or even strings of small diameter. Moreover, aggregates used for road construction are extremely dense materials with high X-ray attenuation, which means that only a setup with high energy would be able to image an aggregate packing of this size. At the same time, the high attenuation of the aggregates and the high-energy beams needed to image them would also complicate the detection of any material with less attenuation present in the specimen, in particular in this case the strings. The strings would likely be hardly distinguishable from the voids and would be particularly be hard to image when very close to or in contact with the aggregates. Despite the number of issues identified in this preliminary analysis, an attempt was nevertheless made to image the aggregate packings with strings, taking advantage of a unique setup available at Empa's Center for X-ray analytics.

The very-high energy X-ray tomograph at Empa's Center for X-ray Analytics (see Abb. 34) consists of a X-/γ-rays source based upon a linear (electron) accelerator (LINAC), manufactured by US Photon (Pulstar PSL-6D), and by a 1D radiation detector with a width of 1500 mm. The LINAC-based source can produced a photon beam with maximum energy of either 4 or 6 MeV (dual operation mode). The beam is collimated into a 2D, fan beam by a Tungsten slit system. In our measurements, the source was operated at 6 MeV. The 1D detector consists of an array of 3828 pixels, with a pixel pitch of 0.4 mm and a pixel width of 0.32 mm. Each pixel is a photodiodes covered by a 10 mm-thick coating of  $\text{CdWO}_4$ , acting as a converter (scintillator) of X-/γ-rays into visible light photons. Such detector (model X-Scan iHE04-M) is manufactured by Detection Technologies Inc., Piisilta (Finland). The source's slit and the 1D radiation detector are mounted on high precision, aligned vertical stages, while the specimen is mounted on a rotation stage, which can hold up to 1000 kg of weight. Such a configuration of high (photon) energy source, wide detector

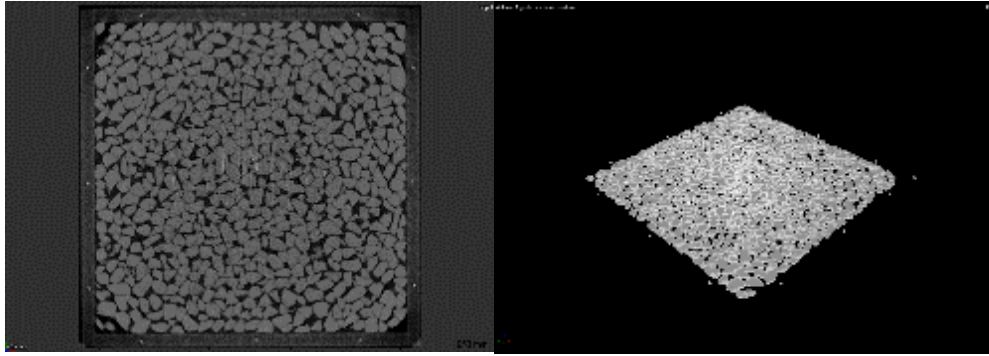
and high-load stage allows to perform tomography on large specimens (up to 70 cm) also made of highly photon-absorptive materials, e.g., a 30 cm-thick steel cylinder, a 90 cm-thick aluminum one or, as in our case, a large wooden box filled with dense aggregates.

The tomographic measurements consisted of acquiring a large number of 1D projection images (radiographs) of the specimen, at each vertical height, while rotating the specimen over  $360^\circ$  with a step of  $\Delta\theta = Y^\circ$ . The cross-section of the specimen's volume at each height is then reconstructed by using an in-house implemented version of a fan-beam filtered back-projection algorithm.

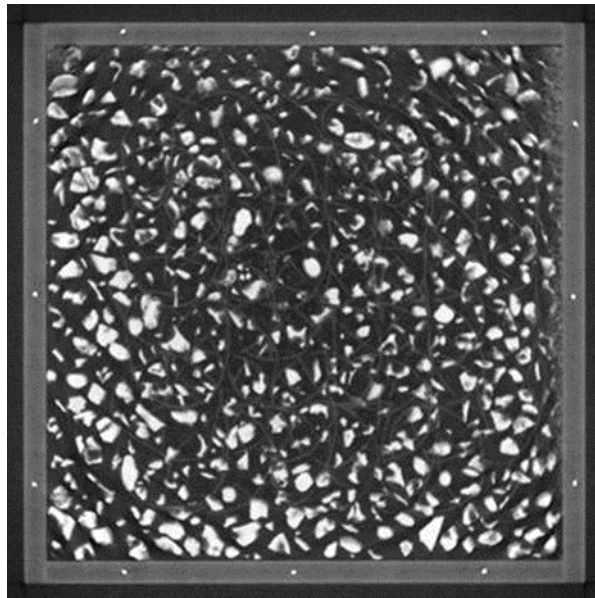


**Abb. 34** photograph of the very-high energy X-ray tomograph at Empa's Center for X-ray Analytics, with details of the setup evidenced.

Several samples were tomographed with the setup to find an optimum configuration. In each case, only a thin slice of the sample was imaged, of about 5 mm thickness. The reason of this limitation is that tomography with this setup is very time (and energy) consuming. Abb. 35 shows a slice of a specimen with only aggregates and no string reinforcement. Both the sample boundaries (in particular, the box) and the individual particles are clearly visible. In Abb. 35, right, a view of the aggregates is shown, which shows that they can be easily segmented. Abb. 36 shows instead a specimen with strings. While the strings are clearly visible to the eye, the contrast with the voids is limited and they could not be segmented by simple thresholding. While it is not excluded that with more sophisticated approaches (see e.g. [24]) a successful segmentation could be obtained, this effort was called off after the preliminary results because of the large amount of time and resources that would have had to be allocated to it. This section has been written as documentation for any reader that would wish to continue with this or similar approaches. One possible idea to increase the X-ray attenuation of the strings would be to paint them with a metallic paint or with a substance with higher attenuation. However, this would bring about stiffening of the fibers, for which reason it cannot be performed before the strings are placed in the sample. Since the strings are buried in the packing and cannot be reached after they are placed, this strategy was not followed further.



**Abb. 35** X-ray tomography of a slice of an aggregate packing (small boxes, cross-section  $50 \times 50 \text{ cm}^2$ ) without strings. The thickness of image in the vertical direction was about 0.6 mm. Left: view from above. Right: rendering of only the aggregates.



**Abb. 36** Figure C. X-ray tomography of a slice of an aggregate packing (small boxes, cross-section  $50 \times 50 \text{ cm}^2$ ) with strings. The thickness of image in the vertical direction (out of plane) was about 0.6 mm.



## 4 Modelling using the Discrete Element Method

### 4.1 Overview

In this section, we report about the development of numerical models for simulating the structural behavior of continuous reinforced granular materials under cyclic loading. In order to understand how the strings deployed in a continuous manner help improving the structural performance of continuous string reinforced structures, we created discrete element models (DEM). The main objectives of this modelling effort were:

- 1) Giving insight on the fundamental mechanisms that govern the deformation of the reinforced aggregate packing;
- 2) Providing the possibility of rapidly exploring the effect of some parameters (material properties, load, string patterns and boundary conditions) that may be difficult to change systematically in the experiments;
- 3) Reducing the amount of experimental effort by complementing the experimental series with additional numerical experiments.

DEM is based on the idea of representing granular materials as a collection of discrete, interacting particles, each with a specific mass, size, and shape and capture a system behavior by modeling interactions between individual particles. In a DEM simulation, the particles are allowed to move and to contact with each other under the influence of external forces such as gravity, friction, and applied loads. The interactions between particles are modeled using contact laws that describe the forces and torques that arise when particles touch each other. Simulations are performed in discrete time steps, during which the positions, velocities, and orientations of the particles are updated based on the forces and torques acting on them. This allows the behavior of the granular material to be studied over time, including phenomena such as flow, segregation, and compaction. This method has been a valuable tool for studying granular assemblies for almost fifty years, although being computationally intensive. As any model, DEM requires careful calibration to accurately simulate real-world dynamic systems.

In the frame of this project, we used the commercial software ThreeParticle/CAE (<https://www.becker3d.com/>) to model the small box ( $50 \times 50 \times 15\text{cm}^3$ ) experimental setup described in previous section. With this software, we can create 3D Simulation for Particle Processes and Particle Flow Simulation [27]. This tool allows to set up a virtual real-world environment from a 3D CAD model and test it. It is possible to model a broad range of parameters and different contact models such as particle dynamics of dry and cohesive materials, static and dynamic response of parts and particles, among others. ThreeParticle/CAE is organized in modules for Pre-processing (Design mode), Solving (Simulation mode), and Post-processing (Analysis, Plot, Image, Video mode and 3D Tools). The models can be prepared using the more user friendly CAE (Computer-aided engineering) or using keyword commands that can be loaded at specific times [28] [29]. The so-called keyword timing is a special feature to automate a running simulation by loading any keyword file with a defined timing by preparing keyword-timing lists. Each keyword command is available to create materials, change interactions, reposition parts or even delete or create particles, among many other possibilities. Therefore, due to the complexity of the simulations and in order to automatize and speed up the creation of new models, instead of using the simpler CAE approach, we used the keyword timing option. We therefore prepared .inp (input) files with all the information required to perform a simulation, including the preparation of the specimen with the different layers of aggregates and strings, its layer-wise compaction plus final compaction and the compressive cyclic loading. We used Matlab scripting to prepare the timing and input files in an automatic manner to automatize as much as possible to steps towards the creation of new models.

Regarding the capabilities of the software, with ThreeParticle/CAE it is possible to create hybrid models containing parts and particles. Parts are continuous 3D surface elements created from built-in geometries like boxes, planes or cylinders or imported from 3D CAD

models. The resulting geometries are allow to have dynamic motion including translation, rotation or even more complex movements, such as sinusoidal paths. Depending of the needs of the model, these geometries can be meshed using, for example, triangular elements. Similarly, using the Finite Element Method, the contact stresses resulting from the interaction with other geometries or particles can also be obtained. However, because the contact detection algorithms check for contacts with each individual mesh element, the amount of them affect computational needs and simulation time. The software has also predefined particles shapes including basic geometries like spheres, boxes, ellipsoids or capsules, among others. Further, more complex particles geometries include a combination of simple geometries like multi-sphere, clusters or triangle meshes. Simple geometries have high calculation performance but are less accurate than geometries that are more complex and in our specific case may be much closer to the shape of the aggregates in the packing.

In order to prepare the models, we designed each component of the test individually according to the geometry and materials of the test setup. Although in this report only the final results of the modelling efforts are presented, we must point out that so far the most suitable combination of modelling conditions was obtained as a result of multiple iterative trial-and-error simulations. As an example, the next chapter briefly reports about one of the multiple preliminary simulations prepared as a proof of concept of the setup and model.

## 4.2 Preliminary simulations

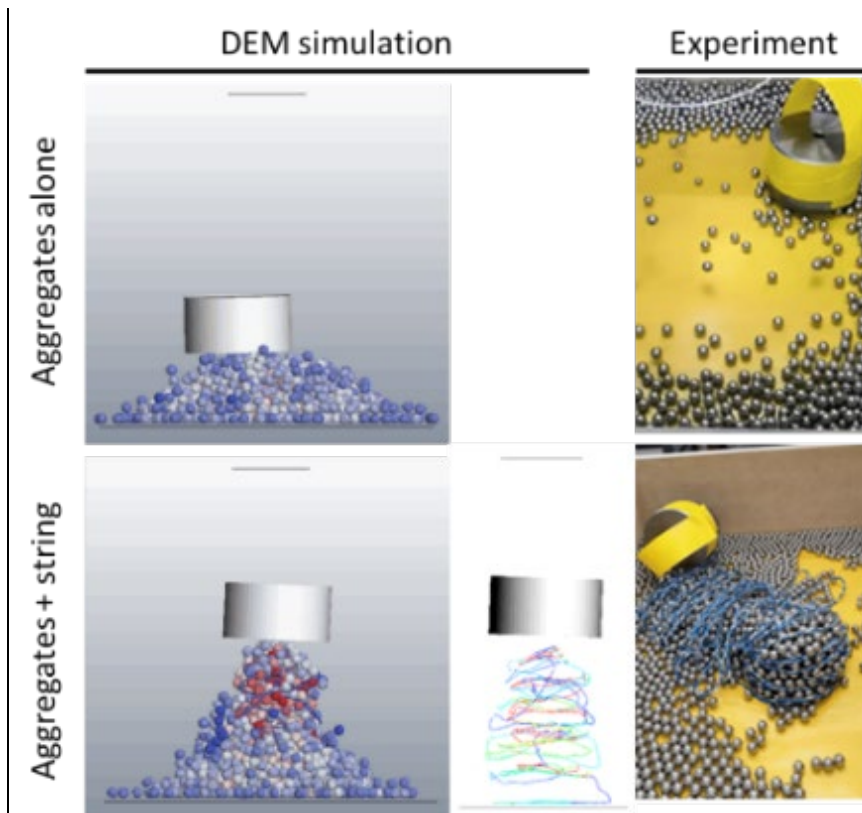
To study the capabilities of the software, we carried out and modelled experiments using ideal spherical particles (steel balls) and, as internal confinement elements, we used strings and other reinforcement elements like rubber bands (see Abb. 37). In this specific case, we manually prepared cylindrical specimens inside a plexiglas tube as a formwork. Once the different layers of string and steel balls filled the plexiglas cylinder, we applied a weight on the top and took the formwork out. We then observed the behavior of the structure and qualitatively evaluated how the reinforcements were able to provide confinement, even in this extreme case, by assessing the dispersion of the balls.



**Abb. 37** experiments using strings (left) rubber band (center) and view of a specimen

Abb. 38 displays a comparison between the results of the DEM simulations (left) and the experiments (right) with (top) and without (bottom) string reinforcement. A detailed explanation about how the string was modeled is presented in the next chapter. A visual assessment of results reveal that DEM is, up to some extent, able to capture the effect of adding a string to the system. If no string is added in the cylindrical specimen, the packing of steel balls (which have almost no contact friction among them) completely collapses after the formwork is removed and the balls scatter all over the floor (upper images in the figure). On the other hand, if strings are present, several balls are released after formwork removal, but the majority tend to form a heap thanks to the string's confining effect (lower images in the figure). With the software ThreeParticle/CAE, it is possible to display the tension in the string using a color bar (see Abb. 38 bottom- center) and therefore assess how the

continuous reinforcement works when deployed inside granular materials. The reader can download File 4 from the repository available at <https://doi.org/10.5281/zenodo.7786624> to see a video of the test and the simulations.



**Abb. 38** DEM simulation and experimental result of aggregate-string system, using ball shaped aggregates.

### 4.3 Simulation of the small box experiment

In this section, we describe the steps required to create a model that simulates the small box tests. In next paragraph, a short description of the different elements required to prepare an accurate model is provided. In the next subsections, we provide details about each single element.

The physical components of the model are the wooden box, the rubber mat, the compaction plate, the aggregates, the string and the loading plate. For the box, for the compaction tool and for the load application disk we used the software's part feature with the actual dimensions of each element. The interaction between the aggregates strongly depends on their shape through mechanical interlocking. Therefore, in order to have a more accurate representation of the actual particles used in the experiments, we scanned a random sample of aggregates and accurately measured their shape. Subsequently, we modelled their shapes using different approaches, such as multi-sphere, triangular meshes representations and superquadratic. Similarly, we represented the strings as a continuous chain of spheres or capsules bonded together with linear finite-element Timoshenko beam elements, which consider axial, shear and bending stresses. In this case we established a von Mises yield stress at which the bonding between the capsules that make up the string ruptures, which simulates the breakage of the string. For the rubber mat, we considered mainly two approaches: on one hand, we used continuous meshed elements using a built-in Finite Element Analysis and on the other hand as a set of cubic particles bonded together

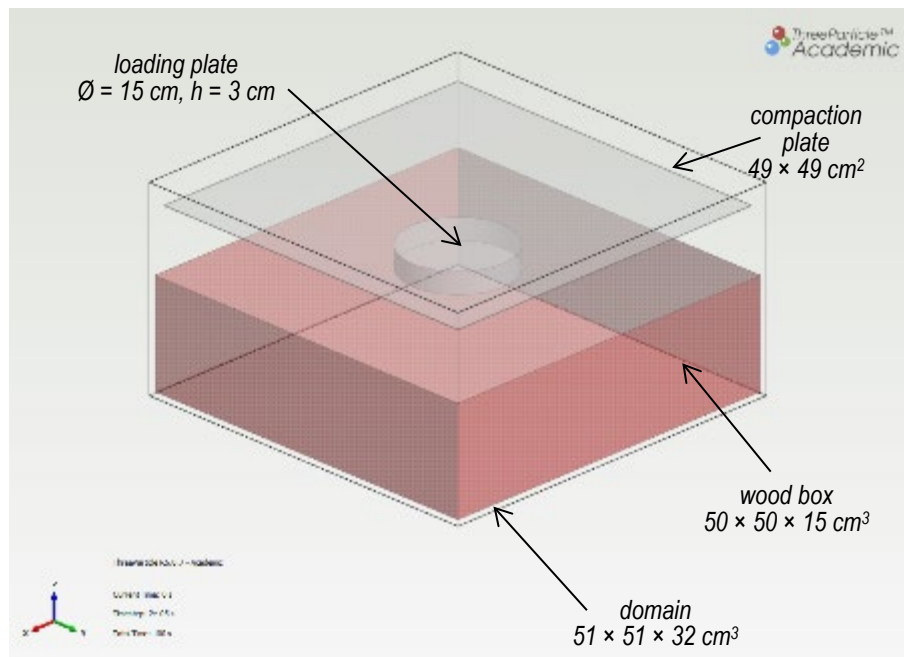


to form the mat. The mechanical properties of the different components were established using different material properties. On most of them, we set the initial values based on the literature. However, for the aggregates, string and rubber mat we used the calibration measurements described in sections 3.2.2, 3.2.3 and 3.2.4 respectively. The interaction contact among the different elements was also modelled for each pair of materials that can get into contact (master model). Apart from the bonding interaction (slave model) among string particles mentioned earlier, we used Hertz Mindlin (no slip) model (HM model), in which the normal force component is based on the Hertzian contact theory and the tangential force model is based on the work of Mindlin and Deresiewicz [22]. Following the work of Illiev [2], particle rotations in 3D were tracked and updated via the representation through quaternions, which allow a compact representation using four-dimensional vectors. We also simulated the procedure to prepare the specimen, in particular with the simulation of the filling and compaction processes. The preparation procedure was indeed found to have an influence on the performance of the model. After trying different configurations like particle generator (creates particles at defined rates) or filling (creates particles in a defined volume) we decided to use the manual generation option, in which it is possible to set the position of each particle as well as the initial velocity of each layer. The compaction, as well as the loading, are loading functions, which in our case were created from the real loads and frequencies though amplitude functions. It is important to mention that the correct determination of the temporal occurrence of each step is crucial for the model to work. A proper timing is used to control the creation or generation rate with any time depending function based on amplitude or a simple start and stop. In the next sections, we describe each element mentioned here more in detail.

### 4.3.1 Parts

#### *Wooden box, compaction plate and loading plate*

Simple geometrical shapes like boxes, cylinders and polygons are already implemented in ThreeParticle/CAE and can be easily created as parts. As the parts are usually defined using mathematical equations, the particle-geometry contact detection is very efficient. Continuous (non discrete) elements like the wooden box, the compaction and loading elements were modelled using parts as a box, a plate and a cylinder respectively (see Abb. 39). In the same figure, the domain shows the volume in which the detection algorithm works, as explained later in § 4.3.6.

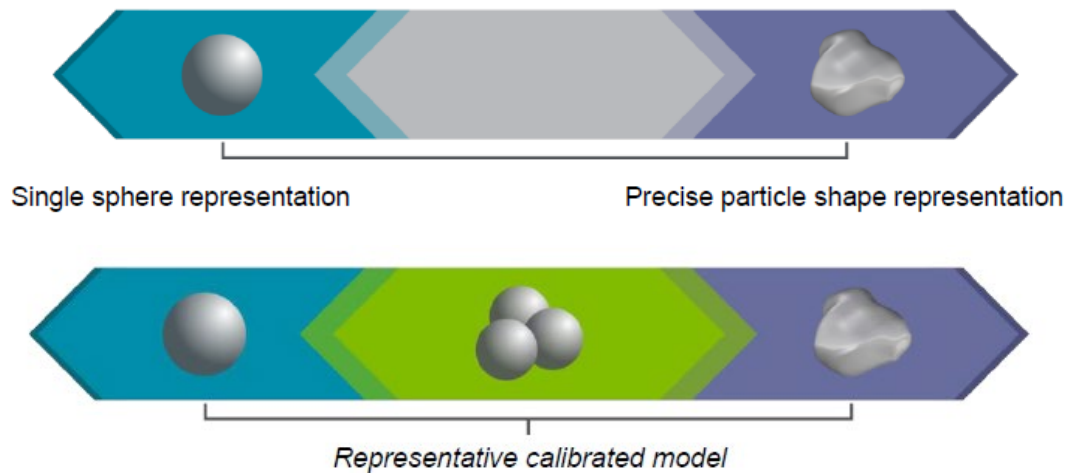


**Abb. 39** screenshot of the software *ThreeParticle/CAE* showing the different parts used for the model.

### 4.3.2 Particles

#### *Aggregates*

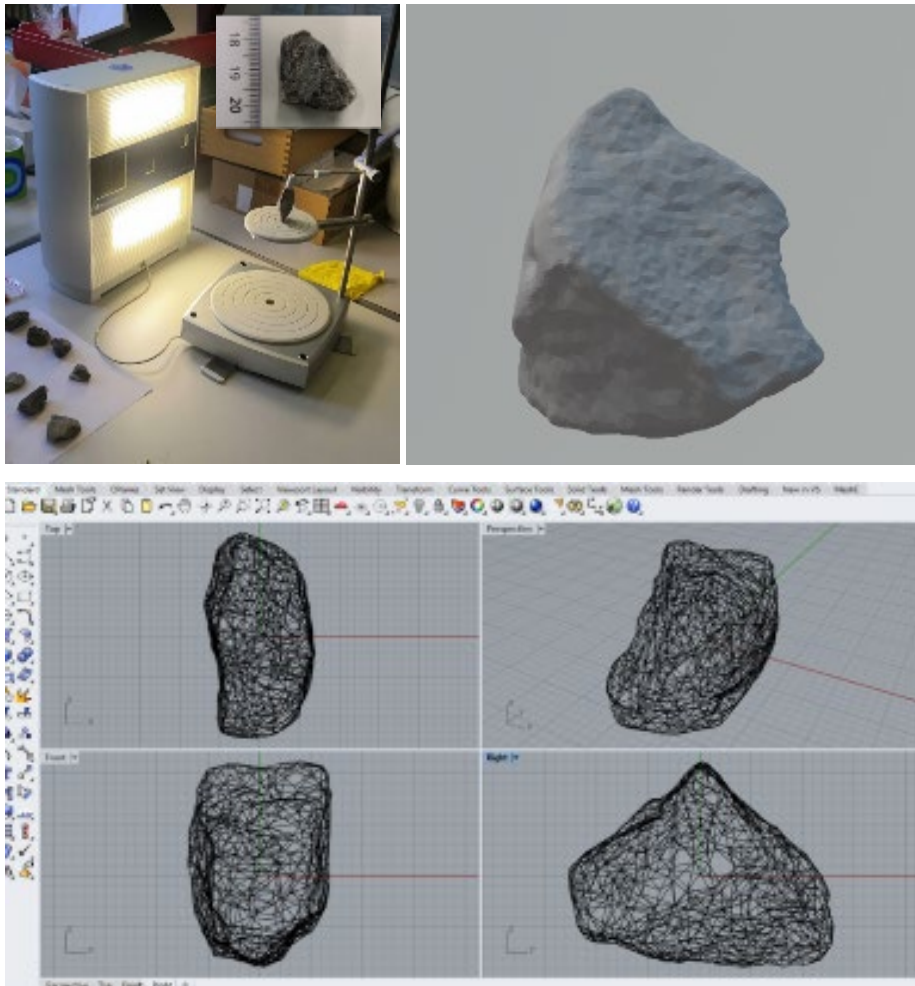
The simplest particle model in DEM are circles (in the case of 2D representations) or spheres (for 3D systems), whose geometry can be easily defined through a radius. The computational effort when simulating granular material behavior with spheres is limited compared to more complex shapes. This advantage of spheres can be exploited to reduce simulation time, especially when dealing with a large number of particles. However, in some applications it is necessary to model particle irregularities as the shape of the particles affects the bulk material behavior (e.g. via mechanical interlocking). The optimal model should be a balance between a detailed real particle representation and the computational effort (see Abb. 40). In order to analyze which is the optimum compromise and to select the best particle representation, a calibration using the results of simple tests is the recommended approach [23].



**Abb. 40** schema showing how to represent actual particles in a DEM simulation (from [23]).

In this work, a representative sample of 100 angular aggregates, size 16-22, were picked randomly and scanned with the Ultra-HD 3D scanner Nextengine (see Abb. 41 top-left photograph). The scanner uses an auto-drive rotating stand to clamp an object (aggregate) and rotate it 360°. This movement allows all surfaces of the aggregate to face the camera, flash and laser, which are responsible for measuring and saving the digital 3D representation of the sample (see Abb. 41 top-right picture). The scanner uses the software Scan Studio to capture the color and the texture of the object up to 0.012 mm resolution and perform basic data processing (see Abb. 41 bottom). In our work, we saved the scans as .stl CAD files. With other self-made processing tools, we converted the files into geometrical parameters ready to be used as input in ThreeParticle/CAE. These parameters depend on the type of granular representation chosen, as explained later in this chapter.

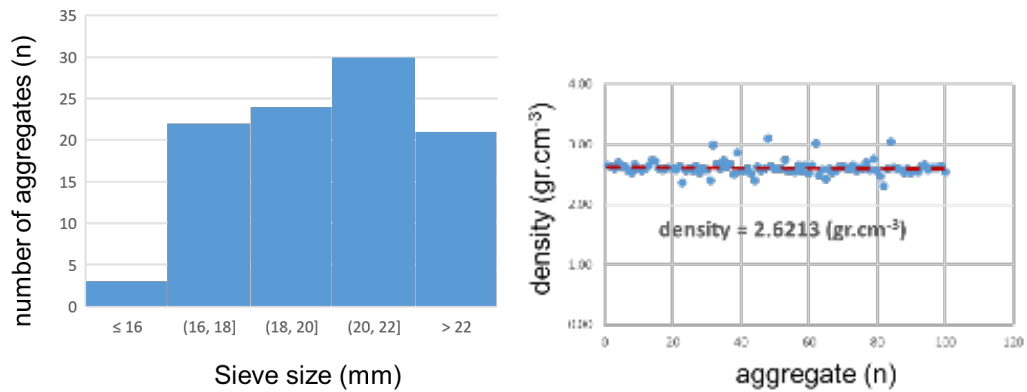
In order to obtain a more precise volumetric characterization of the sample, we sieved the aggregates using openings of 16 mm, 18 mm, 20 mm and 2 mm and we weighed all the aggregates (see Tab. 2). Using the volume information obtained with the scan, we calculated the average density of the aggregates, which were used as an input for the material properties (see § 4.3.3). The sieve analysis and the density measurements are presented in Abb. 42.



**Abb. 41** view of the scanning of one aggregate (top-left), digital 3D representation of the sample (top-right) and tessellation of a 3D aggregate representation using polygon meshes (bottom).

**Tab. 2** mass of individual aggregates of the representative sample

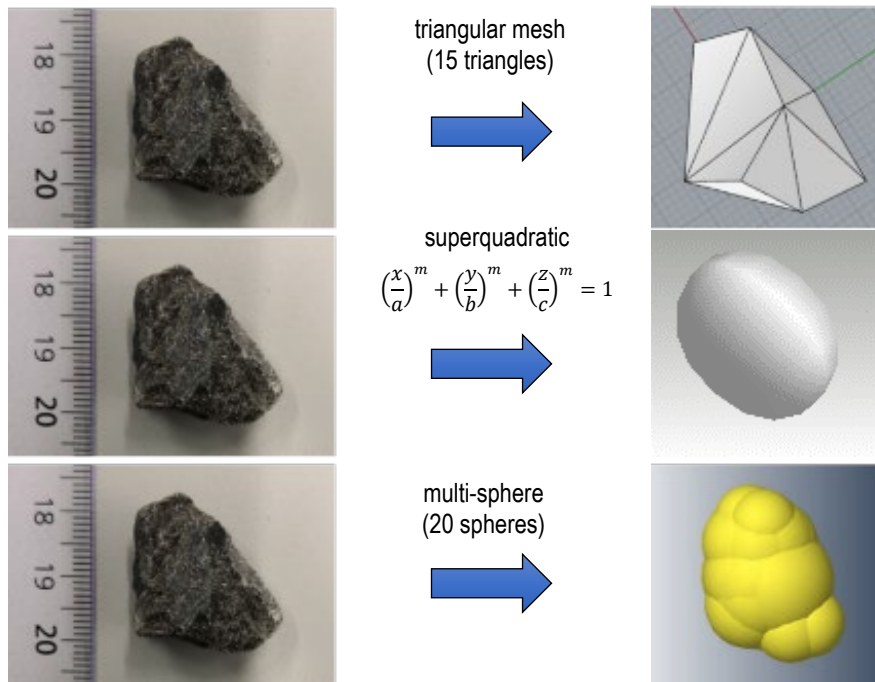
Name	Mass (gram)	Name	Mass (gram)	Name	Mass (gram)	Name	Mass (gram)
nAgg_n_001	20.423	nAgg_n_026	9.714	nAgg_n_051	26.321	nAgg_n_076	18.371
nAgg_n_002	24.795	nAgg_n_027	12.351	nAgg_n_052	15.124	nAgg_n_077	17.444
nAgg_n_003	7.647	nAgg_n_028	16.936	nAgg_n_053	10.618	nAgg_n_078	16.099
nAgg_n_004	19.74	nAgg_n_029	21.523	nAgg_n_054	12.62	nAgg_n_079	6.57
nAgg_n_005	18.344	nAgg_n_030	8.918	nAgg_n_055	27.097	nAgg_n_080	11.673
nAgg_n_006	21.505	nAgg_n_031	9.082	nAgg_n_056	10.169	nAgg_n_081	7.797
nAgg_n_007	10.092	nAgg_n_032	21.058	nAgg_n_057	11.549	nAgg_n_082	3.601
nAgg_n_008	11.211	nAgg_n_033	18.446	nAgg_n_058	7.36	nAgg_n_083	14.902
nAgg_n_009	16.01	nAgg_n_034	8.459	nAgg_n_059	14.478	nAgg_n_084	7.979
nAgg_n_010	6.672	nAgg_n_035	13.346	nAgg_n_060	9.976	nAgg_n_085	8.358
nAgg_n_011	17.976	nAgg_n_036	11.949	nAgg_n_061	15.513	nAgg_n_086	16.463
nAgg_n_012	13.934	nAgg_n_037	21.657	nAgg_n_062	10.488	nAgg_n_087	11.156
nAgg_n_013	6.459	nAgg_n_038	11.348	nAgg_n_063	9.308	nAgg_n_088	5.894
nAgg_n_014	10.373	nAgg_n_039	7.563	nAgg_n_064	14.046	nAgg_n_089	14.698
nAgg_n_015	26.055	nAgg_n_040	10.452	nAgg_n_065	7.335	nAgg_n_090	6.113
nAgg_n_016	17.574	nAgg_n_041	10.095	nAgg_n_066	12.059	nAgg_n_091	6.579
nAgg_n_017	13.119	nAgg_n_042	10.704	nAgg_n_067	14.715	nAgg_n_092	7.704
nAgg_n_018	11.856	nAgg_n_043	11.226	nAgg_n_068	10.061	nAgg_n_093	19.179
nAgg_n_019	10.673	nAgg_n_044	9.191	nAgg_n_069	9.881	nAgg_n_094	19.515
nAgg_n_020	13.681	nAgg_n_045	9.855	nAgg_n_070	9.424	nAgg_n_095	13.424
nAgg_n_021	7.851	nAgg_n_046	8.602	nAgg_n_071	14.439	nAgg_n_096	19.79
nAgg_n_022	17.156	nAgg_n_047	7.605	nAgg_n_072	18.665	nAgg_n_097	13.172
nAgg_n_023	7.814	nAgg_n_048	5.861	nAgg_n_073	7.366	nAgg_n_098	14.566
nAgg_n_024	18.818	nAgg_n_049	17.888	nAgg_n_074	11.689	nAgg_n_099	16.123
nAgg_n_025	13.883	nAgg_n_050	15.132	nAgg_n_075	13.65	nAgg_n_100	9.996



**Abb. 42** size distribution (left) and density (right) of the selected 100 aggregates

In Abb. 43 we show an example of how an aggregate looks like when represented with triangular meshes, superquadratic functions and multi-spheres. Triangular meshes are defined in terms of vertices, edges and faces in which the pyramid is the most simple shape. Superquadratic elements are defined through a surface with a mathematical function (see center of Abb. 43). In multi-spheres, the shape of the aggregate is fitted through a number of overlapping or touching spheres whose centers are fixed relative to each other. Intuitively, an angular aggregate like the one shown at the left of the figure seems to have a more accurate representation with the triangular meshes. However, solving the equations of equilibrium of these types of representation consume higher computational resources and similar results can be sometimes obtained by tuning the contact parameters of the multi-sphere representation. On the other hand, superquadratic functions are, in the case of the particle shapes considered in our simulations, less accurate than the other two methods. Consequently, after a first trial, superquadratic functions were discarded in the further analysis.

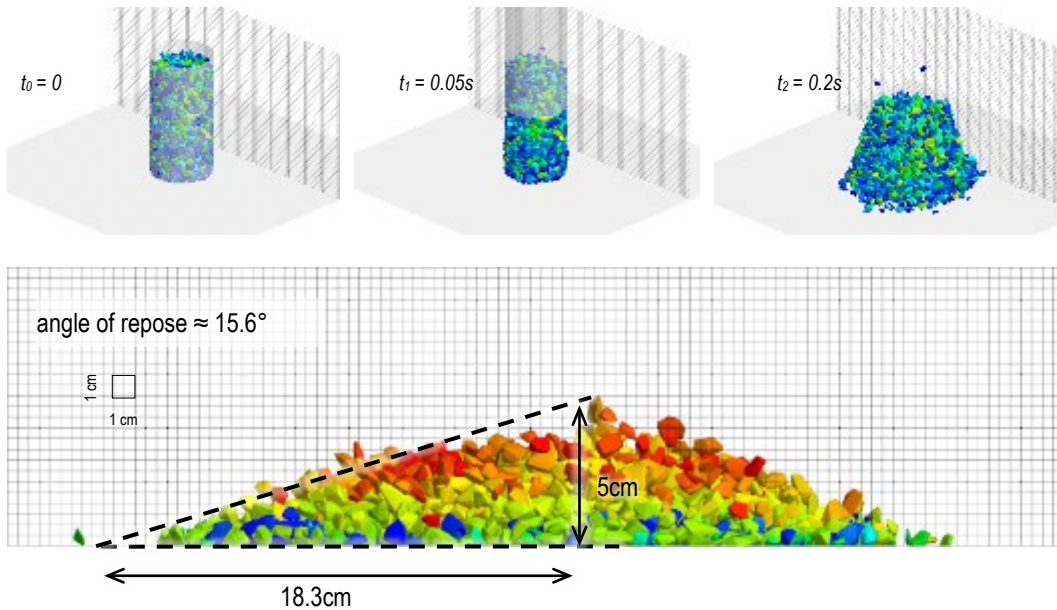
It must be pointed out that, with increasing refinement of the representation (in the example of Abb. 43 we show a multi-sphere with 20 spheres, but we could use from 1 to an infinite number of spheres) the resulting model will be more accurate but, at the same time, more computationally consuming. From these explanations it can be concluded that a clever selection of the best strategy when modeling complex systems (as the ones we want to simulate, which involve a rather large number of particles with complex shapes) requires many trial and error simulations. The importance of experience in the preparation of these type of models is also a significant factor that cannot be neglected.



**Abb. 43** aggregate shape representations using triangular mesh, superquadratic equations and multi-sphere method with 20 spheres.

In order to have an orientation about which type of element and which interaction properties are the most accurate to define the behavior of the aggregates, we prepared several DEM simulations to numerically reproduce the angle of repose tests described in § 3.2.2. Abb. 44 shows an experiment in which a cylindrical container was filled with a random packing of aggregates and then the cylinder was suddenly removed. The aggregates were represented with triangular meshes, as explained above. In the upper part of the figure, several screenshots of the first instants immediately after removal of the cylinder are shown. Similarly as in the procedure in which the angle of repose of the actual aggregates was determined experimentally (see § 3.2.2 above), the angle of repose in the simulation is calculated visually based on the geometry of the reposing aggregates heap. In order to have a close approximation to the test results (calibration), the simulations were repeated several times with different static and rolling friction coefficients and damping restitution coefficients. These parameters are part of the HM contact modelling and will be explained in more detail in § 4.3.3.

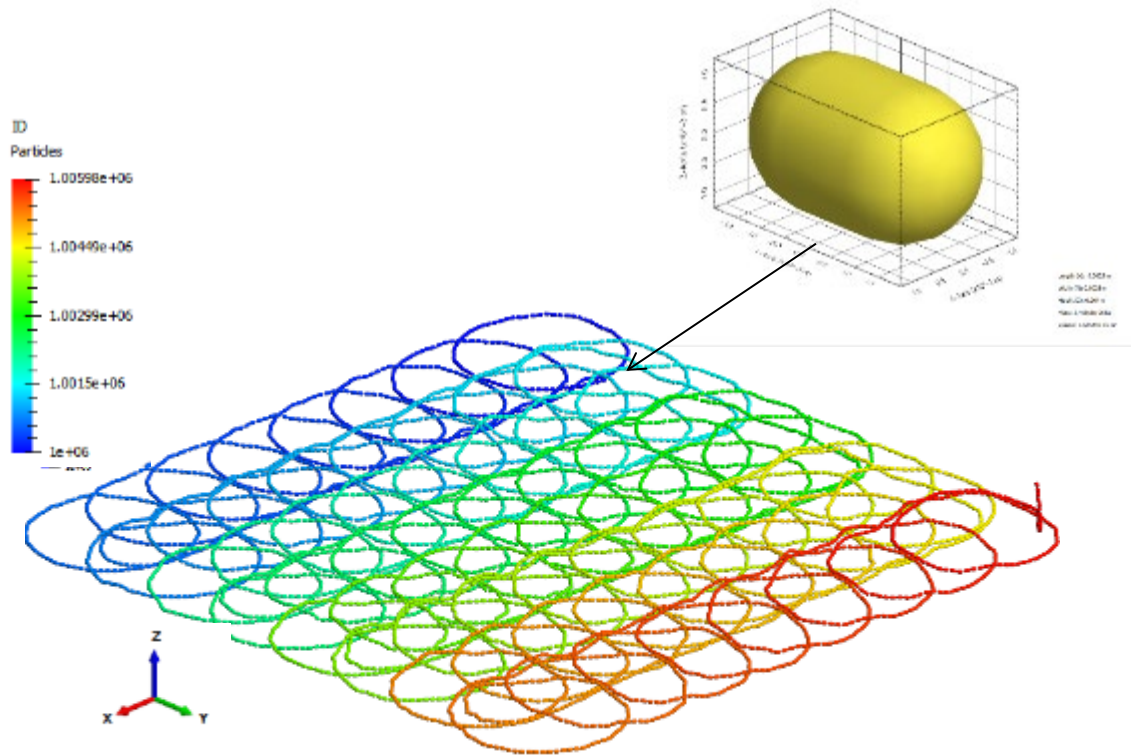




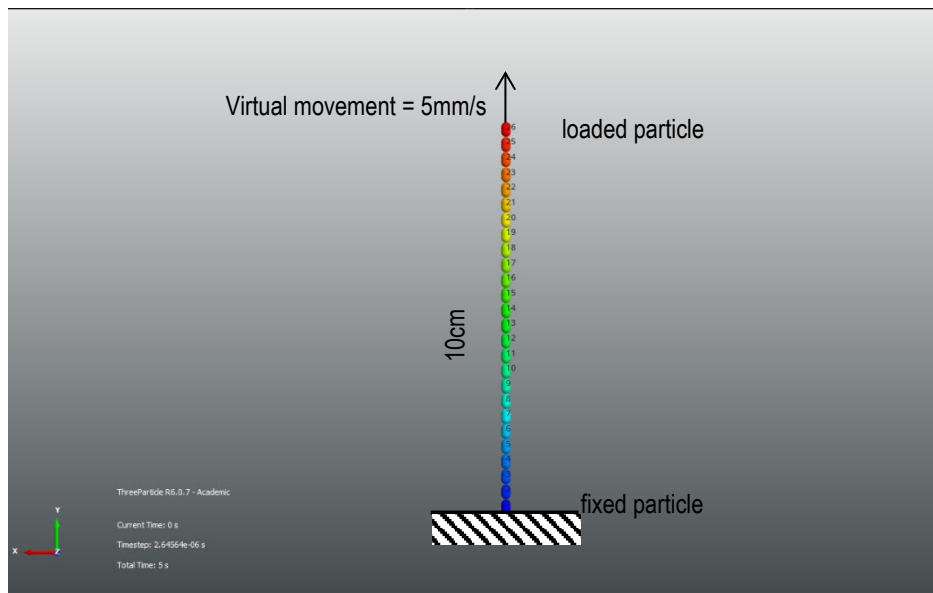
**Abb. 44** calibration of the aggregate to aggregate interaction parameters of triangular meshed representation using the measured angle of repose (see § 3.2.2 for the equivalent tests on the actual aggregates).

### String

In DEM it is possible to model not only the forces resulting from the collision of moving particles but particles can also be bonded together (slave interaction) to resist normal and tangential tension stresses. It is also possible to define a breaking stress at which the bond breaks. In this work, we modeled the strings as a chain of point-like masses connected by linear and radial elastic spring elements (see Abb. 45). We selected two types of elements to model the links of the chain: a sphere and a capsule. The radius of the elements was selected based on the thickness of the modeled string (2.5 mm). Capsule elements with a length of 3.5mm were preferred over spherical ones, since the elongated shape of the capsules allows using fewer elements to describe the same string length. At the same time, this length of the capsules was still able to describe with reasonable accuracy the geometry of the circular patterns (in this case with 6 cm diameter). The location of each particle followed a determined pattern and was generated with Matlab and stored in 5 different files, one for each layer of reinforcement. Similarly as with the aggregates, the bonding parameters of the string links were calibrated using the tension tests described in § 3.2.3. As depicted in Abb. 46, we prepared a model of the string with a length of 10 cm with the bottom element fixed. We then applied a virtual movement to the opposite element, simulating the 5 mm/s movement of the test setup: In this case the parameters changed were the Young's modulus, the Poisson's ratio as well as other parameters as critical von Mises stresses, damping coefficient, reduction factor, bonding radius and damping ratio (see a detailed explanation in § 4.3.3). We performed several simulations in order to tune these values and reproduce the string test results as close as possible.



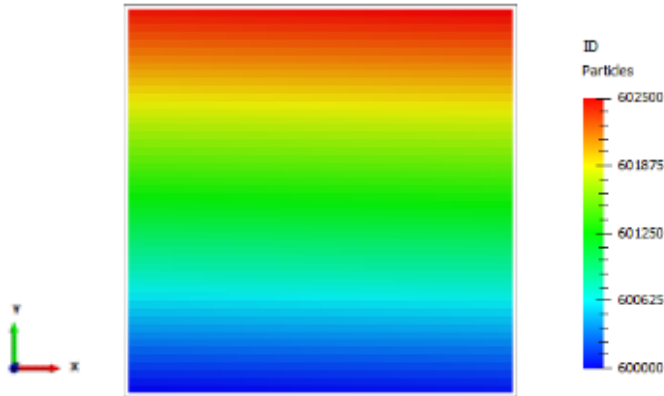
**Abb. 45** modelling of the string made of capsule elements, each reinforcement layer containing about 6000 elements (the exact number depends on the layer).



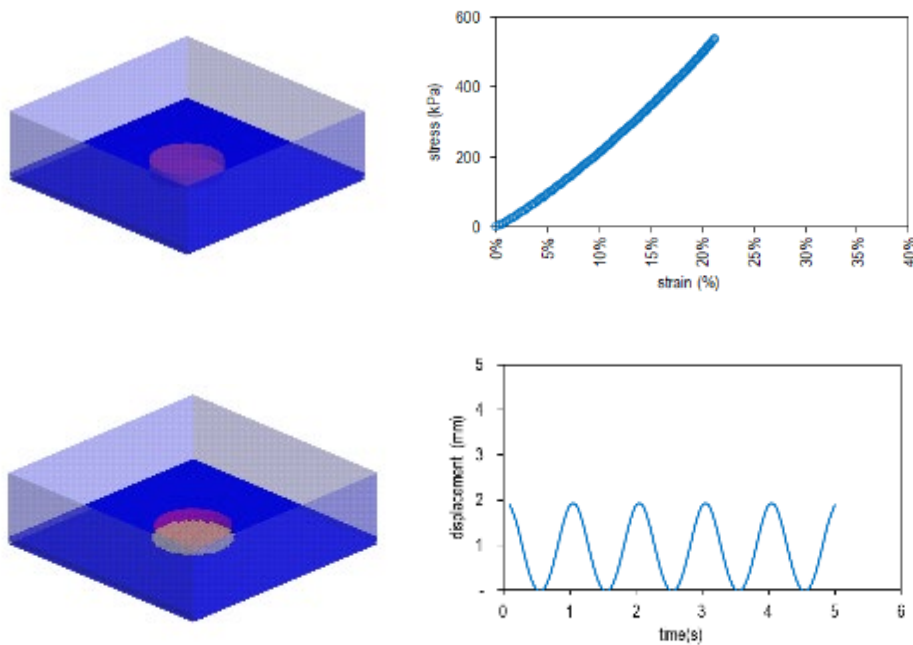
**Abb. 46** DEM for the calibration of the string link bonding parameters.

*Rubber mat*

In the initial modelling efforts we considered the elastic rubber mat at the bottom of the box as continuous meshed elements and tried to obtain the strain-stress tensional state of the element with the Finite Element Analysis solver. However, the simulations of the early stages of the small box experiments proved to be extremely time consuming. Looking for options to reduce the computation time, we finally opted to create one upper and one lower meshes of cubic particles ( $1 \times 1 \times 0.75 \text{ cm}^3$ ) consecutive bonded together (see Abb. 47) on each face, except for the top and bottom surfaces. The reason for dividing the mat in a bottom and top layer was based purely on the optimization of the results. In the same way as we did for the aggregates and strings, we used the rubber mat compression tests described in § 3.2.4 to calibrate the bonding parameters for the simulation.



**Abb. 47** identification of the 2500 cubic particles used to model the top layer of the mat



**Abb. 48** DEM simulation of the static (top) and dynamic (bottom) rubber mat tests. The resulting stress-strain and displacement curves, shown on the diagrams on the right present similar order of magnitudes than the experimental results shown in § 3.2.4.

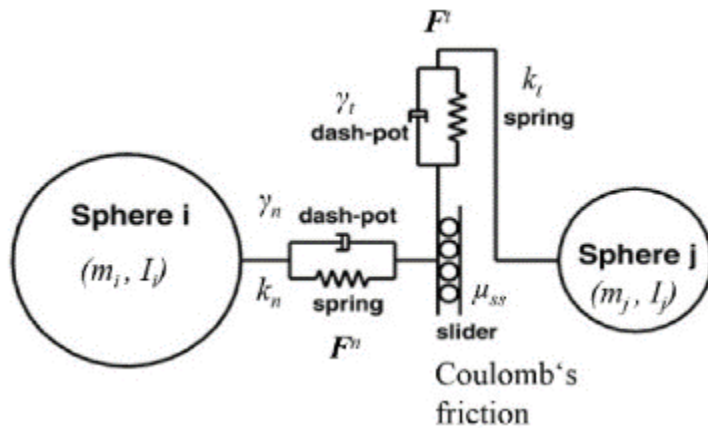
### 4.3.3 Materials and Interactions

In ThreeParticle/CAE it is possible to define solid materials using general parameters that include density and elastic properties to define the stiffness and the Poisson's ratio. In DEM, it is common to use a lower shear modulus than the real physical one, to increase the critical time step. Other parameters as the yield stress or thermal properties are useful to simulate elasto-plastic behavior or temperature dependency, but are not relevant for modelling the box experiments studied in this project.

**Tab. 3.** *materials parameters used in the small box model*

Name	Material	Density (kg/m <sup>3</sup> )	Shear modulus (MPa)	Poisson ratio
'mString'	string	400	10	0.285
'mBox'	box	400	10	0.3
'mAggregates'	aggregates	2620	10	0.3
'mHammer'	compaction plate	7800	10	0.3
'mHydJack'	loading plate	7800	10	0.3
'mGround'	rubber mat (bottom)	750	1	0.3
'mElasticMat'	rubber mat (top)	750	1	0.3

The module "interactions" of the software ThreeParticle/CAE establishes the contact models used to describe physical interactions among materials. These are usually expressed through a combination of ideal functional elements like springs, dashpots and sliders (tangential friction). The HM (no slip) contact model used in these simulations consists of three components: normal and tangential contact forces as well as a normal damping force. The normal contact force is calculated based on the overlap distance between the particles, and is modeled as a linear or nonlinear spring function. The tangential contact force represents the frictional forces between the particles and is modeled using Coulomb's law of friction. The normal damping force is a viscous force that acts to dissipate energy during collisions. Abb. 49 shows schematically the elements of the HM model.



**Abb. 49** schema of the HM contact model (from [25]), where  $m_i$  and  $I_i$  are the masses and moment of inertia of the particles;  $F^t$  and  $F^n$  are the tangential and normal contact forces respectively;  $k_t$  and  $k_n$  are the spring coefficients;  $\gamma_t$  and  $\gamma_n$  are the dashpot coefficients and  $\mu_{ss}$  is the coefficient of the slider.

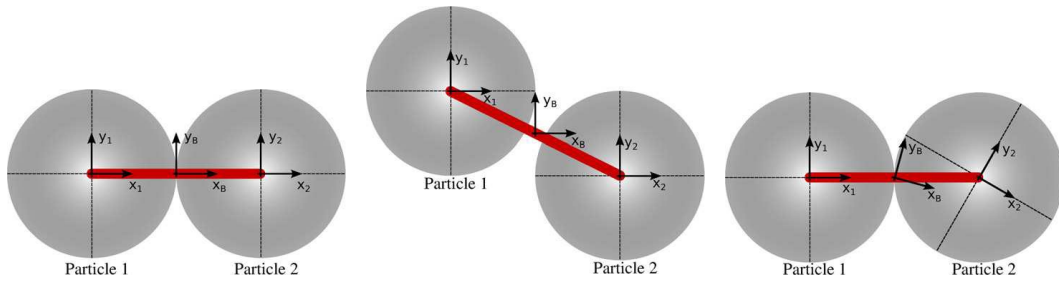
When two particles get into contact, the particle elements begin to overlap and the springs are compressed. This causes an increase in the contact force. The dashpots resist the sliding motion and dissipate energy due to friction. The slider switches to a sliding state when the applied force exceeds the maximum static friction force. As the contact force is decreased, the particles begin to separate and the springs are extended. This causes a decrease in the contact force. The dashpots still resist the sliding motion and dissipate energy due to friction. The sliders switch back to a sticking state when the applied force is less than the maximum static friction force.

The most important parameters that represent the different HM model elements in ThreeParticle/CAE are the static friction, the dynamic friction and the rolling friction coefficients. The static friction corresponds to the case when sliding does not occur during contact. Meanwhile, dynamic friction is related to the situation when sliding occurs immediately after the tangential force exceeds the normal force and static friction limit. Rolling friction describes the particle rolling or rotational movement resistance in contact with another surface. A higher frictional force between the acting particle and surface stops the sliding or scratching of the surface. Another element used in the HM is the coefficient of restitution, which is related to the damping: if the restitution is 0, the collision is considered perfectly inelastic, whereas if the restitution equals 1, the collision is considered perfectly elastic and no kinetic energy is dissipated. A realistic value should be chosen between 0 and 1. Tab. 3 contains all the coefficient values used in the model.

**Tab. 3** master contact coefficients for the HM contact model

No.	Material A	Material B	Static friction	Dynamic friction	Rolling friction	Restitution
1	string	string	0.5	-	0.15	0.5
2	string	box	0.5	-	0.15	0.5
3	string	aggregates	0.5	-	0.15	0.5
4	aggregates	box	0.65	0.55	0.25	0.5
5	aggregates	aggregates	0.6	0.6	0.6	0.9
6	aggregates	compaction plate	0.55	0.45	0.15	0.5
7	string	loading plate	0.50	-	0.15	0.5
8	aggregates	loading plate	0.55	0.55	0.25	0.9
9	loading plate	box	0.50	0.50	0.15	0.5
10	hammer	box	0.50	0.40	0.15	0.5
11	string	rubber mat (top)	0.50	-	0.15	0.1
12	aggregates	rubber mat (top)	0.85	0.75	0.75	0.2
13	loading plate	rubber mat (top)	0.75	0.65	0.25	0.2
14	rubber mat (bottom)	rubber mat (top)	0.75	0.65	0.25	0.2

As mentioned previously in § 4.3.2, passive interaction is used to bond particles in order to model the string and the rubber mat. In ThreeParticle/CAE the bond is modelled by a beam element that obeys a linear elastic material law and allows for finite values for displacements and rotations, following the geometrically exact beam theory for small deformations [26]. The bonding element is built between two consecutive particles with a local bonding coordinate system, where the x-axis and the bonding element lies in the same direction (see Abb. 50, left). If a translational deformation between particles occur, the bonding element (beam) elongates and introduces shear deformation (Abb. 50, center). When the relative orientation of two connected particles changes during the simulation, the bonding element is bent or twisted (Abb. 50, right). For this case, the model parameters are the strength and stiffness of the beam elements defined as: Young's modulus, Poisson coefficient, critical stress (tensile strength of the beam model), bonding radius and damping. Tab. 4 contains all the values used in the model.



**Abb. 50** initial state of bonded particles with the connecting beam element as a bold red line (left), shear displacement (center) and bending deformation (right) (from [26]).

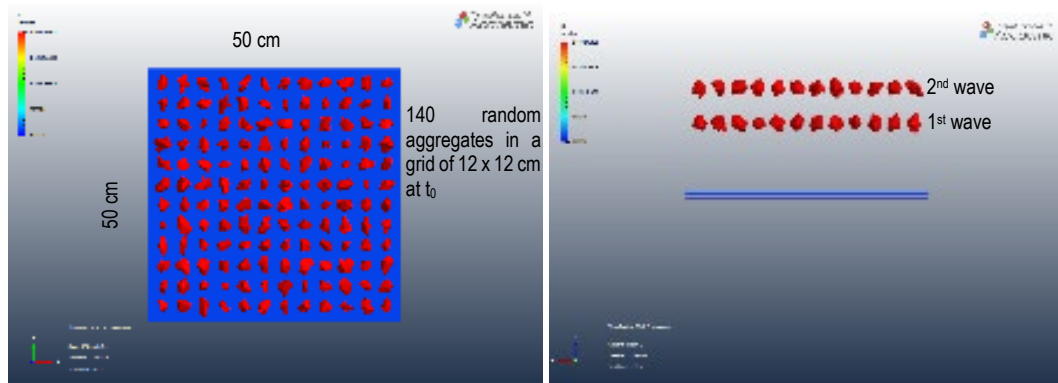
**Tab. 4** slave contact coefficients

No.	Material A	Material B	Young modulus (MPa)	Poisson coeff	Critical stress (MPa)	Bonding radius (m)	Damping ratio
1	string	string	640	0.49	10 e6	0.000612	0,05
2	rubber mat (top)	rubber mat (top)	1.65	0.30	-	0.005631 m	0.7
	rubber mat (bottom)	rubber mat (bottom)	1.65	0.30	-	0.005631 m	0.7

### 4.3.4 Particle generation

The particle generation section in ThreeParticle/CAE is used to generate particles in a smart way and include different types like automatic generation, filling, moving and manual. For our model, the goal of the particle generation was to mimic as close as possible the actual pouring of aggregates for the preparation of the specimens and also the laying of the string in a predefined pattern. After several trials, the approach we used was to manually generate the particles at specific locations on top of the mat, covering the box geometry in a grid of  $12 \times 12$  (see Abb. 51). Due to gravity and due to a given initial vertical velocity, these particles move down until they deposit on top of the rubber mat. With a time delay, several waves of new random particles are generated at the same location. It must be remarked that within any new wave, there is a generated particle mix with uniform distribution, i.e. each of the 100 scanned aggregates have equal probability to be in one of the 140 points of the grid. The procedure is repeated until a specific certain amount of aggregates are added, simulating the creation of a layer. As already mentioned in § 4.3.2, the generation of the strings is predefined in a file that stores the position of each particle.





**Abb. 51** top view of the generation pattern in which is possible to see a  $12 \times 12$  aggregates grid (left) and lateral view were is possible to see the second wave of aggregates (above) generated with a time delay respect to the first one (right)

### 4.3.5 Compaction and loading

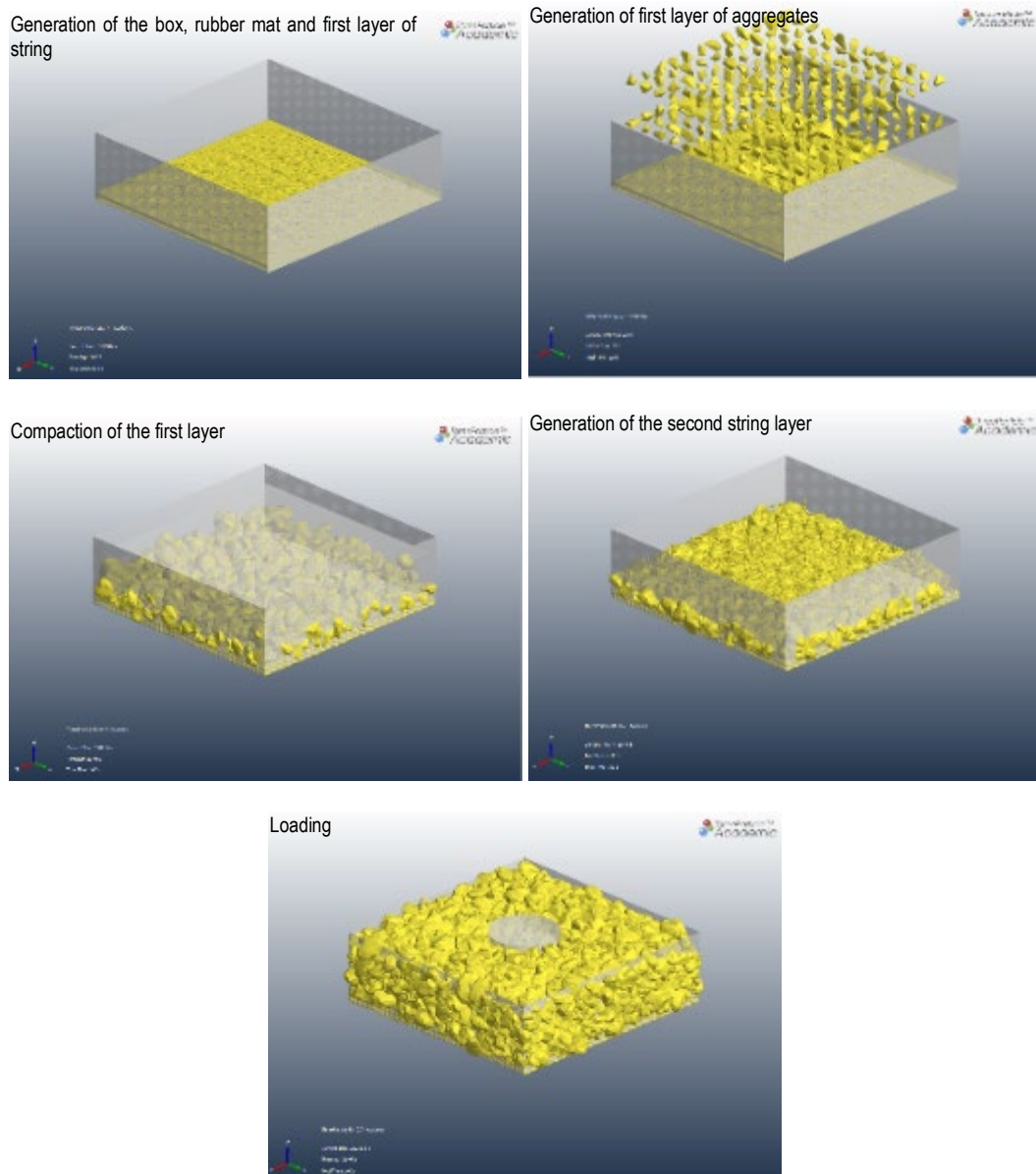
The simulation of these two steps was done through various functions that add time-dependent external loads on both parts and particles. For the model, we had first to define sinusoidal amplitude types. They are used for simulating, on the one hand, the compaction load after generating each layer of aggregates and string. On the other hand, they are also used to simulate the testing loading, which lasted several hours. For the first one, we produced a sinusoidal amplitude function with a maximum load of 3 kN at 20 Hz and a duration of 3 s. For the second one, we produced again a sinusoidal amplitude function with a minimum value of 0.5 kN and a peak value of 9.5 kN. The frequency was also set at 20 Hz. In this case, as it is not possible to simulate several hours of loading, we limited the duration to approximately 2 min (2400 loading cycles). As for the loading, we also added a gravity field to simulate the real-world environment. The gravity of course contributes to the rearrangement of the particles in addition to the imposed load.

### 4.3.6 Domain

As briefly mentioned in § 4.3.1, the domain is the volume in which the contact detection algorithm works. This algorithm is capable to simplify and speed up the identification of collisions between particles and between particles and objects, in each calculation time step. Without it, the detection of collisions would be done by checking the distance between each pair of particles. For spheres, a collision is detected when the distance between them is less than the sum of both radii, which is computationally expensive and becomes much more expensive for shapes that are more complex than spheres. To that end, the domain is subdivided into 3D cells that activate when they contain a particle or a piece. Only these activated cells are checked for contacts and the forces acting on each colliding particle are calculated, resulting in an important reduction of the computational effort. In our simulation, we set the cell size to  $1.25 \times 1.25 \times 1.25 \text{ cm}^3$ .

### 4.3.7 Implementation through keywords programming with Matlab

Due to the complexity of the model and in order to prepare the steps to simulate the setup and the tests, we created a tool to prepare the models in an automatized way, taking advantage of the Keyword timing feature of ThreeParticle/CAE [28]. To that end, as briefly referred in previous chapters, we created several Matlab files capable to change the model by changing different variables. For example, the scripts can automatically, generate the particles to different representations, deploy the string following pre-established patterns, set the material and interaction properties, apply the loads and calculate the timing of different inputs. All Matlab files and auxiliary archives are available for downloading at <https://doi.org/10.5281/zenodo.7786624>, selecting the zipped File 5. As synthesis, Abb. 52 shows the view of the entire simulation process.



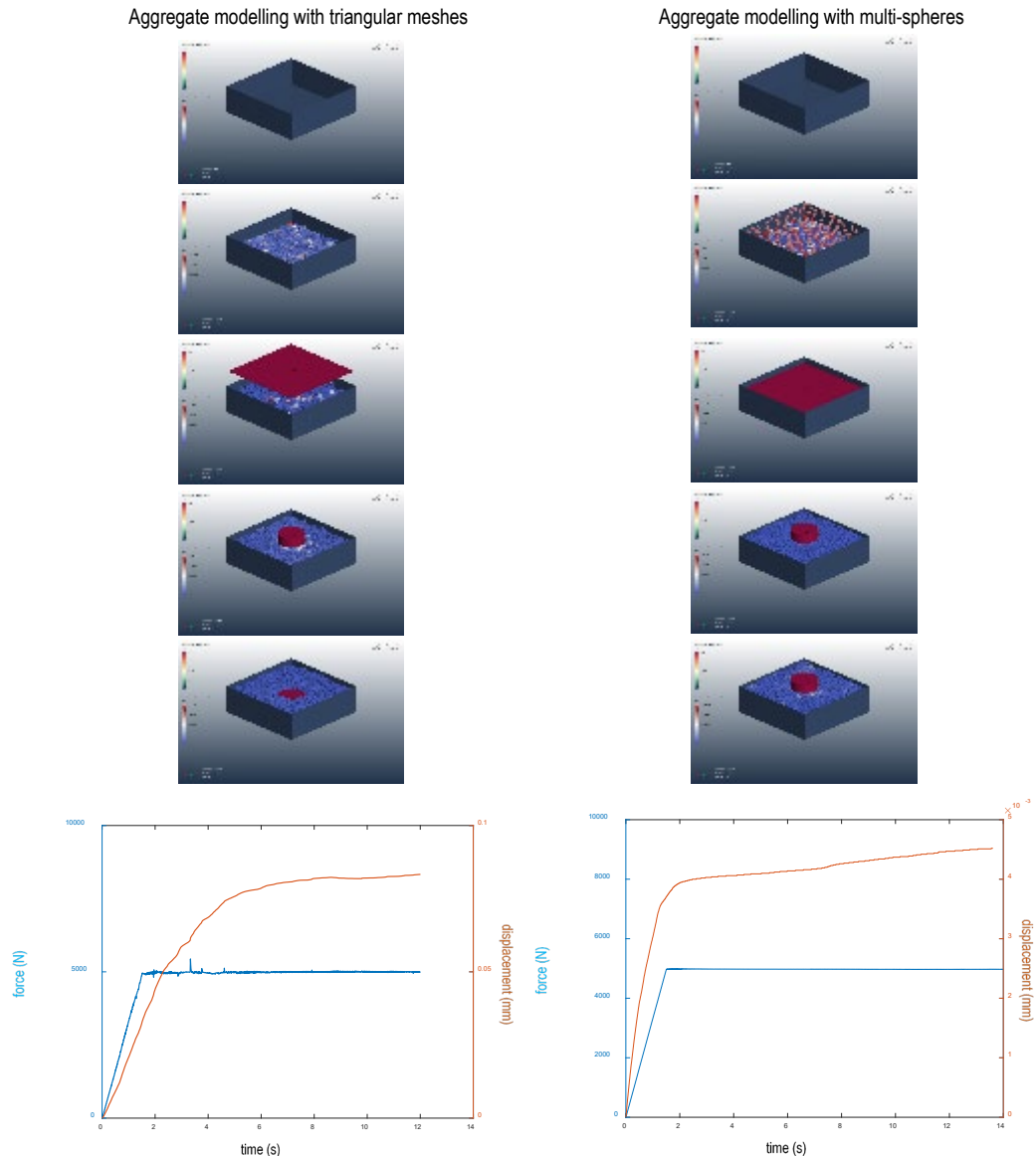
**Abb. 52** panorama of the full simulation process of the small box tests, with a total simulation time of 150 s.

## 4.4 Results

In this section we report about the multiple simulations carried out to find the right set of parameters to achieve a model with similar results (deformation, displacement of the loading plate) as in real tests. It must be pointed out that, for the calibration of these models, we did not only consider the results in terms of deformation of the loading plate, but also we focused on ways to reduce the computational time to acceptable durations (max. 3 days). Another challenge of these models are also the size of the results in terms of hard disk memory: each of these simulations accounted for almost 500 GB.

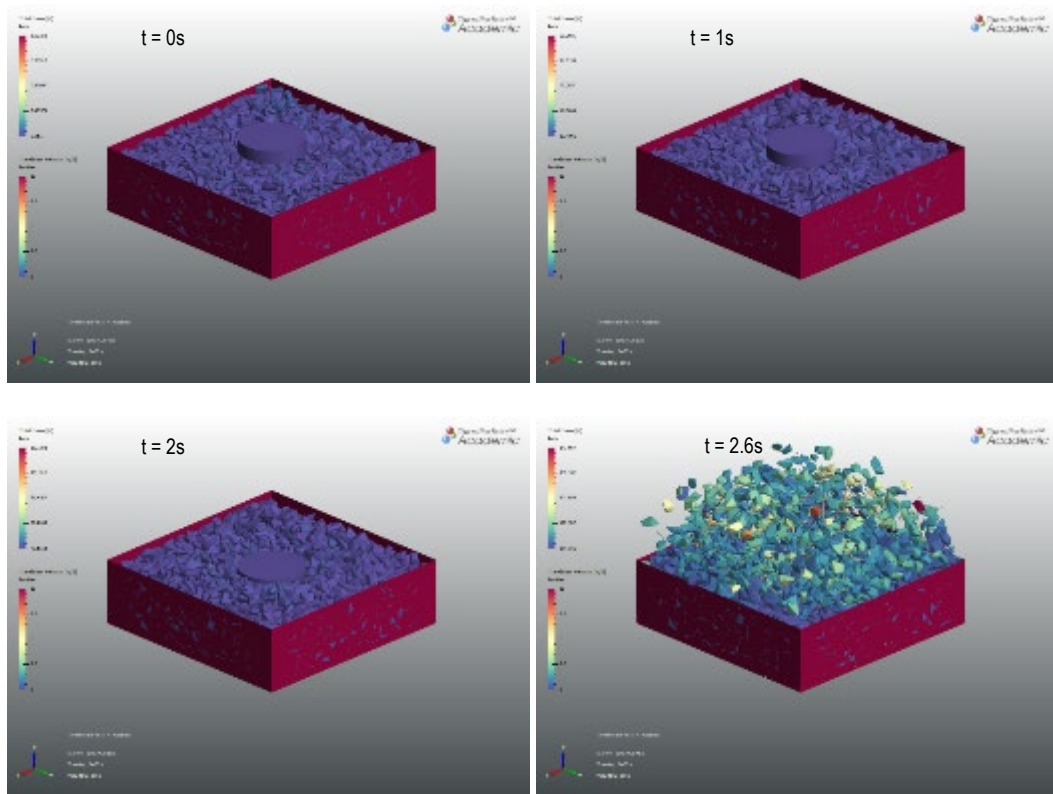
In Abb. 53 we display the results of two simulations. In the first one (see Abb. 53 left) we used triangular meshes to model the aggregates and in the second one (see Abb. 53 right) we used multi-spheres. After 12 s of loading simulation with a sinusoidal load of 5 kN, the permanent deformation reaches 0.085mm for the triangular mesh and 0.0045 mm for the multi-spheres, almost 20 time smaller. From the measurements in the small box samples

this value is about 1 mm, almost 10 times larger than the value obtained from the triangular mesh simulations. We can here conclude, that the modelling of the aggregates with triangular mesh provide more accurate results than with the multi-spheres, but nevertheless the match with the experiments is not satisfactory. The videos of the simulations are accessible at <https://doi.org/10.5281/zenodo.7786624>, File 6.

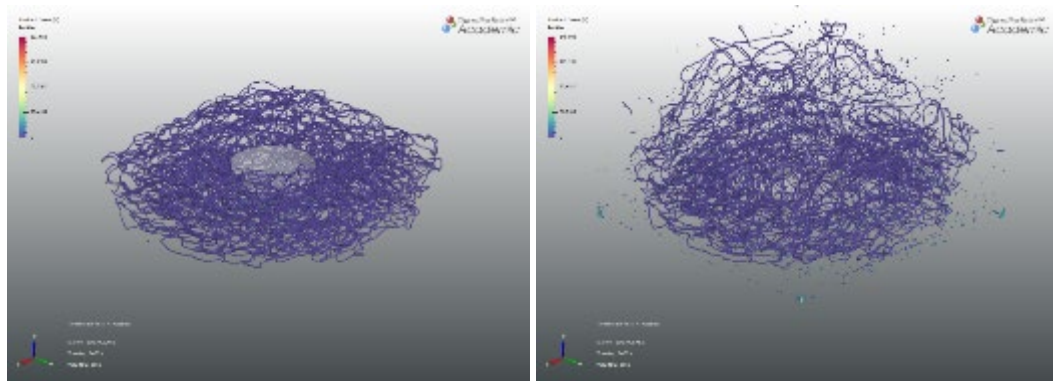


**Abb. 53** comparison of permanent deformation under load of an unreinforced specimen with aggregates made of triangular meshes (left) and multi-sphere clumps (right).

The simulation of specimens reinforced with strings were not providing the expected results and the simulations show that the specimen is collapsing even faster (within little more than 2 s after the load initiates) than the unreinforced specimens (see Abb. 54). The reason of this behavior was, until the preparation this report, still not completely understood. However, the most probable theory is that the sharp edges of the loading plate and the aggregates induce extremely high stress values in the bonding of the string, making them break in very short time step (see Abb. 55). This fragile breaking condition releases a high energy peak, giving the impression that the specimen explodes. This hypothesis and probable approach to avoid this behavior is being consulted with DEM specialists at the time of preparing this report.



**Abb. 54** view of the load progression of a reinforced specimen until failure



**Abb. 55** stress state of the string just before (left) and at the moment of the collapse (right)



## 5 Conclusions and Outlook

In recent research performed at ETH Zurich, it has been shown that a thread or a wire, carefully placed between un-bound aggregates in a layer-wise manner and following certain patterns can induce and improve jamming in aggregate packings to create new types of fully-recyclable, loadbearing structures. In this project, we introduced the concept of "Jammed Architectural Structures (JAS)" into road engineering to develop a unique type of reinforcement for pavements. Instead of vertical structures prepared to withstand mainly quasi static loads, the concept of continuous string reinforcement was extended to the unbound layers of pavements, which have primarily the function of taking repetitive transient vertical traffic loads from the surface and distribute them onto a wider underlying substrate without deforming excessively. The main advantage this novel approach over traditional methods for pavement reinforcement is that in case of repairing or demolishing a pavement, the strings can be easily extracted from the layers, allowing to reuse the remaining unbound aggregates with minimal effort. Placing reinforcement strings in 3D patterns can be performed with robots, which move resembling a knitting needle.

In the first and main part of this report, the experimental work on aggregate packings with and without string reinforcement is described. Aggregates of two different fractions, mainly 16 - 22.4 mm but also 8 - 11.2 mm, were placed into wooden boxes. Mostly, crushed aggregates were used, but also rounded aggregates were used in selected experiments. The string was an eco-friendly, low-priced braided thread made of recycled synthetic and natural leftovers from the textile industry. Strings with 2.5 mm diameters were mostly used, with selected tests with strings of 1.8 mm and 4 mm diameter. The initial tests were performed with  $50 \times 50 \times 15 \text{ cm}^3$  boxes (small boxes), while the main experimental series was performed using  $70 \times 70 \times 25 \text{ cm}^3$  boxes (big boxes) with a 1.5 cm-thick rubber mat at the bottom. A robotic arm with 6 degrees of freedom was used to deposit the string, with an end effector developed in the course of the project that was used to pull the string following predefined patterns in successive layers. Different types of string patterns were employed in the experiments, including circular patterns with different degrees of overlap and rectangular patterns with meshes of different sizes. The specimens were prepared adding consecutive layers of strings and aggregates followed by a manual densification using an earth rammer. For the big box samples, the final compaction was carried out with a sinusoidal load distributed over the entire area of the specimen, until the recorded permanent deformation reached a plateau. The uniaxial cyclic compression tests, with loads imposed by a loading plate, were then carried out with different load types, maximum and minimum values and frequencies.

The main conclusions of the experimental section are:

- Reinforcement of the aggregate packing with strings has a considerable and repeatable effect on the cyclic load carrying capacity of the system. The deformation of the unreinforced specimens was in any case orders of magnitude greater than that of reinforced specimens;
- Smaller deformations, both for the reinforced and the unreinforced specimens, were observed with smaller aggregates. This effect might be due to different packing density of the different size fractions or to the finite size of the tested boxes;
- Rounded aggregates resulted in much larger deformations than angular aggregates with the same sizes, both when unreinforced and when reinforced. This was expected, as jamming is critically dependent on friction between the aggregates;
- The type of cyclic load showed a paramount influence in the performance of the specimens: with a high maximum load and a low minimum load, much larger deformations were observed than when both the minimum and the maximum loads were low or both high;

- The loading frequency had almost negligible influence when the number of cycles was kept the same, which was somewhat expected since these systems only include elastic components and no viscoelastic binder (as would be the case in asphalt);
- Under the geometries and loads employed in this project, strings with 2.5 mm diameter performed as well as thicker strings, while thinner strings ruptured and resulted in larger deformations of the aggregate packings. The 2.5mm diameter strings were in fact able to sustain greater stresses than the thicker strings with about the same elongation;
- A general trend of reduced deformation with increased length of string embedded in the packings was observed, but circular patterns appeared to work better than rectangular patterns. The best performance was observed in circular patterns with overlaps, but the performance of these patterns did not improve when too much overlapping or circles of small diameter were employed;
- A smaller distance between the reinforcement layers in the vertical direction, or equivalently, more layers of string in the specimens, resulted in a reduction of the permanent deformation;
- With X-ray tomography (using a special, high-energy setup available at Empa) it was possible to obtain a 3D image of the reinforced aggregate packings and of the string, but the quality of the images (in particular the contrast of the strings) was too poor to study the effect of cyclic loading on the aggregate packing and on the string. This line of research would need a dedicated effort in the future.

In the second part of this report, we described the methodology to develop numerical models to simulate particle-string systems under dynamic loading. The aim of this section is to achieve an accurate representation of the systems studied in the experimental section. In this numerical work, both the aggregate packing and the string reinforcement were simulated with the Discrete Element Method (DEM). The main aims of this modelling effort were: 1) to obtain insight about the fundamental mechanisms that govern the deformation of the reinforced aggregate packing; 2) to explore the effect of important parameters (e.g. material properties of aggregates and strings, load, string patterns and boundary conditions) in a systematic and simple manner, which may be difficult or impossible in the experiments; 3) to extend and complement the experimental series with additional numerical experiments, e.g. with different geometries and configurations. We used the DEM software ThreeParticle/CAE as a tool for solving the numerical models. In order to automatize and simplify the preparation of different model configurations, we developed a script in Matlab that was able to numerically replicate the preparation and the testing of the specimens. As part of the preparation of the models, we scanned and digitalized a significant number (100) of the aggregates used in the experimental phase. We also obtained the mechanical properties of the different materials and devices used in the experiments (i.e., aggregates, strings, rubber mat), in order to obtain initial values of the materials and contact models.

The main conclusions of the numerical section are:

- The most complex trial models obtained were able to replicate the steps required to prepare the specimens, including pouring of aggregates, deploying of strings and compaction;
- Different particle shape representations for the aggregates were employed. Modelling of the aggregates with multi-spheres – despite being less accurate than using polyhedrons or three meshes - provided the best results with an acceptable computational effort;
- The string was modelled by bonding different capsule elements together;
- The design of the patterns was automatized;



- The complexity of these models is requiring a very important computational effort, with extremely long computation times (up to 4 weeks) on the available hardware;
- While the simulations performed in the frame of this project provided valuable insight and prepared the methods and the tools, future work will focus on optimizing the simulations of the reinforced specimens to obtain rapid results.

The main conclusion of this study is that the JAS concept, originally established in architectural and structural engineering research for vertical structures, can also enhance the performance of horizontal structures under dynamic loading conditions by reducing its permanent deformation with economy of materials. The main advantage of these novel structures compared to traditional pavement reinforcement approaches is their almost perfect recyclability. Clear evidence of this advantage was the large amount of laboratory specimens that could be assembled and disassembled within the frame of this project. However, unlike in JAS, where structures follow architectural designs based on columns and walls with endless possible shapes, pavements or ballast embankments have mostly 2D linear structures with no geometrical singularities. For these quite simple structures, the use of robots to deploy strings might not be the most efficient approach. Analogous to 3D printing technologies, the required time to create a piece is still, and will always be, an obstacle for mass production. Here, we see the use of robots as a way of "rapid prototyping", i.e. a way to easily produce specimens with different reinforcement patterns in order to study the performance of each prototype. Further, this work lays the groundwork for the use of digital technology in the pavement construction landscape, stimulating future discussions about their application in a still quite traditional field. The effort invested in this project is then justified and the lessons learned represent the conceptual basis for future work in this area. Following these considerations, potential continuation of this research line should include the use of rolling tires instead of cyclic compression loads in order to validate the results. Further, possible future topics could consist of the study of the effect of water, different aggregates distributions including RAP and surface surcharge. And, as previously stated, the results could also be used in the future for designing and fabricating a continuous 3D grid.



## Glossar

<b>Begriff</b>	<b>Bedeutung</b>
CAE	Computer-Aided Engineering
DEM	Discrete Element Method
Empa	Eidgenössische Materialprüfungs- und Forschungsanstalt Swiss Federal Laboratories for Materials Science and Technology
ETH	Eidgenössische Technische Hochschule Swiss Federal Institute of Technology in Zurich
FEM	Finite Element Method
HM model	Hertz-Mindlin contact model
JAS	Jammed Architectural Structures
NCCR	National Centre of Competence in Research
MIT	Massachusetts Institute of Technology
UR	Universal Robots




## Literaturverzeichnis

- 
- [1] Partl, M. N. (2018), "Towards improved testing of modern asphalt pavements", *Materials and Structures*, 51(6), 166. <https://doi.org/10.1617/s11527-018-1286-9>
- 
- [2] Iiev, P. (2019), "Mechanical behavior of confined granular materials", *Doctoral Thesis ETH Zurich*, *Ethz.ch*. <https://doi.org/10.3929/ethz-b-000341577>
- 
- [3] Yan, T., Marasteanu, M. O., & Le, J.-L. (2021), "Mechanism-based evaluation of compactability of asphalt mixtures", *Road Materials and Pavement Design*, 22(1), s482–S497, <https://doi.org/10.1080/14680629.2021.1905697>
- 
- [4] Ghafoori Roozbahany, E., Partl, M. N., & Jelagin, D. (2019), "Modelling the flow of asphalt under simulated compaction using discrete element", *Construction and Building Materials*, 227, 116432. <https://doi.org/10.1016/j.conbuildmat.2019.07.158>
- 
- [5] Cates, M. E., Wittmer, J. P., Bouchaud, J.-P., & Claudin, P. (1998), "Jamming, Force Chains, and Fragile Matter", *Physical Review Letters*, 81(9), 1841–1844. <https://doi.org/10.1103/PhysRevLett.81.1841>
- 
- [6] Liu, A. J., & Nagel, S. R. (1998), "Jamming is not just cool any more", *Nature*, 396(6706), 21–22. <https://doi.org/10.1038/23819>
- 
- [7] Han, J., Zhang, Y., & Parsons, R. L. (2011), "Quantifying the influence of geosynthetics on performance of reinforced granular bases in laboratory", *Geotechnical Engineering*, 42(1), 75.
- 
- [8] Zhang, Y. (2007), "Investigation of geosynthetic-soil confinement using asphalt pavement analyzer", *Doctoral dissertation, University of Kansas*, <https://www.proquest.com/dissertations-theses/investigation-geosynthetic-soil-confinement-using/docview/304846700/se-2?accountid=28439>
- 
- [9] Qamhia, I. I., & Tutumluer, E. (2021), "Evaluation of geosynthetics use in pavement foundation layers and their effects on design methods", *FHWA-ICT-21-020*
- 
- [10] Arraigada, M., Perrotta, F., Raab, C., Tebaldi, G., & Partl, M. (2016), "Use of APT for Validating the Efficiency of Reinforcement Grids in Asphalt Pavements", in *The Roles of Accelerated Pavement Testing in Pavement Sustainability: Engineering, Environment, and Economics* (pp. 509–521). [https://doi.org/10.1007/978-3-319-42797-3\\_33](https://doi.org/10.1007/978-3-319-42797-3_33)
- 
- [11] Gramazio, F., & Kohler M. (2008), "Digital Materiality in Architecture", *Lars Müller Publishers, Baden*, 7–11
- 
- [12] Willmann, J., Gramazio, F., Kohler, M., & Langenberg S. (2012), "Digital by material: envisioning an extended performative materiality in the digital age of architecture", in: *Brell-Cokcan, S., Braumann, J. (eds.) Robotic Fabrication in Architecture, Art and Design*, Springer, Wien, 12–27
- 
- [13] Aejmelaeus-Lindström, P., Willmann, J., Tibbits, S., Gramazio, F., & Kohler, M. (2016), "Jammed architectural structures: Towards large-scale reversible construction", *Granular Matter*, 18(2), 28. <https://doi.org/10.1007/s10035-016-0628-y>
- 
- [14] Aejmelaeus-Lindström, P., Thoma, A., Mirjan, A., Helm, V., Tibbits, S., Gramazio, F., & Kohler, M. (2017), "Rock Print: An Architectural Installation of Granular Matter", in *Active Matter*, Skylar Tibbits, 286–296. Cambridge, MA: MIT Press
- 
- [15] Aejmelaeus-Lindström, P., Rusenova, G., Mirjan, A., Medina Ibáñez, J., Gramazio, F., & Kohler, M. (2020). "Rock print Pavilion: Robotically fabricating architecture from rock and string", *Construction Robotics*, 4(1–2), 97–113. <https://doi.org/10.1007/s41693-020-00027-8>
- 
- [16] Rusenova, G., Wittel, F. K., Aejmelaeus-Lindström, P., Gramazio, F., & Kohler, M. (2018), "Load-Bearing Capacity and Deformation of Jammed Architectural Structures", *3D Printing and Additive Manufacturing*, 5(4), 257–267. <https://doi.org/10.1089/3dp.2018.0039>
- 
- [17] Fauconneau, M., Wittel, F. K., & Herrmann, H. J. (2016), "Continuous wire reinforcement for jammed granular architecture", *Granular Matter*, 18, 1
- 
- [18] Iiev, P. S., Wittel, F. K., & Herrmann, H. J. (2018), "Discrete element modeling of free-standing wire-reinforced jammed granular columns", *Computational Particle Mechanics*, 5(4), 507–516. <https://doi.org/10.1007/s40571-018-0186-7>
- 
- [19] Iiev, P. S., Wittel, F. K., & Herrmann, H. J. (2021), "Inversion of force lines in fiber-reinforced jammed granular material", *The European Physical Journal E*, 44(4), 58. <https://doi.org/10.1140/epje/s10189-021-00053-6>
- 
- [20] Conzelmann, N. (2022), "Development of non-convex artificial aggregates for pavements", *Doctoral Thesis, ETH Zurich*, <https://doi.org/10.3929/ETHZ-B-000537041>
- 
- [21] Conzelmann, N.A., Partl, M.N., Clemens, F.J., Müller, C.R., & Poulikakos, L.D. (2022), "Effect of artificial aggregate shapes on the porosity, tortuosity and permeability of their packings", *Powder Technology*, 397, p.117019
-

- 
- [22] Aikins, K.A., Ucgul, M., Barr, J.B., Awuah, E., Antille, D.L., Jensen, T.A., & Desbiolles, J.M.A (2023), **"Review of Discrete Element Method Simulations of Soil Tillage and Furrow Opening"**, *Agriculture* 2023, 13, 541. <https://doi.org/10.3390/agriculture13030541>
- 
- [23] Altair Engineering Inc. (n.d.), **"What is the Discrete Element Method (DEM)?"**, Retrieved January 4, 2023, from <https://www.altair.com/resource/what-is-the-discrete-element-method-dem>
- 
- [24] Kaufmann, J., Frech, K., Schuetz, P., & Münch, B. (2013) **"Rebound and orientation of fibers in wet sprayed concrete applications"**, *Construction and Building Materials*, 49, pp.15-22.
- 
- [25] El-Kassem, B., Salloum, N., Brinz, T., Heider, Y., & Markert, B. (2021) **"A multivariate regression parametric study on DEM input parameters of free-flowing and cohesive powders with experimental data-based validation"**, *Computational Particle Mechanics*, 8(1), 87–111. <https://doi.org/10.1007/s40571-020-00315-8>
- 
- [26] Obermayr, M., Dressler, K., Vrettos, C., & Eberhard, P. (2013), **"A bonded-particle model for cemented sand"**, *Computers and Geotechnics*, 49, 299–313. <https://doi.org/10.1016/j.compgeo.2012.09.001>
- 
- [27] Becker, A. (2022), **"ThreeParticle - User guide"**, BECKER 3D GmbH
- 
- [28] Becker, A. (2022), **"ThreeParticle – Keywords guide"**, BECKER 3D GmbH
- 
- [29] Becker, A. (2022), **"ThreeParticle – API guide"**, BECKER 3D GmbH
-

# Projektabschluss

 <p>Schweizerische Eidgenossenschaft Confédération suisse Confederazione Svizzera Confederaziun svizra</p>	<p>Eidgenössisches Departement für Umwelt, Verkehr, Energie und Kommunikation UVEK Bundesamt für Strassen ASTRA</p>
<h2>FORSCHUNG IM STRASSENWESEN DES UVEK</h2> <h3>Formular Nr. 3: Projektabschluss</h3>	
<small>Version vom 09.10.2013</small>	
erstellt / geändert am:	08.06.2023
<h3>Grunddaten</h3>	
Projekt-Nr.:	ASTRA 2017/005
Projekttitel:	Robotergestützte Verstärkung von Belägen
Enddatum:	30.06.2023
<h3>Texte</h3>	
Zusammenfassung der Projektergebnisse:	
<p>Research conducted at ETH Zurich demonstrated that strategically placing threads or wires between unbound aggregates in a layer-wise manner can enhance the jamming phenomenon in aggregate packings, leading to the creation of fully-recyclable, load-bearing vertical structures such as columns and walls. These structures, known as "Jammed Architectural Structures" (JAS), require the use of a robotic arm capable of precisely deploying the strings according to a digital blueprint. Once these structures have served their purpose, they can be easily dismantled by removing the strings for efficient recycling.</p> <p>The aim of our work was to introduce the concept of JAS to the field of road engineering, particularly for the development of a unique type of reinforcement for pavements. Instead of relying on traditional vertical structures designed to withstand primarily static loads, we extended the concept of continuous string reinforcement to the unbound layers of pavements. These layers primarily function to handle repetitive transient vertical traffic loads from the surface, distributing them over a wider area without excessive deformation.</p> <p>The experimental phase of our study focused on conducting cyclic compression tests on aggregate packings contained within boxes, both with and without string reinforcement. We explored various parameters, such as pattern type, string thickness and length, aggregate size, and loading conditions. The results clearly demonstrated that reinforcing the aggregate packing with strings had a substantial and repeatable impact on the cyclic load-carrying capacity of the system. Furthermore, we developed intricate numerical models using the discrete element method, which closely reproduced the necessary steps involved in specimen preparation, including the pouring of aggregates, deployment of strings, and compaction.</p> <p>Overall, our research successfully showcased the potential of using JAS principles in road engineering, particularly in the context of developing innovative reinforcement techniques for pavements. By incorporating string reinforcement in unbound granular layers, we observed significant improvements in the cyclic load performance through the reduction of the permanent deformation.</p>	
<div style="display: flex; justify-content: space-between;"> <span>Forschung im Strassenwesen des UVEK: Formular 3</span> <span>Seite 1 / 3</span> </div>	





Schweizerische Eidgenossenschaft  
Confédération suisse  
Confederazione Svizzera  
Confederaziun svizra

Eidgenössisches Departement für  
Umwelt, Verkehr, Energie und Kommunikation UVEK  
Bundesamt für Strassen ASTRA

#### Zielerreichung:

According to the proposal, the project's main objectives were to introduce digital technologies into the pavement construction landscape and enhance pavement durability. To achieve these goals, we utilized robotic arms in conjunction with digital design, which was a novel approach in pavement research. The laboratory results indicate a notable improvement in specimen performance through the use of string reinforcement. Therefore, we consider the general objectives of the project to have been successfully accomplished. However, it is important to note that certain aspects of the project faced challenges and limitations. Specifically, we were unable to conduct the planned validation tests involving rolling tires, and some experiments, such as CT scans, did not yield the anticipated results. Further, modeling still needs improvements. These issues present opportunities for improvement and should be the primary focus of any future follow-up projects.

#### Folgerungen und Empfehlungen:

Continuation of this research line should explore the use of rolling tires as an alternative to cyclic compression loads for result validation. Additionally, future research could focus on studying the impact of water, different aggregate distributions (including RAP), and surface surcharge. Modeling can also be improved in a follow up project. The outcomes of this study could also be applied in the future to design and fabricate a continuous 3D reinforcement grid.

#### Publikationen:

So far there is no published paper about the results of the project.

#### Der Projektleiter/die Projektleiterin:

Name: Arrigada

Vorname: Martin

Amt, Firma, Institut: Empa

#### Unterschrift des Projektleiters/der Projektleiterin:



## FORSCHUNG IM STRASSENWESEN DES UVEK

### Formular Nr. 3: Projektabschluss

#### Beurteilung der Begleitkommission:

##### Beurteilung:

Experimental results from this unconventional project have demonstrated that the deployment of string reinforcement through a robotic arm can enhance aggregate jamming and effectively handle dynamic vertical repetitive loading. This approach increases the stress distribution area and reduces permanent deformation, such as rutting. Additionally, the project successfully showcased the application of digital technologies and robots in reinforcing specimens that simulate horizontal structures like pavements. Although modeling tools were developed, further work is required to ensure accurate and efficient simulation of the experimental results. Overall, the project objectives were adequately achieved.

##### Umsetzung:

This is a fundamental research project and therefore it is too early to practically implement their findings.

##### weitergehender Forschungsbedarf:

Several questions, like the effect of rolling tires or the impact of water in the permanent deformation of the reinforced specimens should be answered in future research efforts.

##### Einfluss auf Normenwerk:

The project has no direct influence on standardisation.

#### Der Präsident/die Präsidentin der Begleitkommission:

Name: Bueche

Vorname: Nicolas

Amt, Firma, Institut: BFH

#### Unterschrift des Präsidenten/der Präsidentin der Begleitkommission: